Summer 6-21-2023

UNDERSTANDING THE FLOW DYNAMICS OF THE PEARL RIVER, MS, THROUGH HYDRODYNAMIC MODELING

Nahruma Mehzabeen Pieu

UNDERSTANDING THE FLOW DYNAMICS OF THE PEARL RIVER, MS, THROUGH HYDRODYNAMIC MODELING

by

Nahruma Mehzabeen Pieu

A Thesis
Submitted to the Graduate School,
the College of Arts and Sciences
and the School of Ocean Science and Engineering
at The University of Southern Mississippi
in Partial Fulfillment of the Requirements
for the Degree of Master of Science

Approved by:

Dr. Kemal Cambazoglu, Committee Chair
Dr. Jerry Wiggert
Dr. Maarten Buijsman
Dr. Gaurav Savant

August 2023

ABSTRACT

The Pearl River brings fresh water and nutrients into Lake Borgne regulating conditions for oyster growth in estuarine waters. However, there are no flow measurement stations installed on East Pearl or West Pearl either at the river outlets or after the upstream bifurcation of the Pearl. This study aims to model the Lower Pearl River to understand the flow dynamics in the major branches, and to determine the final outflow distribution into the Mississippi Sound, aiming to improve river forcing for ocean models studying estuarine dynamics of the Mississippi Sound.

Synthetic meandering bathymetry with updated banks is developed and applied to represent major branches of Pearl River and is verified using survey data at East Pearl. A riverine HEC-RAS model is set up, calibrated for 2014, and validated for 2015, 2019, and 2020, The model showed good performance with high values of Correlation Coefficient(>0.85), Nash-Sutcliffe efficiency (>0.6), Wilmott Skill (>0.8), Kling-Gupta Efficiency (>0.7) and low values of Percent Bias (<25%) and Root Mean Standard Deviation Ratio (< 0.7) at stations in Lower Pearl and West Pearl while the tidal discharge at East Pearl is underestimated. Model results help explain the complex flow distribution in Pearl River showing West Pearl as the dominant river branch upstream all year, and East Pearl as dominant downstream during high river inflow The Middle Pearl channels carry the floodplain waters back to East and West Pearl while East Pearl flows upstream and all the river outflow is through the West Pearl-Little Lake during dry months.

ACKNOWLEDGMENTS

I would like to thank my adviser Dr. Mustafa Kemal Cambazoglu for his encouragement, direction, and understanding. I would also like to thank my committee members Dr. Jerry Wiggert, Dr. Maarten Bujisman, and Dr. Gaurav Savant for their guidance and knowledge. A special thank you to Dr. Anand Devappa Hiroji and the students from hydrography Science, especially Peter Komolafe and Olauluwa Oderinde for providing the bathymetric data for the river and for answering my endless repetitive questions. I'm grateful to Gowri Shankar Chinnathambi for providing data from the ADCIRC run and for his valuable advice and suggestions. A big thanks to my friends Tasnim Islam and Shihab Hossain Saran for their ideas which helped me progress in this work, and to many more friends for encouraging me and giving me mental support.

DEDICATION

This work is dedicated to my family. Especially my mother Nayma Akter, and my sister, Syed Ummey Shafura Kanak, two of the strongest women I have known since birth. My open-minded and critical brother Syed Al Nahian and my ever so emotional and cautious father, G.M. Jahangir Hossain. Thank you for believing in me and allowing me to spread my wings. I am where I am, and who I am, because of you.

TABLE OF CONTENTS

LIST OF TABLES

LIST OF ILLUSTRATIONS

LIST OF EQUATIONS

CHAPTER I – INTRODUCTION

The Pearl River is a blackwater river (Duan et al., 2007) that is more pristine (Shiller et al., 2012) than the Mississippi River but has a discharge that is a hundred times lower (Wang et al., 2013). Among the freshwater rivers that drain into the Mississippi Sound, such as Pascagoula, Biloxi, Jourdan, and Wolf, to name a few, the Pearl River is one of the major rivers that bring considerable freshwater into the estuarine system (Patrick, 1995). It is a source of fresh water for many residential areas and the rich marshland ecosystem as it bifurcates into two major branches, East and West Pearl (Figure 1.1). The East Pearl drains directly into Lake Borgne while the West Pearl detours into the Rigolets first, eventually flowing into the Mississippi Sound. The Lower Pearl contributes to 9% of the total drainage basin (Blain and Cambazoglu, 2019), and around 50% of the river basin consists of forests and marshes (Goolsby et al., 2000; Duan et al., 2007).

The Pearl River connects to the coastal area, bringing excess freshwater into estuaries during spring which lowers the bottom salinity of Lake Borgne causing negative effects on the water quality and Oyster Bay (Armstrong et al., 2021). Nearly 13000 structures are located near the Lower Pearl River in Louisiana State (Blain and Cambazoglu, 2019), including in the city of Slidell, where frequent inland flooding is witnessed due to heavy rainfall and coastal flooding happens due to storm surges from the coast (Ding et al.,2012). Diverse and rich marshlands at the coastal downstream section of the Pearl support many plants sustained by the salinity system maintained through the combined effect of elevation, saline Lake Borgne waters, freshwater streamflow, tidal amplitude, dominant seasonal wind direction, and soil type (White & Simmons, 1988). It has been speculated that Pearl River discharge might be lowering the salinity of Mississippi

Sound driving the optimal condition of Oyster production seaward (Adriance et al., 2018). Regardless of such flooding and ecological concerns caused by the excess freshwater input, the specific impact of the Pearl on Lake Borgne and Mississippi Sound salinity and its ecology has been rarely investigated.

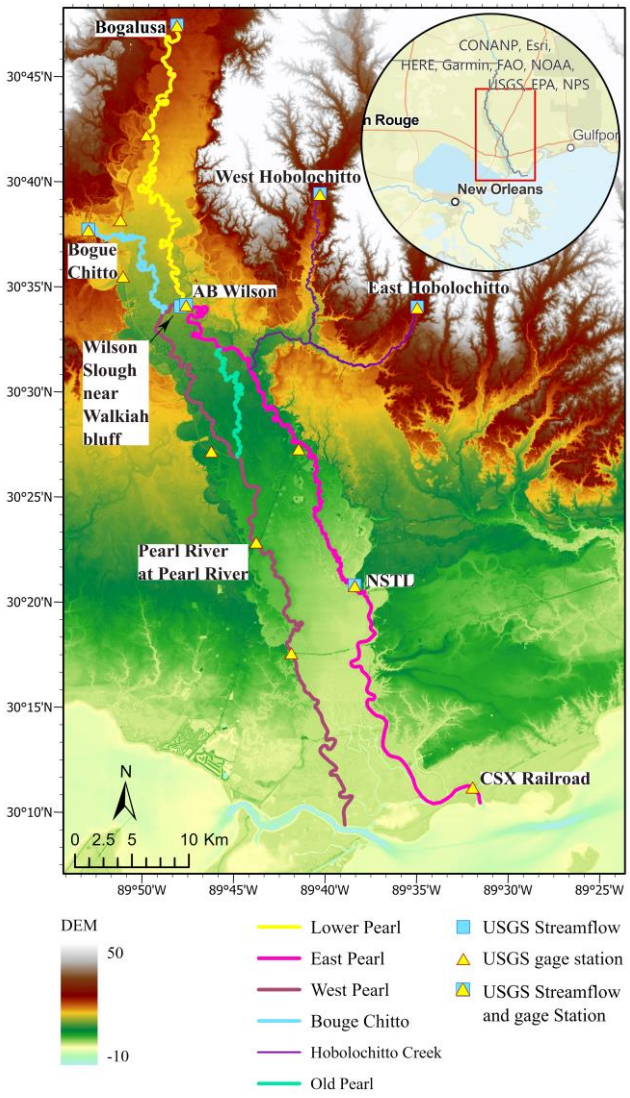

Figure 1.1 *The DEM of the Lower Pearl River, showing its tributaries and USGS monitoring stations naming all the stations used for modeling the area.*

Flow from Lower Pearl River to East Pearl River is low in the dry seasons but becomes significant during wetter periods in high-flow scenarios (Shiller et al., 2012). But the discharge at the inlet of West Pearl River is not continuously measured and East Pearl River is ungauged which makes it difficult to know how much of the flow in East Pearl River is due to the Pearl River or due to Hobolochitto creeks. The knowledge gap is aimed to be filled using a hydrodynamic model. The development, configuration, and results of this model will be discussed in this thesis. The digital elevation model (DEM) used to define the topography was collected from National Oceanic and Atmospheric Administration (NOAA) [https://coast.noaa.gov/digitalcoast/data/coastallidar.html], but the LiDAR data could not capture the river bathymetry, i.e., either the depth was too shallow, or there were blockages along the river causing water to flow through the floodplain instead of the river, or riverbanks were outdated. Improvements had to be made to the riverbanks and channel depth including the effects of the meandering nature of the river. The thesis will introduce a simple technique for synthetic meandering river bathymetry only using a DEM, bank elevations, river slope, and a minimum and maximum depth of the river.

This study investigates if a riverine hydrodynamic model could accurately predict flow patterns using simplified synthetic bathymetry. The flow distribution at branches of the Pearl River is investigated along with the distribution of the flow from the Pearl into the marshlands. The ultimate goal is to provide river forcing using the calibrated and validated model to the Regional Oceanic Modeling System (ROMS) application developed for Mississippi Sound and Bight within the Coupled Ocean Atmosphere Wave Sediment Transport Modeling System (COAWST) to better represent the estuarine system with river

flow dynamics. In the current ROMS model, the flow from Bogalusa station gets distributed by a 40-to-60 ratio into the Mississippi Sound, where the West Pearl is the dominating river branch receiving 60% flow. But river model results in this study show that using constant discharge distribution for a river in the river boundary in coastal models is not representative of the river since the river flow distribution is time variant. The results also show that a significant portion of the flow from Bogalusa (at the upstream section of the Pearl River) is distributed into the swamps and marshlands between the two main branches, so how much of the flow gets distributed and can be included as the river boundary in ROMS can be evaluated by modeling the Pearl. The freshwater outflow from Pearl brings nutrients, sediments and trace elements which interact and affect the salinity in the Mississippi Sound, which impacts the health of Oyster reefs (Sankar et al., 2022). Knowing the variation of discharge from each Pearl branch, and how they interact would help determine the optimal location and period for favorable oyster condition which changes interannually depending on the freshwater input into the Sound and can found by modeling the salinity correctly (Denapolis & Lopez, 2020).

This chapter, chapter one, will explore the background of the study which includes the study area, literature review, the significance of Pearl River, the objective, and the hypothesis of this study. Subsequently, chapter two will focus on the methodology of the work including the challenges faced, and the solutions provided. It will also discuss other similar and previous modeling attempts made in the Lower Pearl River and other similar rivers. Chapter three will show the results of the model in comparison to observations during the calibration and validation period of the study. Chapter four will discuss the

findings of the results and the last chapter, chapter five, of this study will draw conclusions, and provide scope for improvements and future application of the model.

1.1 Study Area

Pearl River originates in Neshoba County, Mississippi, and is the main river system draining the county (Bigelow & Chamberlain, 2001). The southern part of the river called the Lower Pearl River (Figure 1.1) has a meandering length of 715 km (Armandei et al., 2021). The river has an average daily discharge of 373 m^3/s which is the fourth highest in the eastern Gulf of Mexico (Ward et al., 2005). High flow occurs during winter and early spring while low flows are generally during late summer and early fall (Sandeep et al., 2020) and the tidal range for the river is between 1.0 m on spring tide and 0.6 m on neap tide (McKay & Blain, 2010). The Pearl River drainage basin consists of 47% forests, evergreen, deciduous, and mixed, 27% agricultural region (Duan et al., 2007), and 10% marshland or swamps along the river (Pearl River Team, 2000). The river travels through Bogalusa in Hancock County, until it splits, or bifurcates, 26 miles (or 41.8 km) downstream from it into the West and East Pearl River as shown in Figure 1.2 (a).

The East Pearl River, which flows along the border of Louisiana and Mississippi, travels into the state of Mississippi, merges with flow from Hobolochitto Creeks, and empties into Lake Borgne which is connected to the Mississippi Sound. Whereas the West Pearl River travels to Louisiana, combines with the flow of Bogue Chitto and empties into The Rigolets. The Rigolets flow into Lake Borgne before eventually connecting to the Mississippi Sound. Both these rivers show strong tidal signals downstream, especially during low flow scenarios, the tidal flux being much higher than the river outflow, and both these rivers frequently flood and drain the marshlands between them (McKay & Blain,

2010). Each of the bifurcated rivers has tributaries of its own: West Pearl is fed by Bogue Chitto around 2.5 km after the split while East Pearl is fed by Hobolochitto Creek around 17 km after the split. Flow into the East Pearl River gets diverted back into West Pearl River through the Old Pearl River (Figure 1.2) and most of the time, the flow from Hobolochitto Creek, draining a 9.7×10^2 km^2 region of south Mississippi, is the dominating flow maintaining East Pearl River (Shiller et al., 2012), especially true in the dry seasons when a part of the East Pearl connecting to the Lower Pearl becomes almost dry. These rivers also act as important channels for navigation and provide drainage for cities nearby, for example, Nicholson and Pearlington near East Pearl River and Slidell along the West Pearl River.

The bathymetry of Lower Pearl River consists of primarily silt and sand which is easily carried by the high flow in the river and amounts to about 150 million tons annually, being four times higher in spring than in fall (Thorne et al., 2008). As the Pearl bifurcates into the West Pearl River and East Pearl River, the flow is distributed and reduced, which induces the deposition of the sediment at different locations and quantities, and this has significantly changed the course of the river at many locations. Figure 1.1 also shows the USGS streamflow and gage stations, although at first glance it seems that enough monitoring stations are present (Figure 1.1), only a limited number of stations have discharge data, and most of these stations have intermittent data, and many stations have missing data at high flow scenarios. The missing data and river shifts had to be considered while modeling the river which will be further discussed in the methodology, chapter two. The East and West Pearl branches out further downstream creating and sustaining a diverse ecosystem of fauna in the marshlands and bayous. The rivers have a gentle slope (Bush et

al.,2022) almost zero near the coast which is visible in the Digital Elevation Map (DEM) of the area shown in Figure 1.2 (b). Water flows from the West Pearl River into the floodplain between the two main branches which then forms an interconnecting channel system, the Middle Pearl channel system, near the coast. This Middle Pearl channel system transports flow from West Pearl, East Pearl, and the floodplain itself and transports them back to Little Lake and East Pearl River directly further downstream.

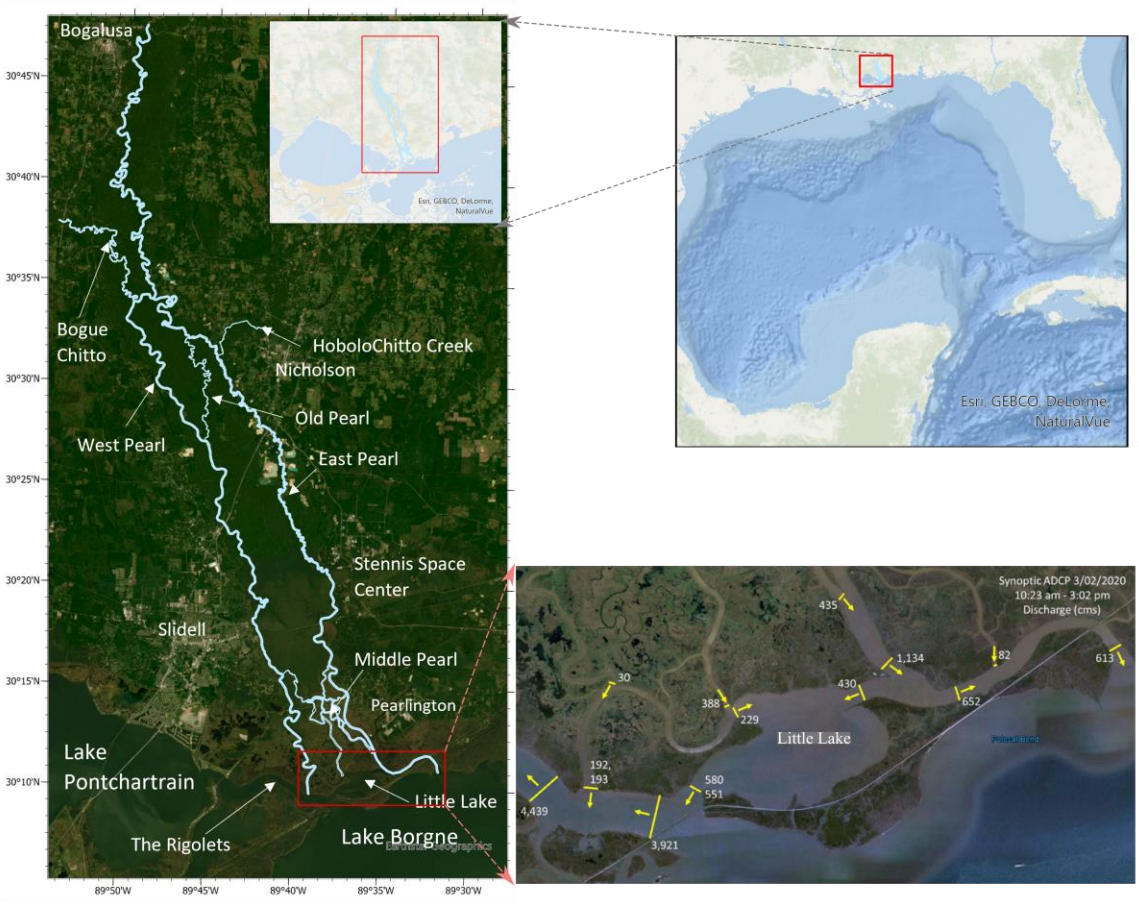

Figure 1.2 *: Extent map of the study area showing (a) The satellite imagery of the Pearl River with areas of interest. (b) zoomed satellite imagery of the Pearl River outlets and the discharge distribution measured using ADCP on March 2nd, 2020 (collected by Kulp et al,2020).*

Flow through Little Lake is complex as it is connected to West Pearl and East Pearl and has an outlet directly to the Rigolets south of the outlet of West Pearl. A survey on the

Pearl River outflow was conducted on March 2nd, 2020, by The Coastal Hydrodynamics and Sediment Transport Laboratory at the Pontchartrain Institute for Environmental Sciences (Kulp et al., 2020). The survey was done using a vessel-mounted Acoustic Doppler Current Profiler (ADCP) in tandem with a differential global positioning system (DGPS) and measured discharge along transects shown in Figure 1.2 (b). It revealed the outflow from Little Lake into The Rigolets to be almost 3 times higher than the outflow of West Pearl River. For this Little Lake was considered as one of the major outlets of our Pearl River model. But why is a river model necessary? The significance of this model and the problems it aims to address will be discussed in the next section.

1.2 Flooding and Ecological Impacts

The extensive floodplain around the East and West Pearl River experiences frequent flooding due to high upstream discharge, rainwater runoff, and high tides associated with the superposition of spring tides with Ekman transport caused by offshore forcing or storm surge during storm events (McKay & Blain, 2010). The freshwater input into the Mississippi Sound due to Pearl River alone is around 10.3 X 10^9 m^3 per year (Eleuterius, 1976), but over the years this freshwater input has been altered by dams, channelization, sills, spillways, and other such diversions (Armandei et al., 2021). These alterations have affected the Mississippi Sound and oyster production (DeHaan et al., 2012) since the freshwater input lowers the bottom salinity of the oyster bay and this is seen to reduce oyster production (Turner, 2006). The freshwater also brings nutrients into Lake Borgne, potentially causing algal blooms and hypoxia, and this is especially felt in spring as it contributes to the salinity decline in the Rigolets, the northwest portion of Lake Borgne, and the Mississippi Sound, significantly reducing oyster production (Armstrong

et al., 2021; Soto et al., 2023). But how much of the freshwater from Pearl contributes to the drastic salinity decline has not been well explored.

As the Bonnet Carré Spillway operates, freshwater is released into Lake Pontchartrain which makes its way to the Mississippi Sound through Rigolets, and another major contributor of freshwater through the Rigolets is the West Pearl. Compound flooding in the West Pearl caused by heavy rainfall and coastal surge during Hurricane Isaac flooded Slidell and caused 500 structures to be flooded (Warren, 2013). West Pearl is the primary cause of inland flooding into Slidell, but despite these, there are no flow monitoring gage stations in the West Pearl to measure and predict flow scenarios and to understand the impact of the silty freshwater into the salinity and sediment regime of Mississippi Sound. This study aims to fill this gap with the development and application of a high-resolution hydrodynamic riverine model.

1.3 Previous Pearl River Models

The hydrodynamic models are convenient tools to understand estuarine systems because of the way they can describe the various processes at different spatial and temporal scales and the way they can introduce or replicate different scenarios (Armandei et al., 2021). So, many hydrodynamic models have been developed for the Mississippi Sound area to comprehend the salinity and temperature variation in the GOM (Schmalz, 1983; Ahsan et al., 2002; Vinogradova et al., 2005), to study the water quality (Dortch et al., 2007), and to understand the flooding impact due to cyclones (Alarcon and McAnally, 2012). But none of the models mentioned have included a riverine system in their models, rather they have only considered a single source from the rivers so they are missing the riverine freshwater dynamics into the estuaries, overlooking an important aspect of how

estuaries work (Sklar and Browder, 1998; Nilsson and Breggren, 2000) and thus could not simulate the salinity within the sound with high accuracy. The inclusion of river hydrodynamics is essential to model and predict compound flooding impacts accurately on the Mississippi coast during storm surges (Ding et al., 2012). The Pearl was also modeled to simulate flood water levels during the Big Bay dam embankment failure in 2004 using HEC-RAS 1D simulation (Yochum et al., 2008) north of Bogalusa and modeled water level matched the high-water marks well. But for the lower Pearl River, south of Bogalusa, the topography is flat, and there was a lack of a well-defined channel. Altinakar et al. (2010) built on this with a 2D model for the confluence of the Pearl River with a CCHE2D-FLOOD model, suggesting that the 1D flow hypothesis would not apply to the gentle slope. However, the modeling attempts of Altinaker et al. (2010) showed inconsistency between modeled and observed owing to the uncertainties in DEM and using an average Manning's roughness coefficient, n-value for the mesh. Both issues were addressed and improved on in the model described in this thesis using land use maps and synthetic bathymetry coupled with high-resolution DEM.

A Pearl River modeling approach has been made in the past (McKay and Blain, 2010) where the Lower Pearl River was modeled using Advanced Circulation (ADCIRC) model and a simplified synthetic bathymetry for the East Pearl River was used to better forecast and predict the flooding pattern surrounding the Lower Pearl River. However, their model did not include the West Pearl River, which our model has found to be the primary cause of flooding in the Pearl River Basin. They also used aerial bathymetric data (4 m resolution) and had to incorporate synthetic bathymetry into their DEM as well but did not show the comparison and basis for their synthetic bathymetry. The model could forecast

the water depth and currents accurately with the exception being the coastal regions of the East Pearl River, overestimating the water level because the synthetic bathymetry overpredicted the depth up to 10 m near Lake Borgne. The model in this work avoids this error by implementing an equation for the synthetic bathymetry to have a depth restriction that limited the depth between 3 m to 7 m, the depths observed during field trips to the East and West Pearl through the Little Lake.

Pearl River was incorporated into another model by Ding et al. (2012) who investigated the effects of coastal storms on the Pearl River basin, and in turn tried to model the effects of the fresh-water input from the river into the Mississippi Sound by modeling the whole area with the coastal model, CCHE2D-Coast. They generated a new refined mesh system to represent the bathymetry and improved the bathymetry itself by incorporating more cross-sectional field data refining the work from the previous modeling effort by Bunya et al. (2010), but their grid overlooked the finer braided channels and the floodplain within the Lower Pearl River, which our model captured. The lack of the Middle Pearl Rivers and floodplain produced flooding unrepresentative of the actual inland flooding. Their model also did not incorporate the Pearl River bifurcation or its unsteady river dynamics and had to utilize synthetic channels along with measured bathymetric data into their DEM, by relating the depth to the one-third power of the channel width, but they did not incorporate any depth restrictions and thus produced cross-sections unrepresentative of the system. It was found during the modeling attempts that the bathymetric data has changed since its last measurement as seen by the significant shifting of riverbanks in many locations along the Lower Pearl River network, so using the old bathymetry would not be representative of the current river system.

A more advanced attempt at Pearl River modeling was presented by Blain and Cambazoglu (2019) who expanded into the modeling of Lower Pearl River by developing an ADCIRC model, incorporating a more refined mesh, more braided channel network within the lower marsh, higher resolution lidar bathymetry of 1 m resolution while including the surge and tide as well. It no longer showed overestimated water level downstream of the East Pearl and the simulated water level agreed with the observed data, but there was a high discrepancy in the West Pearl River. The model would produce accurate results for low flow conditions but showed impractical levels of water level and current for high discharge conditions. The high flow condition would result in uncharacteristic overtopping of water from the bank which was because the model could not represent the local bathymetric condition, here too the synthetic bathymetry generated overly deep channels at wider sections which our bathymetric equation restricts. A gap persisted in modeling all the flow scenarios of Pearl River but the very recent modeling work by Armandei et al. (2021) tried to close the gap by modeling the Pearl River in 3D. Their modeling work coupled two hydrodynamic models, one for the Pearl River and the other for the Western Mississippi sound, using Visual Environmental Fluid Dynamics Code (VEFDC). The system only included a few major branches of the braided river downstream as the main aim of the work was to incorporate and understand the impact of fresh-water input into the Mississippi Sound. However, their model overpredicted or underpredicted the flow, water level, and salinity which might be due to the coarse polygon mesh used to represent the river and its branches, which our model avoids. This lack of research initiative into the flow dynamics and salinity impacts of the Pearl River needs to be addressed to assess the actual flood scenario of the Pearl, the continued maintenance of

the two major branches of the river, and finally investigate the effect, if any, of its salinity impact into the Mississippi Sound.

An extensive survey program was attempted by Thorne et al. (2008) in a report which studied the pattern of sediment transport to predict future sediment deposition volumes and rates by looking at sediment load data at four stations upstream of Bogalusa from 1959 to 2005. But the sediment transport in the rivers which also has tidal influence downstream along with occasional storm surge and unstable bathymetry make it a dynamic problem, the solution of which cannot be a linear one as suggested in the report. Extensive surveys to determine the sediment load at various locations would not be feasible and might even be detrimental to the vast amount of marshland ecosystem (Perra et al., 2020). The safest, most affordable, and most effective way of addressing this issue would be to set up a 2-dimensional sediment transport model for the LPR to simulate the accumulation and removal of sediment along the braided system of the basin. And for this, the formation of a well-calibrated and validated hydrodynamic model is essential, which may be used to understand the dynamics of sediment division as a follow-up work.

1.4 Objective and Hypothesis

The main objective of this study is understanding the flow dynamics of the Lower Pearl River, upstream and downstream of the split near AB Wilson, including the discharge distribution at each of the Pearl branches and the discharge variability. One of the tasks to achieve this is to develop a functioning hydrodynamic model in HEC-RAS 2D, which would allow for the investigation of the flow division once calibrated and validated. The second task to achieve this objective is to develop a synthetic parabolic meandering bathymetry equation to represent silty rivers such as the Pearl. This will also determine

how well the synthetic bathymetric equation used in this study represents the river and its flow. But the primary goal of this study is to provide improved and dynamic river boundary data for the ROMS model, an ocean model studying estuarine circulation and dynamics in the Mississippi Sound.

The initial model runs in steady state condition and literature review helped develop the hypothesis which is set for two conditions: at high flow and low flow, at two different locations: the split and the outlet. In 1999, an earthen trapezoidal weir was constructed at the mouth of the West Pearl to prevent the East Pearl from drying up during low flow conditions (Roberts, 2012). The following hypothesis is based on this report, cross-section at the bifurcation at the station AB Wilson and on the previous analysis by the USM modeling group (Sandeep et al., 2020 and Sandeep et al., 2021). Hypotheses for the split or the bifurcation are:

- At high flow conditions, the flow will be divided by 50-50 between East and West Pearls.
- At low flow conditions, West Pearl branch would dominate, carrying more flow than East Pearl.
- Bogue Chitto flow is restricting the flow into West Pearl.

Whereas for the outlet:

- At high flow conditions, East Pearl would be the dominating river branch carrying most flows from Bogalusa.
- At low flow condition, there will be a 50-50 split between East and West Pearls with similar outflow from both branches.

As the flow from Bogue Chitto enters West Pearl 2.5 km (1.53 miles) downstream of the split at AB Wilson, it creates a tailwater condition, i.e., the water level downstream acts as a wall or obstacle, in the West Pearl which restricts flow through the weir (Roberts 2012). When the flow from Bogue Chitto is high, it might also affect the flow split between the East and West Pearl. The modeling described in the next chapter will be used in addressing these hypotheses.

CHAPTER II – METHODOLOGY

The 2D hydrodynamic riverine model used for this study is HEC-RAS, Hydrologic Engineering Center River Analysis System, which was developed by the Army Corps of Engineers in the Hydraulic Engineering Center (Brunner, 2017). The model is freely e downloadable (Munoz et al., 2021), has a dedicated forum, is constantly updated with upgraded features and bug fixes, and can also be used to simulate a wide variety of events. These reasons have made HEC-RAS a popular hydrodynamic model used globally to simulate high flood events (Lian et al.,2013; Ray et al.,2011; Mejia & Reed, 2011), flash flood modeling (Chowdhury et al., 2023; Fink et al., 2006), and flood inundation mapping (Astite et al, 2015), to name a few. HEC-RAS can model rivers in 1D, 1D/2D combined, and 2D. The type of modeling used to simulate a river would depend on river morphology (Pappenberger et al., 2005; Horritt and Bates, 2002) and expected flow conditions (Gori et al., 2020). A 1D model performs better at rivers with steep, well-defined channel side slopes which would prevent lateral flows when water levels fluctuate quickly (Horritt and Bates, 2002). A 2D model is more applicable for flat rivers, at the confluence of rivers, or where lateral flows occur (Bush et al., 2022), which is how the Pearl River was modeled by Altinakar et al., 2010, who suggested that 1D flow hypothesis is inapplicable for flat floodplains where cross-sections are not well defined. As described in the previous section, the Pearl River is relatively flat (Bush et al., 2022), and has multiple tributaries and lateral flows from the marshy floodplains, hence a 2D model is used in this study to represent the Pearl River flow dynamics.

The 2D model would require input boundary condition data, terrain data-topography and bathymetry, a mesh or grid, and a terrain roughness indicator, among other

parameters. Topo-bathy data is initially taken from the Digital Elevation Model (DEM) containing a 3-dimensional raster image of the depths in the study area. The DEM was collected from Coastal Topographic Light Detection and Ranging (LiDAR) data provided by the National Oceanic and Atmospheric Administration (NOAA). The DEM was constructed using LiDAR data collected over several years and during that time the LiDAR was not equipped with a green light to measure below water level. The DEM did not contain the river bathymetry of Lower Pearl or any of its branches and tributaries, so the bathymetry of the river and its branches were not captured resulting in blockages in river channels (Figure 2.3). Moreover, there was a significant shift in the riverbanks at many locations of the river, affecting the flow rate and flooding, so these locations also needed to be updated. The issues discussed caused all the river flow to spill into the floodplain in the initial modeling attempt. This chapter of the thesis will focus on the modeling challenges due to modeling data and the methods used to reduce the uncertainty at each parameter.

2.1 Modeling Data

The data required to set up an unsteady or time-variant 1D, 1D/2D combined, or 2D model are input hydrographs which are discharge time series at the upstream boundary while the downstream boundary may have discharge time series, water level time series, or normal depth with friction slope (Bush et al., 2022; Bhuyian & Kalyanapu, 2020). These upstream and downstream data act as initial values to solve the 2D Saint Venant equation to determine discharge and water level anywhere between them. 2D models also require topography or bathymetry data in the form of a raster file or DEM which is used to calculate the river area, wetted perimeter, and top width of the equation. The topography is also used

to determine the flood extent within the floodplain. The better the accuracy of the DEM, the better the model performance with respect to observations (Horritt and Bates, 2002; Altinakar et al., 2010). 2D models have the added advantage over 1D using spatially varying Manning's n value for roughness based on the land cover map which was implemented in the model. The modeling of forests in the floodplain was done by assigning a higher roughness value for the forest location based on land use maps. But certain errors are associated with each of these parameters, such as uncertainty associated with boundary conditions (e.g., input and output hydrographs), physical parameters (e.g., topography and bathymetry measurements, roughness estimates), and numerical parameters (e.g., time step) (Pappenberger et al., 2005; Bush et al., 2022). This section is dedicated to the parameters used, i.e., the data source, specification, the uncertainty associated with each parameter, and the techniques used to reduce them.

2.1.1 Water Level and Discharge Data

One of the main data required to run the model is input hydrographs, upstream and downstream of the river channel. Table 2.1 lists all the streamflow and water level data collected from the US Geological Survey (USGS) website in the study area (Figure 2.2(b)). The table shows 15 stations but Lower Pearl River and its main branches, East Pearl, and West Pearl Rivers, have a total of nine USGS gage stations (Figure 2.2 (b): 1,2,8,10, 11, 12,13,14,15) and only 4 streamflow stations (Figure 2.2 (b): 1,4,9,13), with intermittent discharge data. Some stations have data intervals of 30 or 15 minutes, but sometimes the interval changes in between the data period. The table also shows the percentage of data missing at each station which was calculated considering the data at 1-hour intervals. The

accuracy of the gage height measurements is also listed in Table 1.1, collected from USGS website.

At some stations like Bogalusa, the data could be linearly interpolated to fill the gaps with no errors since the data exhibited little gaps between time intervals (few missing hours) and little to no tidal variation. But other stations like AB Wilson (station 8: 02492110) had months of data missing in a single year, mostly during high-flow seasons. Fortunately for this station, 97% of the water level data was present which was used to determine a rating curve for the station. The generated rating curve, a relationship between stream gage height and streamflow, filled in the missing discharge values based on the existing gage height data in that station. The data for NSTL (station 13: 02492620) is no longer available on the USGS website but it was collected from the USGS office directly, though the data was provisional. Among these stations, stream flow at stations Bogalusa (Station 1: 02489500) and Bogue Chitto (Station 4: 02492000), with 30-minute intervals, was used as upstream boundary conditions in the HEC-RAS model for flow in the Lower Pearl and Bogue Chitto respectively.

The flows of West and East Hobolochitto (stations 6: 02492360 & 7: 02492343 respectively) were combined to give the flow for Hobolochitto Creek which flows into East Pearl River as its tributary and at times, its primary source. The water level at CSX railroad station (station 15: 301141089320300) was used as a downstream boundary condition at the East Pearl outlet which captured the tidal forcings and wind set-up downstream. Both the data at Hobolochitto and CSX railroad had a 15-minute data interval. But there are no discharge or water level stations at the outlet at West Pearl and Little Lake. Normal depth as the outlet boundary condition could not capture the tidal fluctuation, so water level data

from the ADvanced CIRCulation (ADCIRC) model, was used as the downstream boundary condition (15-minute intervals) at both West Pearl and Little Lake. ADCIRC results of water levels from simulations conducted using the unstructured finite element mesh, SL15, containing a little over two million nodes, were used. The ADCIRC mesh had a higher resolution (~200 m) near the coast and coarser elements (~2000 m) at sea, which was forced by tide data from ADCIRC tidal database during the HEC-RAS run period and wind data from ECMWF's ERA5. SL15 is verified to predict tides well but ADCIRC results with tidal and wind data forcing was verified at the NOAA tides and current station Pilot Station East SW Pass shown in Figure 2.1. ADCIRC model results downstream of East Pearl had low bathymetry because of its proximity to the coast, so its observation data from USGS station CSX railroad was used instead as the downstream condition for East Pearl.

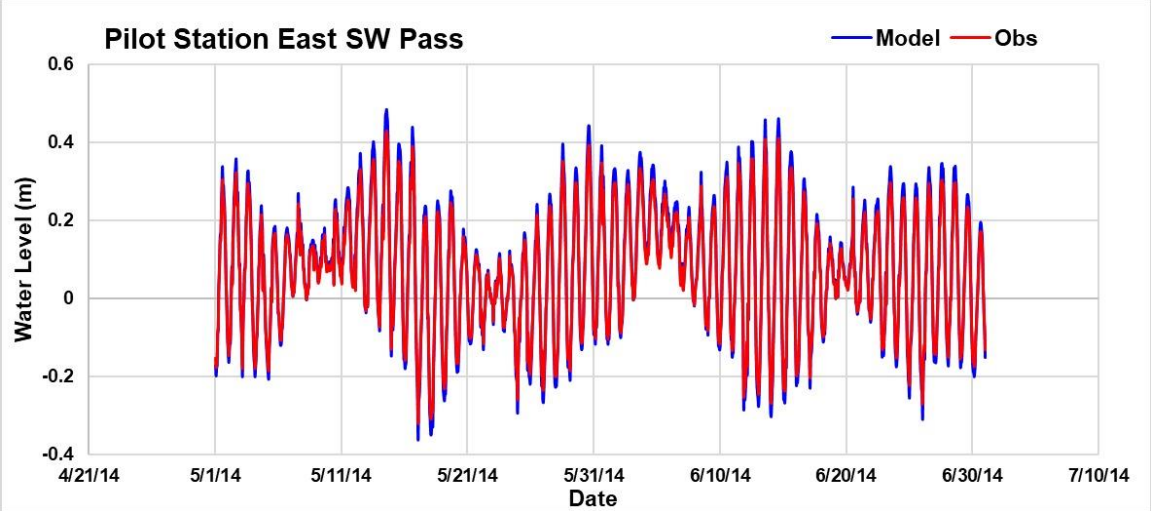

Figure 2.1 Comparison of water level between ADCIRC model (blue line) and observation (red line) at the NOAA tides and current station, Pilot Station East SW Pass for a period of 2 months.

Table 2.1 *: USGS water level and flow measuring stations in the study area, the period in which data is available, the hourly data missing from this available data as a percentage and the accuracy of the data.*

Double Asterix is for the station used as a boundary condition of the model and a single asterisk is for calibration and validation stations.

SL. no.	Station ID	Station Name	Data Type	Data Availability	% Missing Data	Accuracy (ft)
1	02489500	Pearl River near Bogalusa, LA**	Water level	2007-10-01 to 2023-05-06	0.79	1
			Discharge	1995-10-01 to 2023-05-06	1.26	Not available
2	02490193	Pearl River at Pools Bluff near Bogalusa, LA	Water level	2007-10-01 to 2023-05-07	4.34	0.16
3	02490200	Pearl River Navigation Canal Lock and Dam No. 3	Water level	2007-10-01 to 2023-05-07	1.85	0.2
4	02492000	Bogue Chitto River Near Bush, LA**	Water level	2007-10-01 to 2023-05-07	5.34	0.22
			Discharge	1995-10-06 to 2023-05-07	0.31	Not available
5	02492100	Pearl River Navigation Canal Lock and Dam No. 2	Water level	2007-10-01 to 2023-05-07	1.10	0.2
6	02492360	West Hobolochitto Creek NR Mcneill, MS**	Water level	2007-10-01 to 2023-05-07	2.38	0.1
			Discharge	1996-10-01 to 2023-05-07	1.17	Not available
7	02492343	East Hobolochitto Creek NR Caesar, MS**	Water level	2007-10-01 to 2023-05-07	3.07	0.1
			Discharge	1996-10-01 to 2023-05-07	2.04	Not available
8	02492110	East Pearl River AB Wilson SL At Walkiah Bluff, MS*	Water level	2007-10-01 to 2023-05-07	2.99	0.1
			Discharge	2007-10-01 to 2023-05-07	44.84	Not available
9	02492111	Wilson Slough Near Walkiah Bluff, MS*	Discharge	2007-10-01 to 2023-05-07	44.84	Not available
10	02492519	Pearl River Navigation Canal Lock and Dam No. 1	Water level	2007-10-01 to 2023-05-07	2.77	.01
11	02492511	East Pearl River at I-59 Near Nicholson, MS	Water level	2007-10-24 to present	46.76	0.16
12	02492600	Pearl River at Pearl River, LA*	Water level	2007-10-01 to 2023-05-07	1.34	0.07

Table 2.1 (Continued)

13	02492620	Pearl River At NSTL Station, MS*	Water level	2010-01-01 to 2022-06-21	3.44	Not available
			Discharge	2011-10-01 to 2022-06-21	1.7	0.16
14	02492700	Pearl River at I-10 Near Slidell, LA	Water level	2016-10-04 to 2023-05-07	0.76	0.11
15	301141089320300	East Pearl River at CSX Railroad NR Claiborne, MS**	Water level	2001-08-22 to 2023-05-07	2.98	0.01
			Discharge	2008-10-01 to 2009-09-30	6.61	Not available

2.1.2 Manning's n Estimation

Manning's n value represents the channel roughness and friction side slope in the bathymetry (Bhuyian & Kalyanapu, 2020). This parameter is usually modified to calibrate HEC-RAS in the river system (Bush et al., 2022). Initially, a single value of Manning's n was applied to the refined river mesh (0.025) and to the entire floodplain (0.06). But for distributed 2D model, the model accuracy may be increased by using distributed modeling parameters (Pappenberger et al., 2005). It essentially means that to obtain a better result, Manning's n would have to be considered along the whole topography, i.e., in the bathymetry and floodplain. Munoz et al., (2021) used a National Landcover Database to set a default roughness value depending on the land cover. Similarly, a land cover map was collected for the study area from NOAA, Office of Coastal Management DIGITAL COAST. 2016 NOAA C-CAP Regional land cover was used to identify land use in the area. The shapefile was loaded into HEC-RAS through RAS-Mapper, and the model converted it to a raster-based input parameter based on the nearest neighbor method (Munoz et al.,2021). HEC-RAS manual was used to set Manning's n value for each land use. The Manning's n value used and the area for each land use type is shown in Table 2.2. Figure 2.2 (a) shows the land cover map of the area retrieved from NOAA. Sands labeled

in the figure legend do not appear in the model domain, so no area had this type of Manning's n value assigned to it. The Manning's n in the river was found using different values for a month of the wet season and a month of the dry season described in Chapter 3.

Table 2.2 *: The area type based on land use maps of the study area, the area each area type covers, and Manning's n value assigned to it.*

Area Type	**Area (km^2)**	**Manning's n**
Urban Area	128.84	0.12
Roads	360.80	0.06
Bare Land	996.55	0.05
Dense Forest	3122.47	0.10
Mixed Forest	1650.67	0.08
Grasslands	364.33	0.07
Moist soil	101.54	0.04
Marshland	714.89	0.04
Floodplain	49.55	0.04
Waterbody	2416.87	0.03

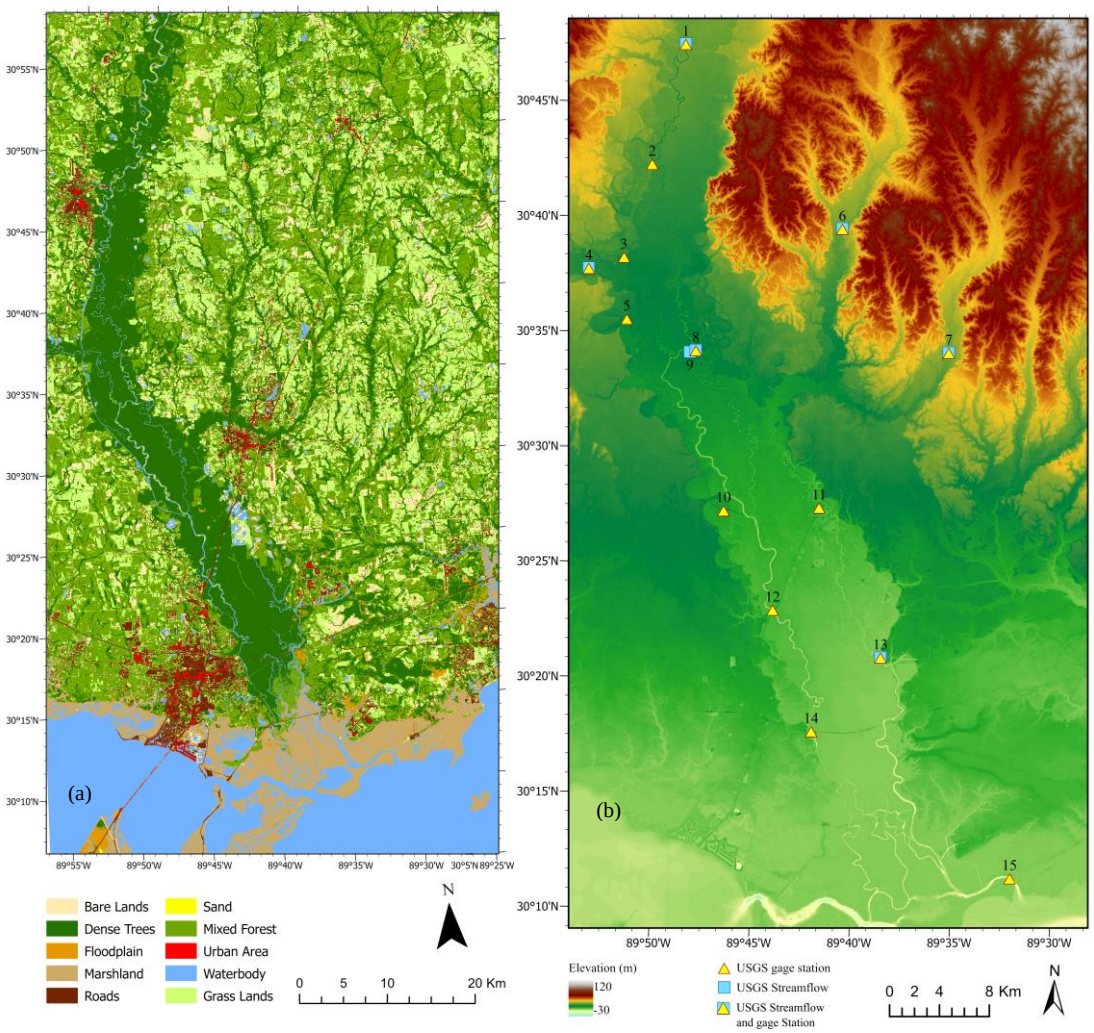

Figure 2.2 *:(a) The Land Use map of the Lower Pearl River Study area; (b) NOAA DEM of the Lower Pearl River showing the river branches and the USGS water level station (yellow triangle) and discharge data stations (blue square)*

2.1.3 Digital Elevation Model (DEM)

The Digital Elevation Model or DEM is a raster image containing the height and location of an area. It sets the flow path by introducing 3D depth planes for water to flow within the river (bathymetry) and floodplain (topography). One of the main factors affecting the accuracy of the 2D flow is the resolution of the DEM, i.e., the floodplain and the river channels (Horritt and Bates, 2002; Altinakar et al., 2010; Munoz et al., 2021).

Initially, the bathymetry data was taken from the DEM from Coastal Topographic Lidar data provided by the National Oceanic and Atmospheric Administration (NOAA) of 1/9th Arc (~ 3m) resolution, Continuously Updated Digital Elevation Model (CUDEM) - Ninth Arc-Second Resolution Bathymetric-Topographic Tiles, the highest resolution publicly available at the time and covering the entire study area. However, as mentioned earlier, the DEM was constructed using LiDAR data collected over several years (2005 to 2014), only the bathymetric measurement data south of the I-10 highway was collected in 2014 and stitched together with the data collected during 2005. The model was initially run with the DEM downloaded as is, but water flowed into the floodplain rather than the river itself due to several blockages along the river pathway as shown in Figure 2.3. Upon further investigation, it was found that the DEM did not contain river bathymetry.

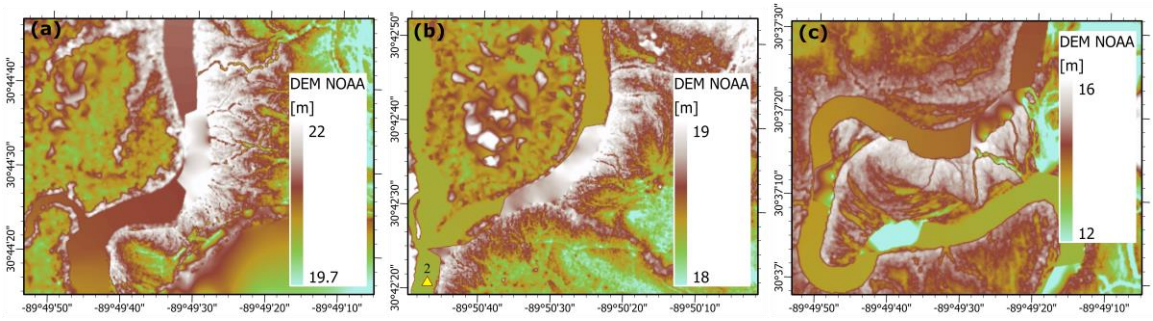

Figure 2.3 *: Some of the blockages along the Lower Pearl River caused disruption in the natural flow through the river. (a) is upstream (b) is in the middle (c) is near downstream of Lower Pearl River.*

A survey conducted in 2014, and once again in 2019, had bathymetry of some of the rivers and the point elevations obtained. The survey had cross-section data from Lower Pearl, Bogue Chitto, West Pearl, East Pearl, and Old Pearl. But on importing the data into Google Earth, it did not cover the whole river as shown in Figure 2.4. Significant portions of the river bathymetry were missing which the DEM could not capture as well.

Furthermore, the bathymetry points were no longer inside the river of the recent Google Earth imagery (Figure 2.4 (a), (b) and (c)). The data aligned when using 2014 imagery, suggesting the riverbank had shifted in the five years since 2014. The implication was that some of these survey data were unusable, further prompting the construction of a synthetic bathymetry to represent the streamflow in the area, the results of which will be explored further in chapter 3.

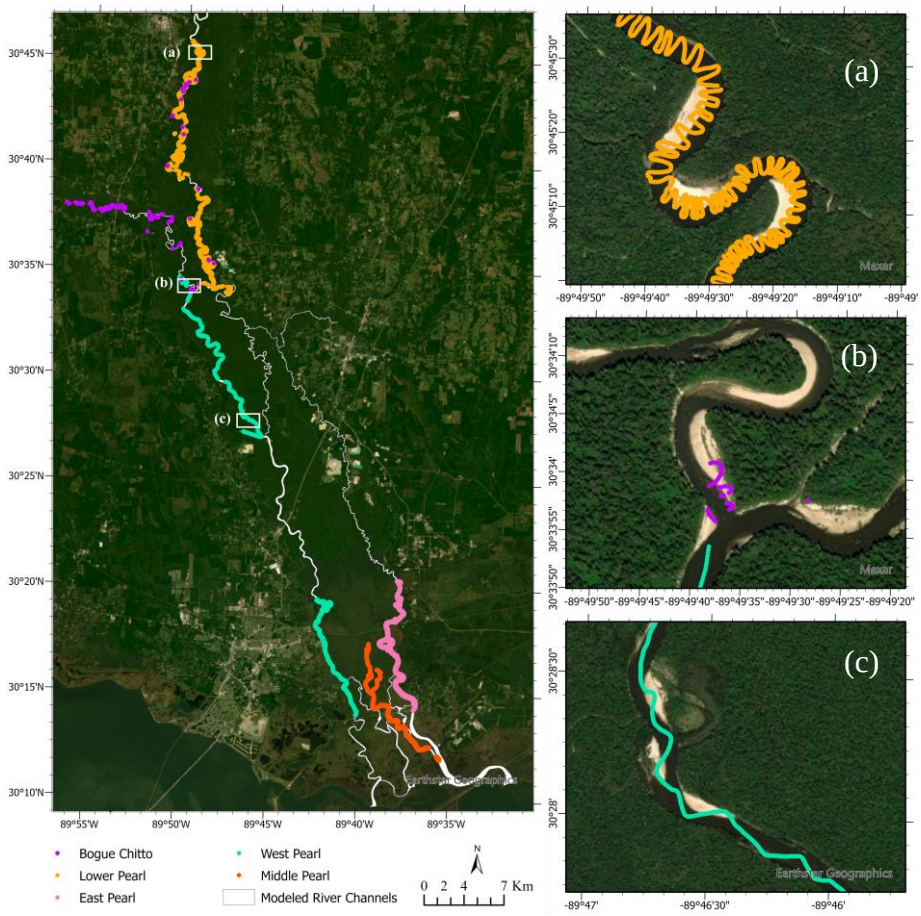

Figure 2.4 *: The satellite imagery of survey bathymetry data (colored dots) of rivers in the Lower Pearl River system. The right shows the zoomed area for locations (a) at the Lower Pearl River, (b) downstream of Bogue Chitto, and (c) at West Pearl.*

Figure 2.4 shows some of the mismatches between surveyed bathymetry collected in 2014 and the recent Google Earth imagery of 2019. Figure 2.4 (a) is zoomed portion

upstream of Lower Pearl River, showing the shift in collected and observed river system, one of many locations. Figure 2.4 (b) shows the downstream of Bogue Chitto River while 2.4 (c) shows the middle portion of West Pearl. The location of the zoomed portions is shown in the larger map on the right in Figure 2.4. The shifts in surveyed bathymetry and river flow suggest there have been a riverbank shift, but are they significant enough to be considered? Did they change the river path too much? The following section will discuss these questions.

Bathymetric data were also collected in a survey by USM's Hydrographic Science students at Quay wall (Figure 2.5), a location where ships and boats can berth, near Stennis Space Station in East Pearl. The data was provided as point elevation with datum with respect to mean low water level during November of 2021 (Figure 2.5 (b)). Recent bathymetry data was collected at a larger section of the East Pearl near Stennis Space Center (Figure 2.5 (a)) during May 2023. A raster was generated from the point elevation bathymetry data of 2021 using Inverse Distance Method (IDW) in Arc GIS Pro, the exact location of the data in the study area is also shown in the extension map, but the 2023 data was in raster form. Since the data from 2023 was very recent, the synthetic bathymetry could only be compared with the 2021 bathymetric data. Figure 2.5 (b) shows the thalweg depth of this small portion of East Pearl varies between 3-7 m; a depth cap assumption made during the formation of synthetic bathymetry to be discussed later. The figure also shows that the river shows significant meandering, and the thalweg is skewed completely to one side of the bank at the highest bends. This data was crucial in re-evaluating the synthetic bathymetric equation; from an equation that has thalweg at the center, to an equation where thalweg deepens and shifts according to the meander bend. The data in

Figure 2.5 (b) was used to compare and generate synthetic bathymetry. More on the method is discussed in Chapter 2.1.3.2 and the comparison of the data is done in Chapter 3.2.

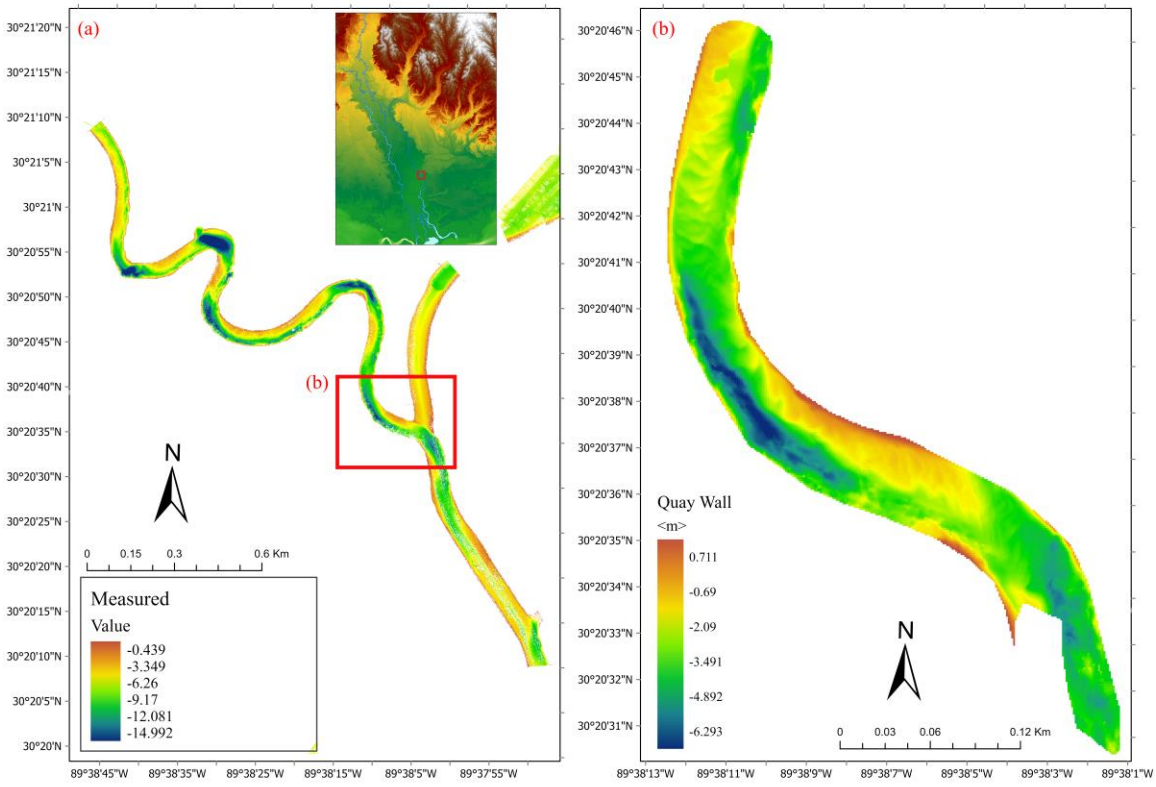

Figure 2.5 *: The Digital elevation of bathymetric data collected for East Pearl River (a) near the Quay Wall in 2023 and (b) at Quay Wall near Stennis Space Center in 2021.*

2.1.3.1 Change to Riverbanks

The banks of the river were digitized using the latest Google Earth Pro satellite imagery from 2019. When the digitized riverbanks were compared to the riverbanks in the NOAA DEM, the riverbanks were observed to have shifted significantly. Since the data was taken, the river has meandered significantly at several locations changing the channels' travel time and capacity. Figure 2.6 shows the shifts in the bank lines from the year the data was collected for the NOAA DEM (2005) to the year 2019, google earth imagery. These banks were digitized manually, the blue polygons are the digitized river from the

DEM (old), the pink polygons are the digitized banks from the google earth image of 2019 (current) and the green polygon is the intersection (overlap) between the two, which shows the area of the river which remained unchanged (common) found using the intersect tool of ArcGIS Pro. The magnitude of the area change was found by subtracting the old area from the common area to get the total depositional area. Similarly, the current area was subtracted from the common area for the erosional area. Differencing the depositional and erosional areas provided the net change in river areas, an indicator of riverbank changes. This was found for each of the major river branches and the values are shown in Table 3.

Table 2.3 shows the extent to which the rivers shifted from their last record which was in 2005 for the river section above Highway 90 and 2014 for sections below Highway 90. The table shows the erosion, and accretion of the river and the net change in the river sediment for the 14 years period until 2019. For Bogue Chitto, the erosion is highest, where the mouth of the river itself changed after 2017, possibly after heavy rainfall caused by Hurricane Harvey in 2017. A more efficient way to update the bank would be by using the Normalized Difference Vegetation Index (NDVI), as done previously by Bhuyian & Kalyanapu (2020). But cloud cover and the width of some of the tributaries (<= 30 m) would make that difficult.

Table 2.3 *: River shifts from the last recorded data (2005) to the current year (2019).*

River Name	**Total erosional area (km^2)**	**Total depositional area (km^2)**	**Net change (km^2)**
Lower Pearl River	0.804	0.564	0.240, deposition
East Pearl River	1.485	1.509	0.024, deposition
West Pearl River	1.612	1.927	0.315, deposition
Bogue Chitto	0.260	0.456	0.196, deposition

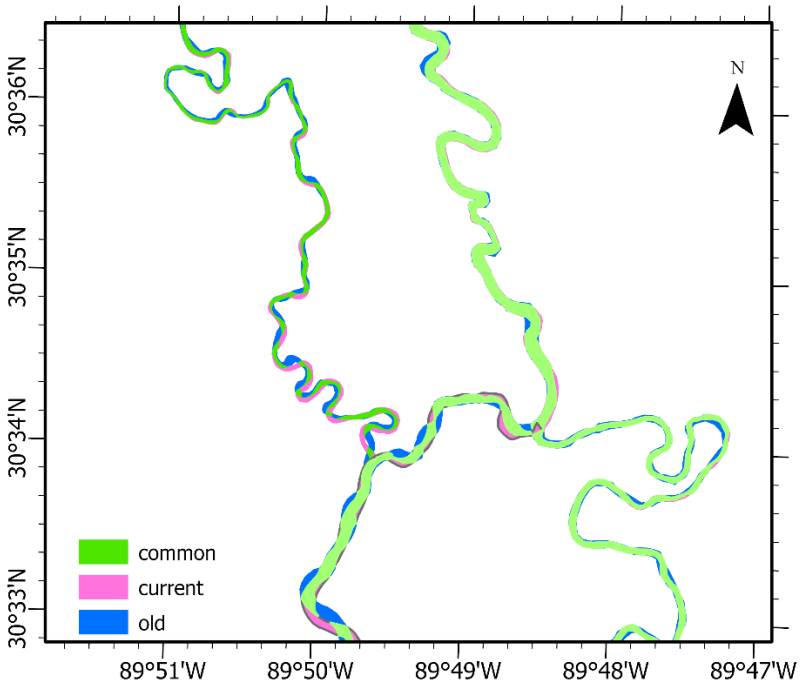

Figure 2.6 *: The riverbanks change from 2005 when the DEM data was collected to 2019.*

2.1.3.2 Implementation of Synthetic Bathymetry

Blockages within the river were observed in several locations in the Lower Pearl DEM before and after its bifurcation into the East and West Pearl, causing the flow to spill into the floodplain before moving downstream the river. Not only this but the depth of the rivers within the DEM was so small that it meant the LiDAR could not detect the full bathymetry, rather it reflected only the water surface in most locations. Figure 2.3 (b) shows the location of the first blockage which was discovered in the initial model simulation due to unexpected flooding of the river on the surrounding floodplain. The cross-section of the measurement location of Figure 2.3 (a) is shown later in Figure 2.9 (b) revealing that the depth of the river was too small as shown by the blue line representing the bathymetry from NOAA DEM. The initial plan was to set up a simple synthetic parabolic bathymetry, owing to the silty nature of the river, to account for the depth issue.

The steps used from the generation of synthetic bathymetry to the running HEC-RAS are shown in the flow chart in Figure 2.7. The following steps were followed to generate a DEM with synthetic bathymetry.

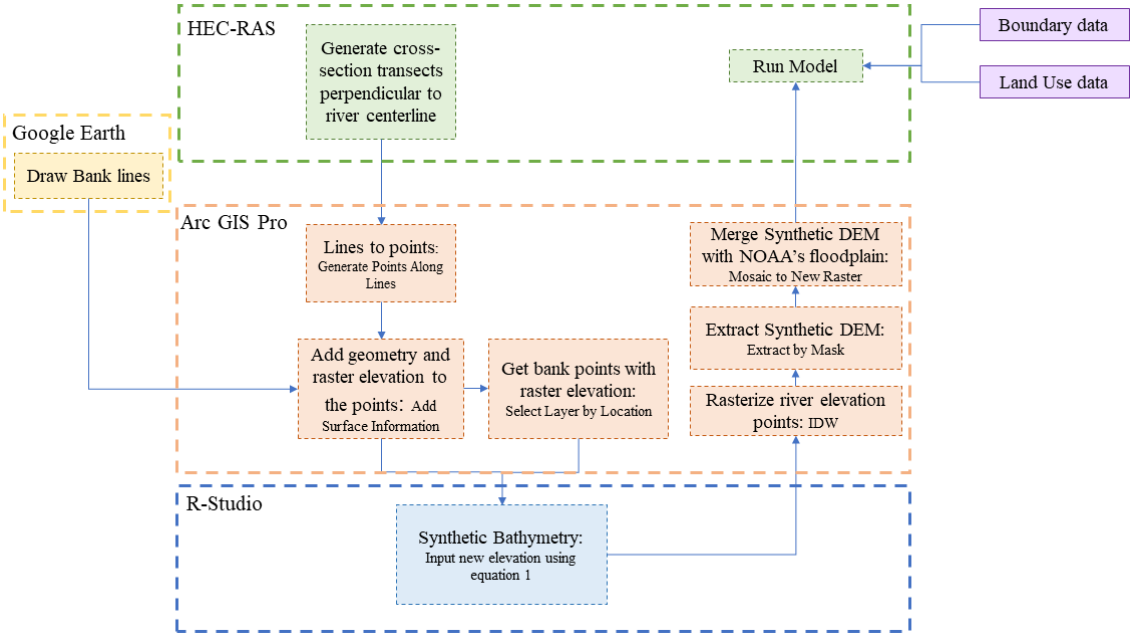

Figure 2.7 *: Flow Chart showing the sequence of methodology to run the create the synthetic DEM and run HEC-RAS.*

1. Cross-section transects were generated perpendicular to the river centerline. The transects were generated in HEC-RAS and were made to cross the riverbanks. (See Figures 2.10 and 2.11 (b))

2. The transect lines were converted to points in Arc GIS Pro using the tool 'Generate Points Along Lines'.

3. The x and y coordinates of the points were generated in Arc GIS Pro and raster elevation from NOAA DEM was extracted at each of the points using the tool 'Add Surface Information'.

4. The left and right bank drawn in Google Earth is imported into GIS and converted to points by the tool “Select Layer by Location”.

5. The R-code is run containing the synthetic bathymetry equation.

6. The new bathymetry points are imported in Arc GIS Pro and converted to raster by Inverse Depth Weighted (IDW) interpolation method.

7. The specific portion of the river is cut out using “Extract by Mask” and merged with the existing NOAA DEM.

8. The new DEM, input boundary data, and floodplain roughness information from Land use data are used to run HEC-RAS.

The points generated in step 5 were 3 m apart and the width of a cross-section was calculated from the bank which was at a higher elevation. The initial synthetic bathymetry was dependent on the channel width, the slope of the riverbank, particularly the bank which was at a higher elevation, and the minimum and maximum depth of the river. The elevation was calculated starting from the higher bank (refer to Figure 2.10) using Equation 1, and Equation 2 was used for the elevation of the lower bank. The width was recalculated to be zero in the middle of the x-section, a positive value from the higher bank and a negative value from the lower bank using equation 3. The terms α_l and C was used to ensure the elevation reaches the bank elevation.

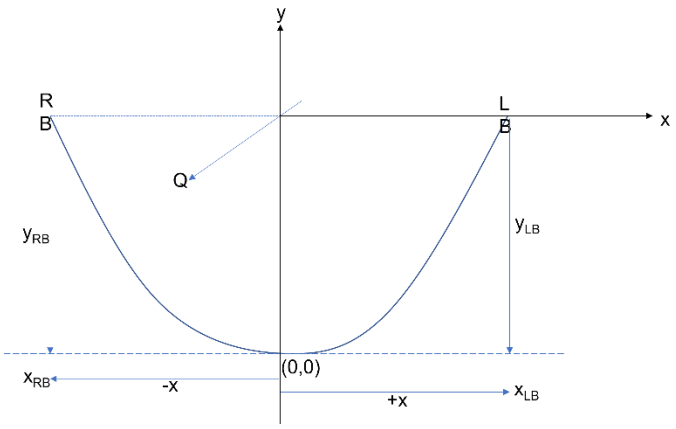

Figure 2.8 *: The design of parabolic synthetic cross-section and its dimension terms*

Equation 1

$$y_{syn,h} = \alpha * \left(x_{syn}\right)^2 + C$$

Equation 2

$$y_{syn,l} = \alpha_l * \left(x_{syn}\right)^2 + C$$

Equation 3

$$x_{syn} = 0.5 * (total\ crosssection\ width) - x$$

Where, *x*= width of the cross-section measured from the left bank.

α = 0.011, a constant after calibration

$y_{syn,h}$= depth of the channel at the higher bank for x_{syn}>0,

$y_{syn,l}$ = depth of the channel at the higher bank for x_{syn}<0,

Equation 4

$$C = y_{higher\ bank} * \alpha * \left(x_{left\ bank}\right)^2$$

Equation 5

$$\alpha_l = \frac{y_{lower\ bank} - C}{(x_{lower\ bank})^2}$$

Pearl is a very silty river transporting large volumes of silt into the Sound (Thorne et al., 2008) and is morphologically active. Several attempts have been made to develop a synthetic bathymetry representative of such morphologically active riverine system to make up this data gap which are parabolic or triangular in nature (Williams et al., 2017; Bhuyian et al., 2019). But some formulas required a water level station upstream of the river to be fitted or had the condition that there would be no lateral flow or significant tributary. The Lower Pearl had significant flow, tributaries, and no water level station on some major portions of East Pearl, hence they could not be used. This simple parabolic cross-section representing silty rivers does not have such conditions. This cross-section equation derived from the basic parabolic equation depended on the cross-section width and the slope of the banks. Because the cross-section is dependent on channel width, the river had too deep channels with depths of 12-20 m at some wider sections of the river, and the channels were very shallow with depths of 1-2 m at narrower sections. A survey was done in November which showed minimum and maximum depth varied between 3 to 7 m, so a depth cap was used to limit the cross-sectional depth between 3-7 m. Equation 6 was used if depth was lower than 3 m and Equation 7 was used if the depth was higher than 7 m. The rest of the parameters were re-calculated to generate the synthetic depth of the river after repeating Equations 1, 2, 4, and 5.

Equation 6

$$\alpha = \alpha_{min} = \frac{3}{\left(x_{higher\ bank}\right)^2}$$

Equation 7

$$\alpha = \alpha_{min} = \frac{7}{\left(x_{higher\ bank}\right)^2}$$

The formulation of x_{syn} made sure the cross-section always had a centerline at mid-width, the cross-section was divided into the left and right sections and the equation was initiated from both banks, meeting at the center where x_{syn} is 0. This equation generated a parabolic cross-section, deepening the river and removing the blockages as shown in Figure 2.8. The cross-sections shown are at Lower Pearl before bifurcation (Figures 2.9 (a), (b)) and after bifurcation (Figure 2.9 (c)), where the blue line represents the cross-section from unaltered NOAA DEM while the red line shows the cross-section after implementing the synthetic bathymetry. The cross-section at Figure 2.9 (b) is for the same location as in Figure 2.3 (b), showing the blockage, its removal, and deepening of the river.

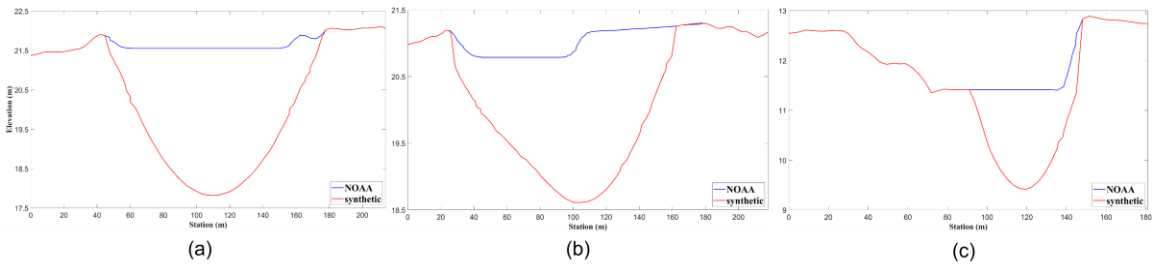

Figure 2.9 *: The cross-sections in the NOAA DEM before and after synthetic bathymetry before the bifurcation (a) at a blockage location (b), and at East Pearl 1km after bifurcation (c).*

USM hydrography department collected side scan sonar data for East Pearl River at the Quay Wall, near Stennis Space Station, in a field survey (Figure 2.5). The synthetic bathymetry equation was verified using the data. The bathymetric data suggested significant meandering in the river, skewing the thalweg nearer to the outer bank of the river bend. The meandering effect contradicted the synthetic parabolic shape, which had its deepest part at the channel center. So, the synthetic bathymetry equation had to be re-evaluated, now considering the river bend. The meandering effect was brought by modifying the x_{syn} term using Equation 8, where the centerline would shift according to the river bend.

Equation 8

$$x_{syn} = [\{0.5 - (d_L - d_R) * 0.65\} * total\ crosssection\ width] - x$$

In this equation d_L and d_R is the distance between consecutive left and right bank stations shown in Figure 12. When the river bends to the right as shown in the figure, i.e., if $d_L < d_R$, the center point (zero) is closer to the right bank and the opposite is true when the river bends towards the left. The cross-section was divided into left and right sections this time as well, but unevenly depending on the river bend. The synthetic bathymetry equation was applied again but this time from the bank with the higher width section, i.e., emphasis was given to the bank with the higher width from the center point (zero). The value of α was modified to be dynamic by considering the river slope and cross-sectional width and calculated with equation 9.

Equation 9

$$\alpha = \frac{max\ (x_{LB}, x_{RB})}{total\ width\ of\ \ xsec} * (slope)^{0.5} * (total\ width\ of\ the\ xsec)^{\frac{1}{3}}$$

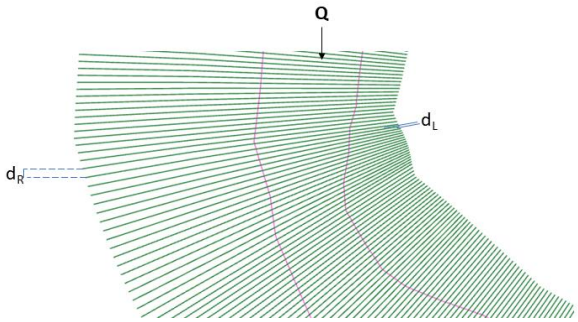

Figure 2.10 *: An example river section showing the river bending towards the right. The green lines show cross-section transects and the purple lines show the riverbanks.*

Again, depth was calculated from two sides of the riverbank, meeting at the deepest part of the channel. This modified synthetic bathymetric equation depends on the bank location (*x*, *y*), a DEM, and the water level slope of the channel. The bank elevation was collected from DEM (z). The equations 1, 2, 4, 5, remains the same to calculate $y_{syn,h}$, $y_{syn,l}$, C and α_l with modified α value calculated using Equation 9 and the calculation starting from the bank with the higher width section. Again, when the depth is smaller than 3 or greater than 7, the value of α is changed to Equations 6 and 7 to force the depth to be between these two depth ranges as explained above. The effect of meandering the cross-section is found by running the model with both the meandering and non-meandering DEM and the discharge and water level hydrographs were plotted (appendix E) to see an improvement in modeling the water level with the meandering effect. Figure 2.11 shows the raster section of the blockage shown in Figure 2.9 (b) before and after implementing synthetic river bathymetry in Figure 2.11 (a) and 2.11 (c) respectively. Figure 2.11 (b) shows the cross-section transects imported from HEC-RAS. The cross-sections were fitted into the river perpendicular to the channel centerline and at 3 m intervals. The shift of the thalweg from the centerline as the channel gets closer to one bank can be seen in Figure 2.11 (c).

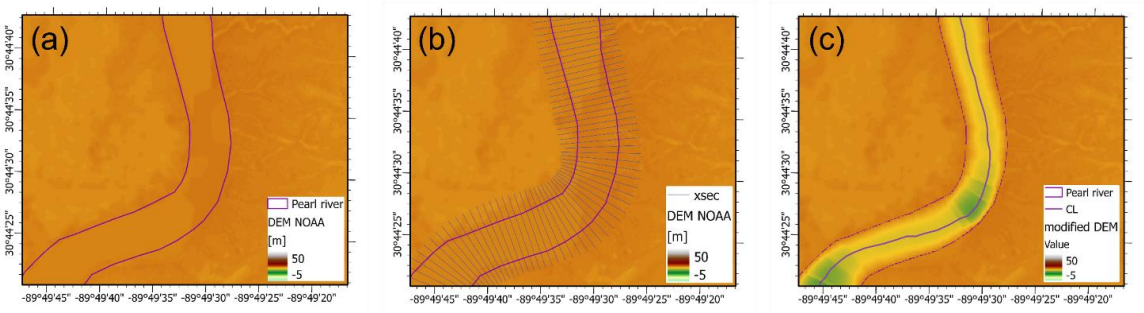

Figure 2.11 *: The LPR upstream of bifurcation (a) The initial NOAA DEM with the channel blockage highlighted with the black box, (b) The cross-section transects at every 3 m where the synthetic bathymetry was implemented, (c) The DEM after stitching the synthetic bathymetry and black line showing the skewed thalweg of the channel.*

The synthetic bathymetry was compared with the surveyed raster data at the Quay wall collected in 2021. The cross-sections shown in Figure 2.12 show the synthetic meandering cross-section in red (synthetic_m), measured bathymetry as black, synthetic non-meandering (synthetic_nm) in yellow, and the bathymetry from NOAA DEM as blue. The figure indicates that both the depth and the location of the deepest location of the synthetic bathymetry get closer to the measured values once the meandering effects are included by shifting the thalweg closer to a bank and by deepening the channel. Lilly pads near the riverbanks prohibited the surveyed data from covering the depth till the riverbank, so straight lines in the observed cross-section (black line) is only interpolated data and there is a mismatch in bank elevation. More cross-section comparisons are shown in the Results chapter.

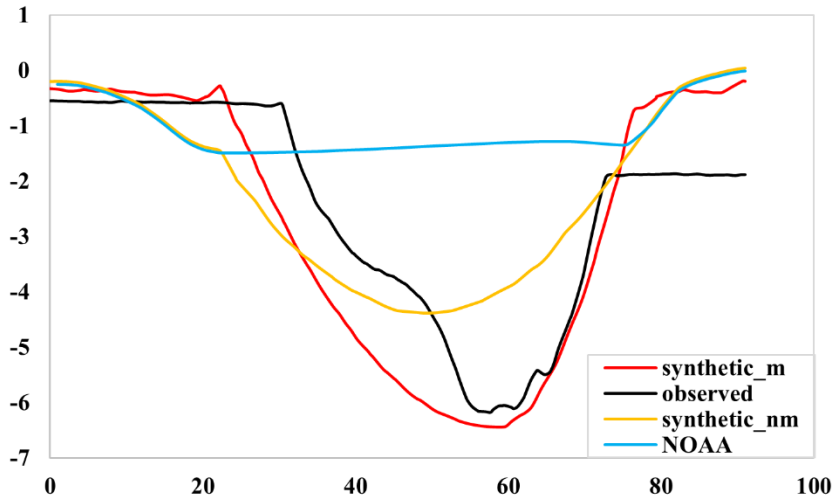

Figure 2.12 *: The cross-sections in the NOAA DEM before and after synthetic bathymetry before the bifurcation (a) at a blockage location (b, and at east Pearl 1km after bifurcation.*

2.2 HEC-RAS Grid Generation

HEC-RAS has multiple solver options: the diffusion wave equation, its fastest and most stable solver, the shallow water equation with a Eulerian-Lagrangian (SWE-ELM) approach to solve advection as it incorporates full momentum equations, and the Shallow water equation solver with a Eulerian approach (SWE-EM) which is its latest equation update, the slowest and more conservative equation causing more instabilities. In this study, SWE-ELM was used to conserve the momentum at the outflow boundary. The model is running on a variable resolution mesh created in HEC-RAS with the main channels refined to have 10 m cells with the highest cell size being 100 m^2 size and the lowest being 18 m^2, at bends and transitions between the river and floodplain, while it is 80 m cells in the floodplain as shown in Figure 2.13 with total number of 865,000 cells. Initially, the model was run with a finer mesh having approximately 2.5 million cells, with resolutions of 6 m within the river, 30 m in the floodplain, and 12 m in between. But this

grid was computationally too expensive, being at least 4 times slower than the current mesh. But for comparison, the model hydrograph results of both the coarse and fine mesh were computed and compared. The hydrographs suggest that the fine mesh and coarse mesh provide identical results, hence the coarse more computationally efficient mesh was selected. Figure 2.13, as a whole, is a map of the model domain showing the refined area in purple polygon and the boundary conditions in red lines. Equations are solved in each cell once boundary conditions are imposed at each end of the channel mesh.

The river flow is used as the upstream boundary at the top of the Lower Pearl River at Bogalusa station, Bogue Chitto and Hobolochitto Station shown by the downward arrows in Figure 2.13 while the downstream conditions are the tidal water levels at the West and East Pearl Rivers along with a third boundary in the Little Lake shown by the upward arrows. The red box shows an example of refinement within the channels and the yellow box shows the Middle Pearl which were not captured by the original NOAA DEM but were captured after using synthetic bathymetry. The USGS water level station 301141089320300 at the CSX railroad near Claiborne is used as the downstream condition for East Pearl. But for West Pearl River, the nearest water level station is approximately 26 km upstream of the river end fully missing the tidal fluctuations, therefore water level fluctuations created by ADCIRC were used at both West Pearl and Little Lake boundaries. The water level fluctuations at West Pearl and Little Lake are different from East Pearl; East Pearl is exposed to Lake Borgne directly has a higher water level whereas West Pearl flows into the Rigolets and has a lower water level. After the model is set to run, it solves the flow equations at each mesh cell using the data provided.

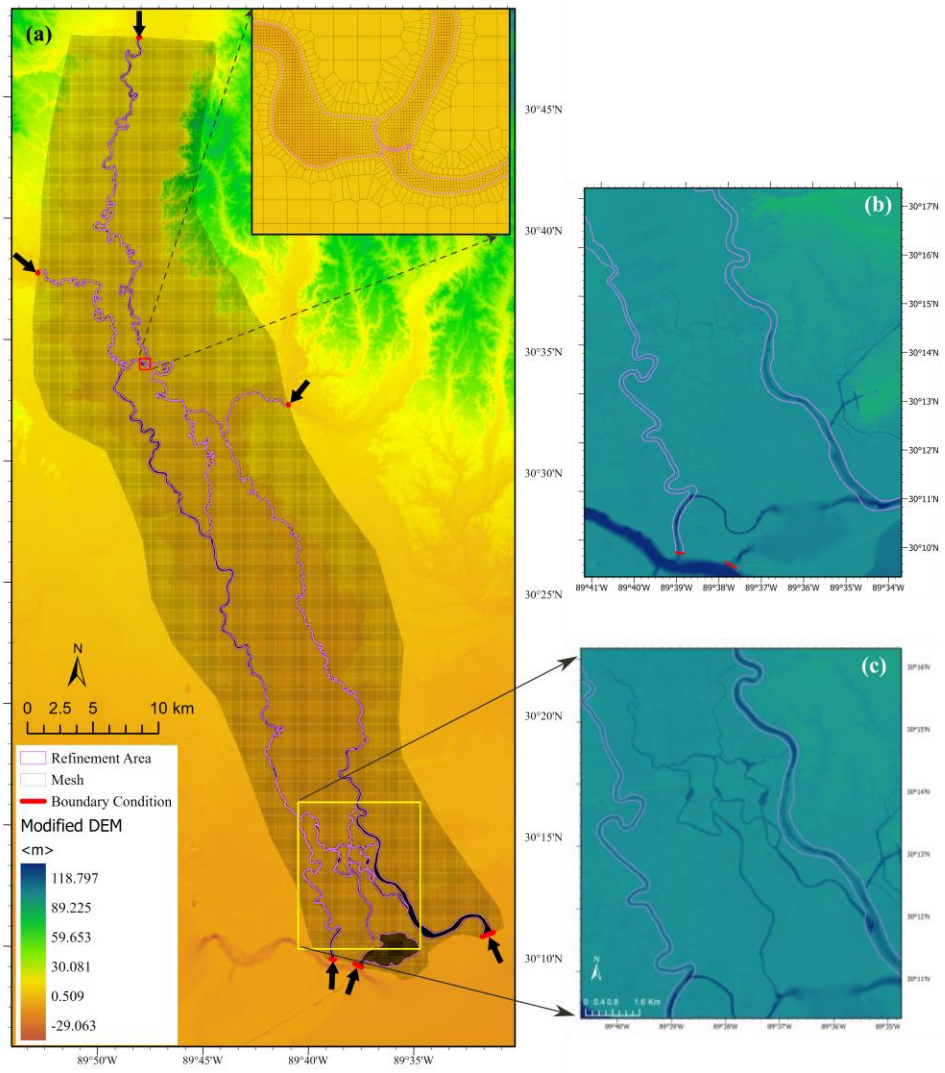

Figure 2.13 *: Map showing (a) the computational grid in the zoomed bifurcation area (inset at top right), location of boundaries, refinement area, (b) the Middle Pearl channels before adding synthetic bathymetry and (c) the Middle Pearl channels after adding synthetic bathymetry.*

2.3 Model Performance Metrics

To check the ability of the model to reproduce measured data, the model must go through a calibration and validation process (Williams & Esteves, 2017). In calibration, the model results are tested for a specific period, where model parameters such as the friction co-efficient are adjusted until the model results match known values of flow at a location

for a given duration, preferably 1 to 2 years (McAlpin et al., 2019, Jones et al.,2018). The model must be verified if the changed parameters are correctly chosen. The adjusted parameters must be tested again to check their accuracy with another set of known values for another 1 or 2 years, at a different period and at the same location (McAlpin et al., 2019, Jones et al.,2018, Williams & Esteves, 2017), i.e., the model must be validated. The calibration and validation are done at three of the USGS stations shown in Table 1 with an asterisk: USGS station 02492110 (AB Wilson, station 8 of Figure 2.2 (b)) for the Lower Pearl River, USGS station 02492620 (NSTL station, station 13 of Figure 2.2 (b)) for East Pearl and USGS station 02492600 (Pearl River at Pearl River station, station 14 at figure 1.1) for West Pearl. Since there are no discharge stations at West Pearl, only a water level comparison will be made at the Pearl River at Pearl River station.

The ability of the model to be properly calibrated and validated is tested by utilizing statistical parameters. The parameters used are correlation coefficient (R2), Root Mean Standard Deviation Ratio (RSR), and Nash-Sutcliffe efficiency (NSE), which measures the overall fit of the modeled hydrograph (strength and direction) with respect to the observed hydrograph in a linear relationship (Munoz et al.,2021; Jain and Sudheer, 2008, Moriasi et al., 2007). Nash-Sutcliffe efficiency (NSE) evaluates how the mean square error of the model compares with the variance of the observed flow (Santos et al.,2018), to test the overall fit of the modeled and observed flow (Moriasi et al., 2007). The model performance will also be tested by using the ratio of root-mean-square error to standard deviation of observed flows (RSR) shown in Equation 12, which standardizes RMSE by comparing the model's error with the standard deviation of the observation, being a better indicator of the model performance than RMSE (Wijayarathne and Coulibaly, 2020). The NSE and R2 are

frequently used to evaluate the overall fit of hydrographs (Jain and Sudheer, 2008, Moriasi et al., 2007). Percent bias or PBIAS shown in equation 13 is used to determine the overall tendency of the model to over or under-estimate the observation (Gupta et al., 1999). PBIAS zero suggests perfect agreement between model and simulation, a positive value indicating model underestimation and over-estimation for negative values.

The Overall skill of the model was judged by two parameters: Willmott Skill or Model Skill (MS) and Kling-Gupta Efficiency (KGE). Wilmott Skill shown in equation 14 (Willmott 1981) is a popular metric used if the model setup is sufficient to simulate the process observed. The Skill score ranges from 0 to 1 where 0 indicates poor performance, such that there is no link between the model and observed, and 1 indicates the model and observed match perfectly (Munoz et al.,2021; Cambazoglu & Haas, 2011). KGE (Gupta et al., 2009) shown in Equation 15, is also used quite frequently in recent times to address model performance (Lahmers et al., 2021; Castaneda-Gonzalez et at., 2018; Gelati et al., 2018). KGE breaks down NSE into its components and assesses a model's performance by comparing the model's linear correlation with the model, standard deviation, and mean of the model with that of observation. It varies between 0 to 1 where 1 indicates perfect agreement between the model and observed while 0 indicates poor agreement. Although some authors consider negative values of KGE to be unsatisfactory (Schönfelder et al., 2017), and this was also shown mathematically by Knoben et al. (2019), Rogelis et al. (2016) considered KGE < 0.5 as unsatisfactory, and this will be considered in this study as well.

Table 2.4 shows the range of performance parameter values defining model performance as collected from several studies. Knoben et al. (2019) cautioned on using ad-

hoc values of these performance parameters to assess a model, but for this study, these ranges are considered soft guidelines. The Manning's n value is tuned so that the model performance is satisfactory at the calibration station based on the performance metrics, and the model is considered calibrated if the improvement is not observed upon further modification of Manning's n (Tetra Tech and Allen Engineering & Science, 2018).

Equation 10

$$R^2 = \frac{\sum_{i=1}^{n}(M_i - M_i^{mean}) * (O_i - O_i^{mean})^2}{\sum_{i=1}^{n}(M_i - M_i^{mean})^2 * \sum_{i=1}^{n}(O_i - O_i^{mean})^2}$$

Equation 11

$$RSR = \frac{RMSE}{STDEV_{obs}} = \frac{\sqrt{\sum_{i=1}^{n}(M_i - O_i)^2}}{\sqrt{\sum_{i=1}^{n}(O_i - O_i^{mean})^2}}$$

Equation 12

$$NSE = 1 - [\frac{\sum_{i=1}^{n}(O_i - M_i)^2}{\sum_{i=1}^{n}(O_i - O_i^{mean})^2}]$$

Equation 13

$$PBIAS = \frac{\sum_{i=1}^{n}(O_i - M_i)}{\sum_{i=1}^{n} O_i}$$

Equation 14

$$MS = 1 - \frac{\sum_{i=1}^{n}(M_i - O_i)^2}{\sum_{i=1}^{n}(|M_i - O_i^{mean}| + |O_i - O_i^{mean}|)^2}$$

Equation 15

$$KGE = 1 - \sqrt{(r-1)^2 + \left(\frac{\sigma_{sim}}{\sigma_{obs}} - 1\right)^2 + \left(\frac{\mu_{sim}}{\mu_{obs}} - 1\right)^2}$$

Where, M_i represent Modeled parameter at specific time and O_i represents the observed parameter at the time, i, through equations 10 to 14. In Equation 15, r is the linear correlation between model and observation, σ_{sim} and σ_{obs} are the standard deviation of model and observation respectively while μ_{sim} and μ_{obs} are the mean of model and observation respectively.

Table 2.4 *: Table showing the Range of each performance parameter classifying the model performance (collected from Salis et al.,2019; Pan et al.,2013; Cho et al.,2013; Moriasi et al.,2007).*

Performance Rating	**RSR**	**NSE**	**PBIAS (%)**
very good	0.00 < RSR < 0.50	0.75 < NSE < 1.00	PBIAS < ±10
Good	0.50 < RSR < 0.60	0.65 < NSE < 0.75	±10 < PBIAS < ±15
Satisfactory	0.60 < RSR < 0.70	0.50 < NSE < 0.65	±15 < PBIAS < ±25
Unsatisfactory	RSR > 0.70	NSE < 0.50	PBIAS > ±25

CHAPTER III – RESULTS

Incorporating the synthetic bathymetry into the DEM and updating the banks showed a marked improvement in the flooding patterns as seen in Figure 3.1 for the Lower Pearl River, which shows the initial modeling attempt using synthetic non-meandering bathymetry. When the model was run with the original NOAA DEM, the water would spill out of the river because of unrealistically low river depths and flow into the floodplain (Figure 3.1 (a)) even at low flow conditions (when flow in Bogalusa is 60 m3/s or ~2118 ft3/s). But with synthetic bathymetry, the flow is contained within the river (Figure 3.1 (b)). Full blockages in the river also caused the flow to shift into the floodplain, avoiding the river (Figure 3.1 (c), this was also prevented by the implementation of synthetic bathymetry (Figure 3.1 (d)). But there are several marshes and lakes between the rivers that stay flooded, and the synthetic bathymetry is not so deep as to restrict the formation of the wet channels seen in the spatial water level map in Figure 3.1 (e) when run with NOAA DEM and Figure 3.1 (f) when run with the modified DEM. The synthetic bathymetry was modified to account for channel meandering afterward and this chapter will show some comparison plots between the synthetic bathymetry and the recently observed bathymetry from 2021.

The model with synthetic river bathymetry and riverbank updates was initially run at steady state conditions at low, medium, and high flow conditions to check how the inflow and outflow from the East Pearl and West Pearl Rivers vary in such different scenarios. Once the integration of the synthetic bathymetry with meandering effects into the DEM is fully completed, at first, the model was calibrated varying the Manning's n value in the various river channels.

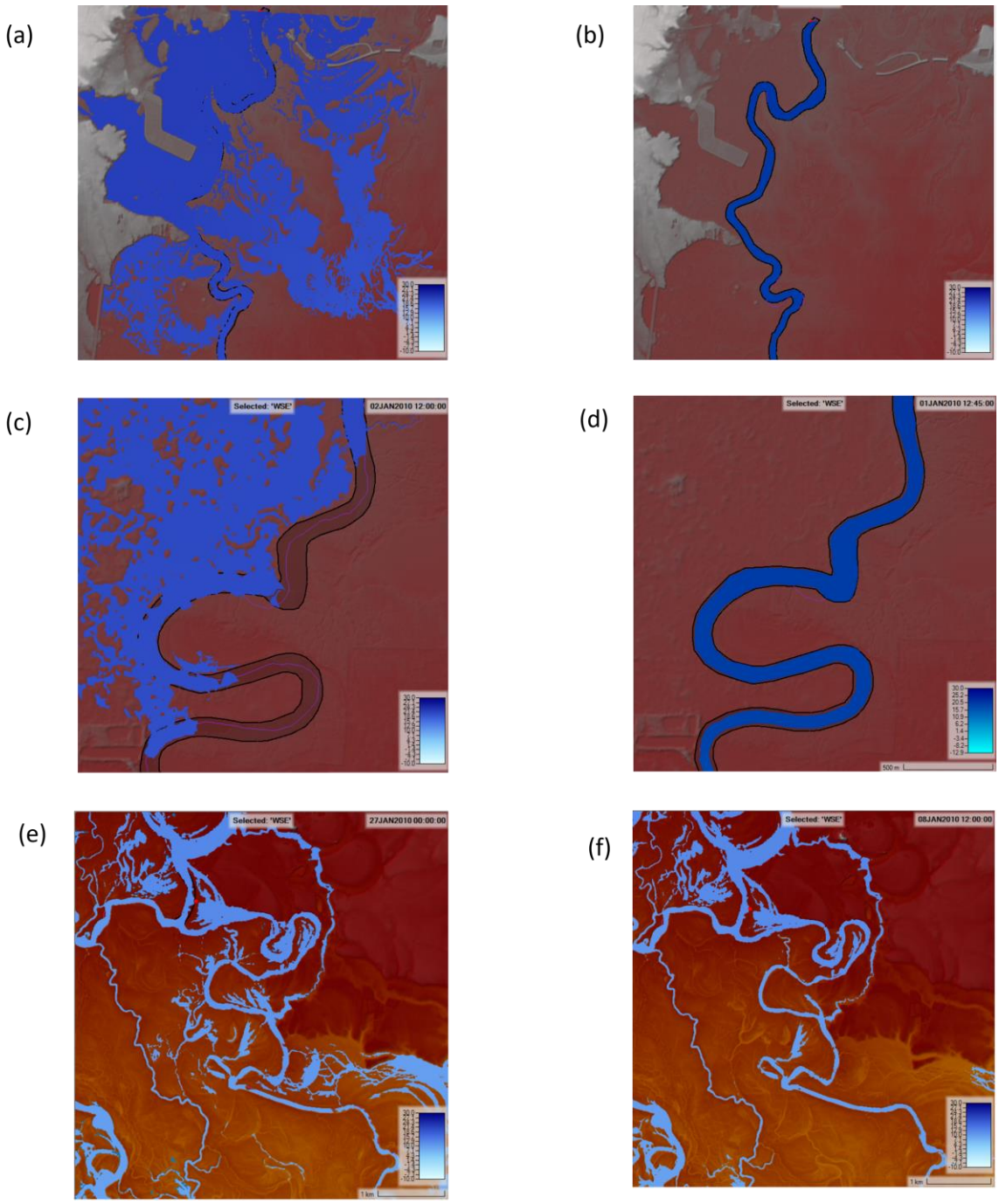

Figure 3.1 *: The flooding scenario in the Lower Pearl River. Figures (a), (c), and (e) is run before implementing synthetic bathymetry while figure (b), (d), and (f) are after the parabolic bathymetry was fitted into the DEM.*

The Manning's n value varies between 0.025 at small rivers with widths less than 30 m (Te Chow. V, 1959) but alluvial sand beds may have Manning's n varying between 0.018-0.035 (LeFavour, G.& Alsdorf, D., 2005). Manning's n values as low as 0.015 (Timbadiya et al., 2015) were used to represent river flow, 0.011, and 0.013 (Jahandideh-Tehrani et al., 2020) have been used to represent flow in tidal rivers. The sediment in Pearl is mostly silt and sand (Thorne et al., 2008), so for this study, it was found a lower range of Manning's n, varied from 0.01 to 0.015, represented the river channel flow better. 2014 was used to check for calibration, a wet month (April) and a dry month (July) were selected for checking the model performance at a variety of n values. The model is then run with the calibrated Manning's n value in 2014 and is validated in entire 2014 and 2015. The model is also run for 2019 (appendix A) for validation in a wet year with multiple Bonnet Carré spillway openings and on 2020 (appendix B). The results from each of these runs will be shown in the subsections of this chapter. The discharge values at the Pearl River outlet locations of East Pearl and West Pearl will be used to run the ROMS model in a later study to check how a better representation of the river flow affects coastal salinity and temperature.

3.1 Steady State Run: Flow Division

To check the model's initial performance and stability, it was run with a high flow of 2000 m3/s (70,490 ft3/s) at the Bogalusa (BL) and 100 m3/s (~3530 ft3/s) at Bogue Chitto (BC) stations, and the value was compared to the flow recorded at the mouth of the Pearl River using ADCP (Kulp et al., 2020). The model showed a higher outflow in the East Pearl (45% of the input discharge instead of 40%) and the West Pearl (15% of the input discharge instead of 10%) and a very low outflow from the Little Lake (5% compared

to 25% in the observed ADCP report). This might be because tidal boundary conditions were not used at the West Pearl and Little Lake for these initial simulations. Such boundary conditions updates were implemented for realistic simulations provided in section 3.3.

The model was run in HEC-RAS with various steady flow conditions at the upstream boundary and normal depth at the downstream boundary condition to check the model's stability. The hydrographs obtained at East Pearl and West Pearl River right after the bifurcation at AB Wilson are shown in Figure 3.2 (a) and (b). The BC in the figure represents flow at Bogue Chitto and the BL represents Bogalusa. The model was run at medium-high, medium, and low flow in steady-state conditions to check the model's stability. The figure shows when the inflow into the model was medium-high (BC flow 50 m3/s and BL 400 m3/s) in blue, medium in orange (BC flow 50 m^3/s and BL 200 m^3/s), and low in grey (BC flow 10 m^3/s and BL 60 m^3/s). These representative flow conditions were determined by analyzing the 10-year flow records at BL and BC measurement stations. Figure 3.2 shows that the flow across both East Pearl and West Pearl branches varies depending on the upstream flow conditions, so using a constant river flow as a boundary in coastal models will not be representative of the river. The use of time-varying discharge is recommended for riverine modeling efforts to understand the Pearl River dynamics.

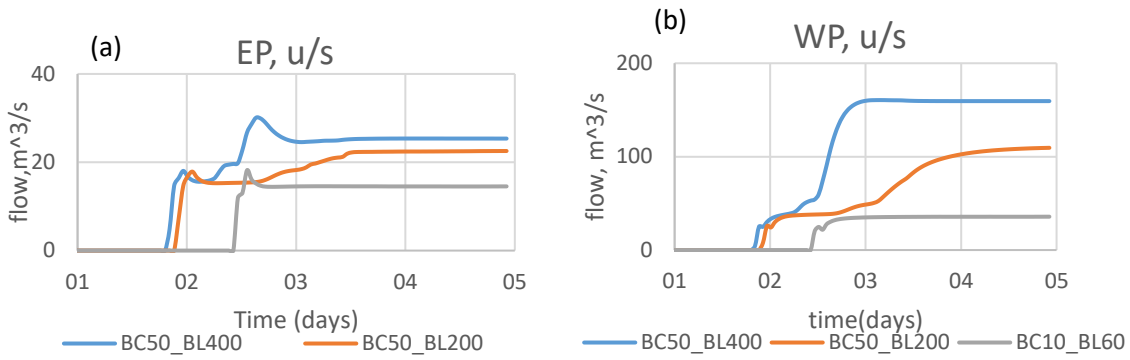

Figure 3.2 *: flow hydrographs East Pearl (a) and West Pearl (b) Rivers right after the bifurcation at station AB Wilson.*

3.2 Verification of Synthetic Bathymetry

Bathymetric data were collected near Stennis Space Center along the East Pearl River (Figure 2.5), as discussed in section 2.1.3. The vertical datum for the bathymetric data was North American Vertical Datum of 1988 (NAVD 88). Figure 3.3 shows the difference between the observed and synthetic meandering bathymetry at East Pearl River. Warm colors represent areas where synthetic bathymetry is deeper than observed and cooler colors represent areas where observed bathymetry is deeper than synthetic. At a location where the bend is strong, the observed bathymetry shows a high depth (> 14 m) which exceeds the upper depth cap of 7 m of the synthetic bathymetry by double. The observations show such a deep bathymetry at only one of the bends in the surveyed area. There may be clay deposits at the other bends which are erosion resistant, but unfortunately there is no survey data to confirm this.

Another section of the river is also zoomed in (Figure 3.4) to further investigate the bathymetry difference. The thalweg line, or the line connecting the deepest point of cross-sections in the channel, is shown in Figure 3.4, for both the surveyed and synthetic bathymetry (including meandering effects). The figure also shows the difference plot found

by subtracting the digital elevation of synthetic bathymetry from the observed, measured at Quay Wall. As the elevation values are negative, blue color represents depth where the observed bathymetry was deeper than the synthetic and the red color represents depth where the synthetic bathymetry was deeper than observed. The difference is larger when the thalweg does not match. The figure also shows cross-section plots at three locations showing the shift of thalweg from the centerline, or the mid width of each cross-section in the channel. Immediately to be noted is that the cross-section plot in the observation does not extend to the synthetic plot, and that is because the observation did not measure to the end of the bank because of Lily pads, making it impossible for the instrument to reach the banks.

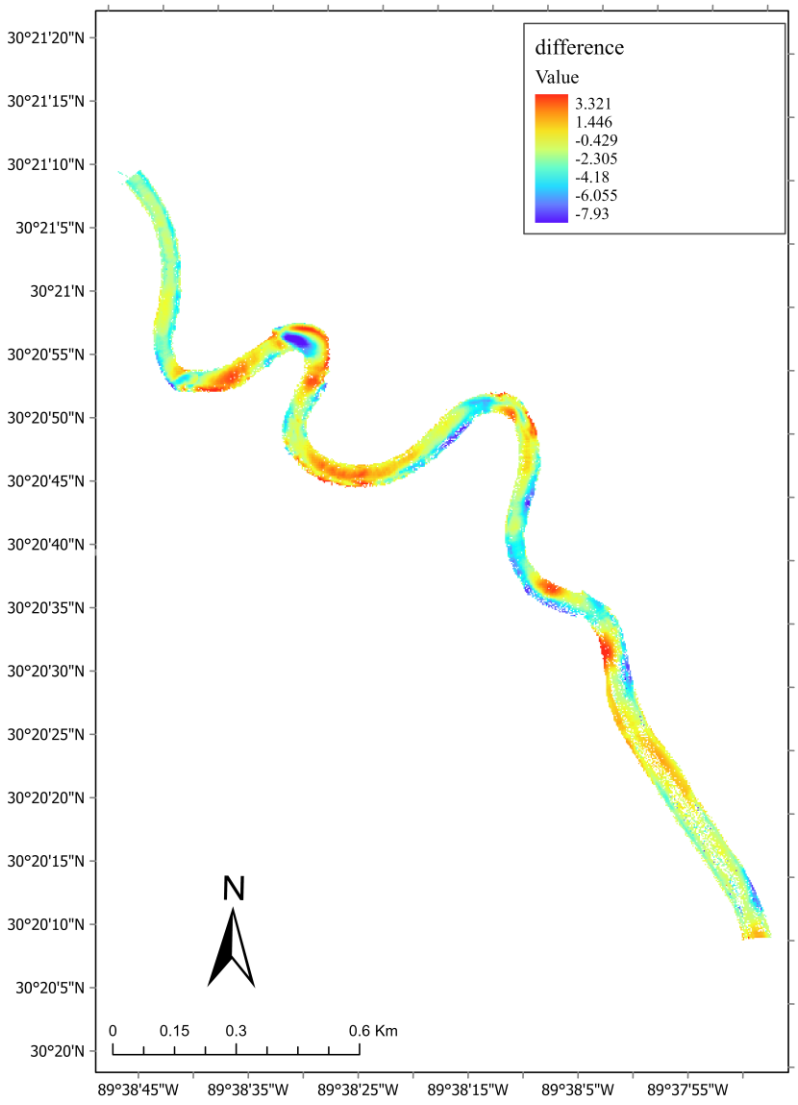

Figure 3.3 *: The difference in bathymetry between the observed elevation and synthetic elevation at East Pearl near the Quay wall.*

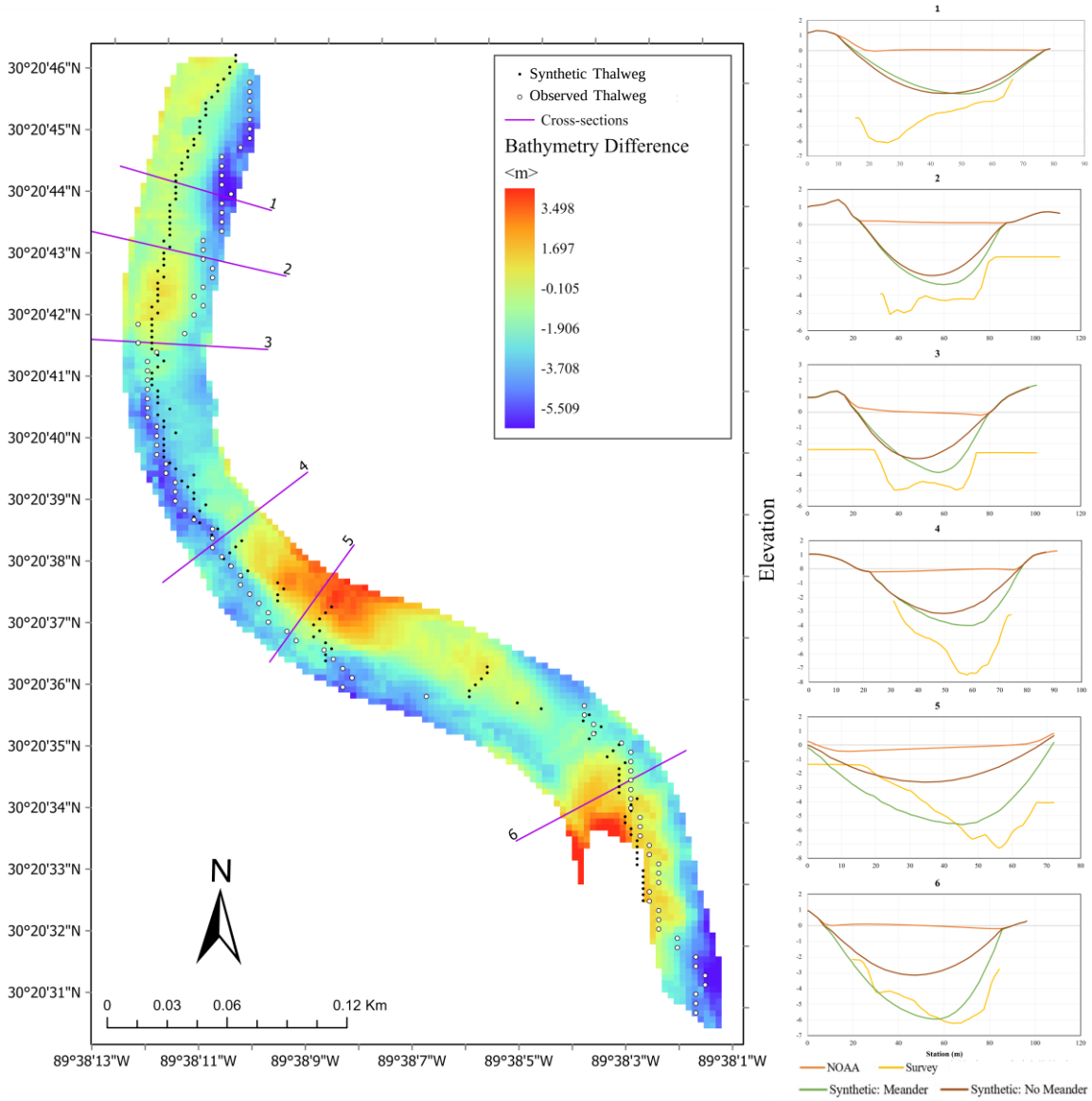

Figure 3.4 *: The difference in bathymetry between the observed elevation and synthetic elevation at the Quay Wall in East Pearl. The figure also shows the thalweg of the synthetic (black dots) and observed (white circles) cross-sections and their locations at specific locations where data are most different and most similar.*

The cross-section plots also suggest the bathymetry will be much deeper at sharp bends than what is suggested in the model. At the top section, the thalweg of synthetic and observed bathymetry do not match, suggesting the synthetic bathymetry should have a stronger meandering effect. In the future, bathymetry should be used with a greater

meander effect i.e., a value higher than 0.65 in Equation 8 to increase the meandering effect of synthetic bathymetry. Preliminary experiments were conducted with higher meandering, i.e., with values higher than 0.65, which generated too deep channels. Further modifications are needed to improve the equation. There is a difference of about 5 m at some sections of the river, but it is critical to note how much difference it creates in the modeled water level and discharge predictions. This is shown in the following sections of this chapter.

3.3 Model Calibration

The model was calibrated at multiple stations: at the station "AB Wilson" before the East-West split, at the station "Pearl River Station at Pearl River" for West Pearl River, and at the station "NSTL" near Stennis Space Station for East Pearl River (refer to Figure 1.1). There are no discharge measurement stations at the West Pearl River, the station "Wilson Slough Near Walkiah Bluff" has very intermittent discharge where the high flows are missing, so the station was not used for calibration purposes and the water level station (station 02492600: "Pearl River Station at Pearl River) was used instead. Figure 3.5 shows the flow and discharge hydrographs at the mentioned stations at Manning's n value ranging from 0.01 to 0.015 for July 2014 representing a dry (low flow) summer season. The values of R^2, RMSE, and NSE are shown in Table 3.1 which shows that for Lower Pearl River, the NSE of the water level (WL) hydrographs and discharge (Q) hydrograph is lower for n value of 0.015, although the RMSE is slightly higher than for other n values. Even though parameters indicated better performance at n =0.01, sharp peaks were observed in the discharge value of the model, indicating possible instability issues. This was further investigated and confirmed 30 m downstream of the Bogalusa station i.e., the upstream

boundary condition (Figure 3.5 (c) and (d)). Sharp peaks in discharge were also observed for an n-value of 0.011. For both West Pearl and East Pearl Rivers, an n value of 0.01 resulted in better performance values as per the highest R^2, lowest RMSE, and highest NSE for both WL and Q hydrographs.

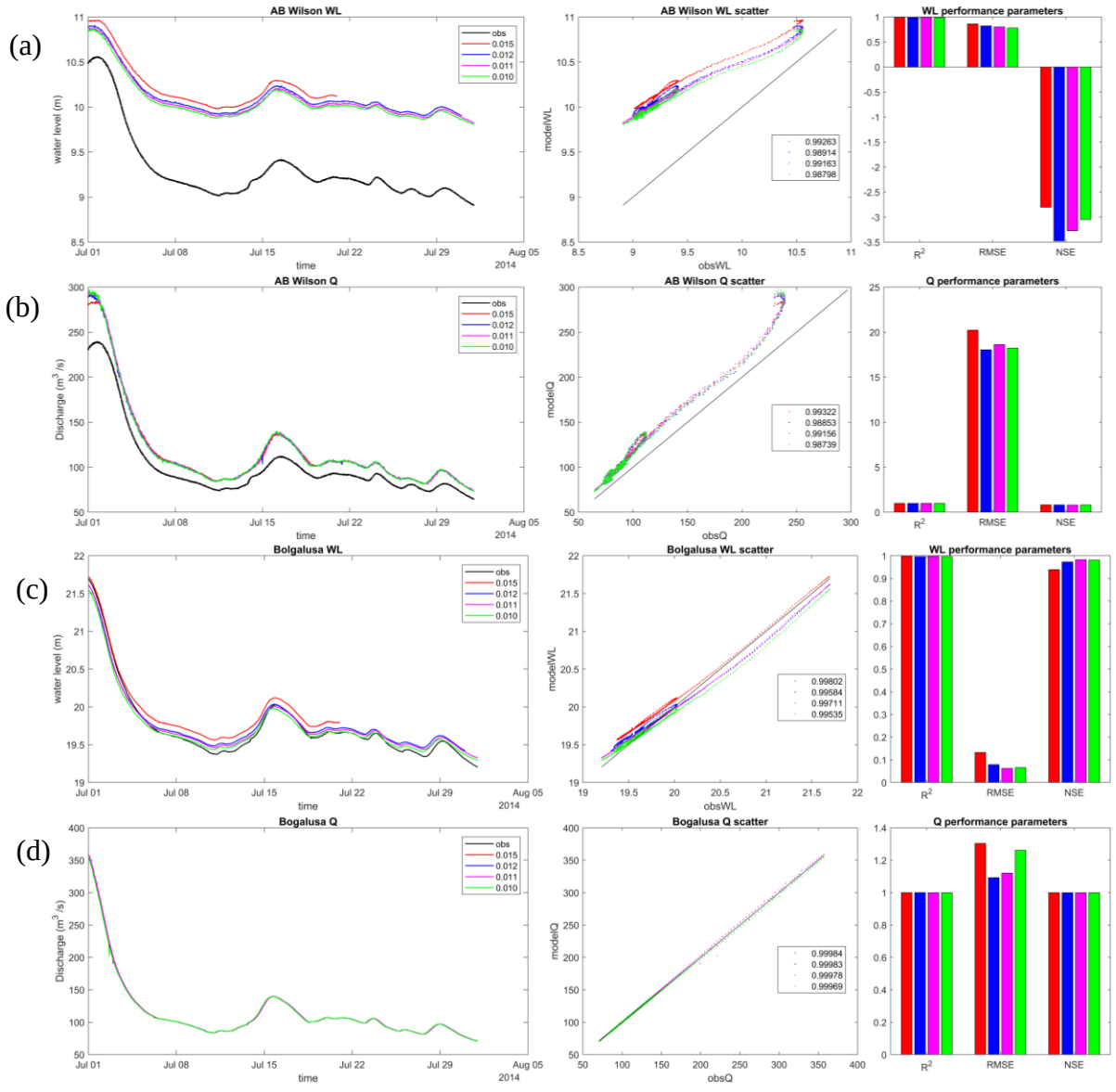

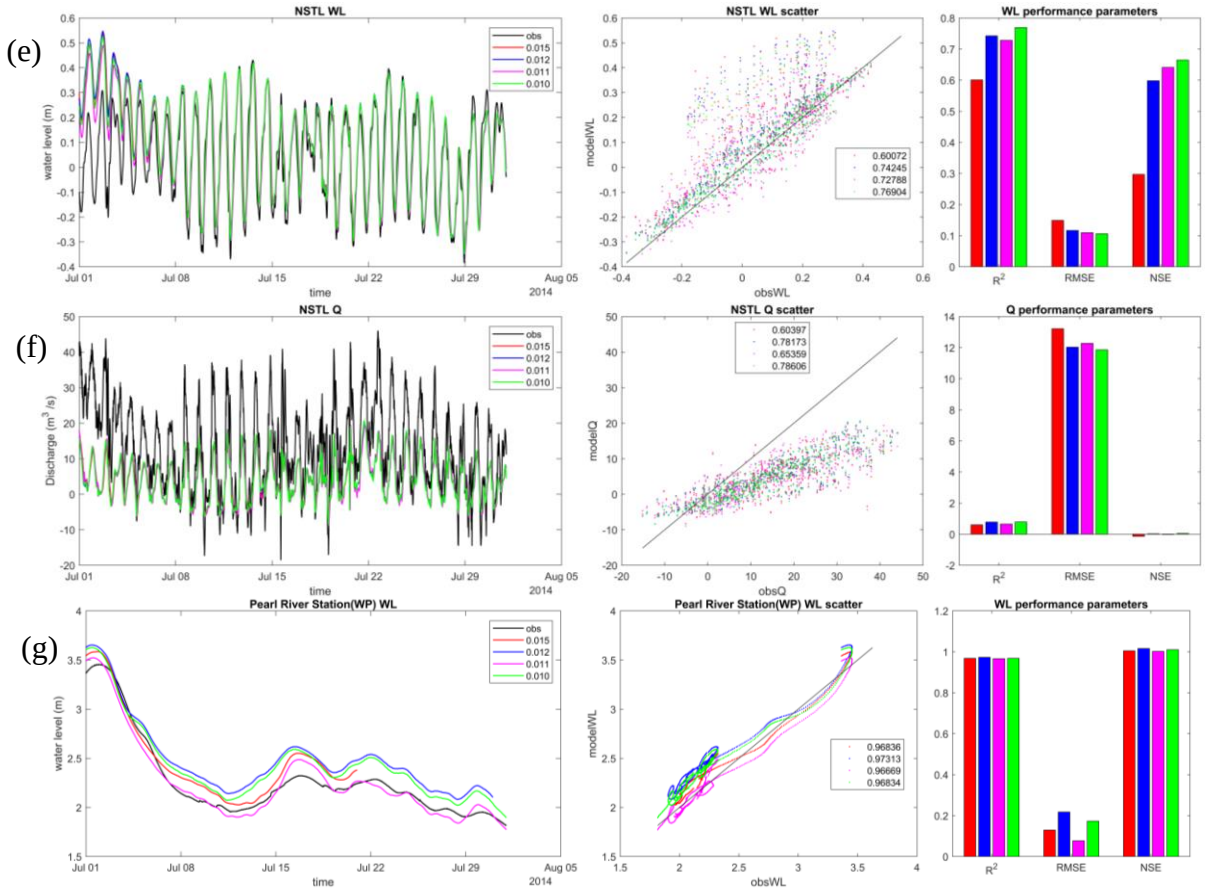

Figure 3.5 *The stage hydrographs (WL) and Discharge hydrographs (Q) at various stations along the channel in July 2014, their corresponding scatter plot, and a bar plot showing the performance parameters R^2, RMSE, and NSE.*

The flow and discharge hydrographs at the mentioned stations at varying Manning's n values representing a wet (high flow) spring season were plotted in Figure 3.6. The performance parameters for April 2014 are also listed in Table 3.2. Again, for the Lower Pearl River, an n value of 0.015 shows a high R^2 value (0.96), lower RMSE (0.21), and highest NSE (0.6) values for water level at AB Wilson. While for West Pearl River and East Pearl River, at stations Pearl River station and NSTL respectively, the model skill is lower but the model results match water level observations better at an n value of 0.01 with a high R^2 value (0.93 and 0.76, respectively), lowest RMSE (0.119 and 0.702, respectively), and high NSE for West Pearl (1.0). Although NSE values for water level at

NSTL (<0) suggest the model's poor performance, the NSE for discharge at NSTL (>0.5) suggests the model satisfactorily simulates the discharge. The discharge variation at NSTL is tidally influenced making it a challenge to simulate this station, which could only be accomplished for a lower value of Manning's n. For these reasons, a Manning's n value of 0.015 was used in the Lower Pearl River upstream of the split and a value of 0.01 was used at both West and East Pearl Rivers. The tributaries, Bogue Chitto and Hobolochitto, and the middle channels, Old Pearl River and Mid Pearl River channels had low width, so their n value was also kept at 0.01.

(a)

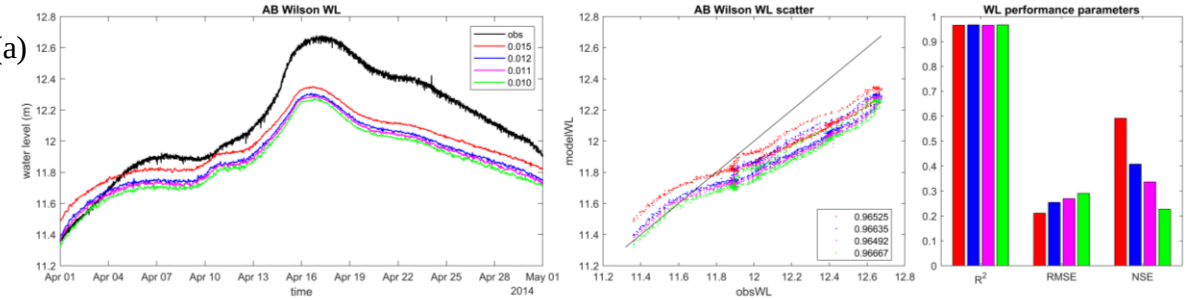

(b)

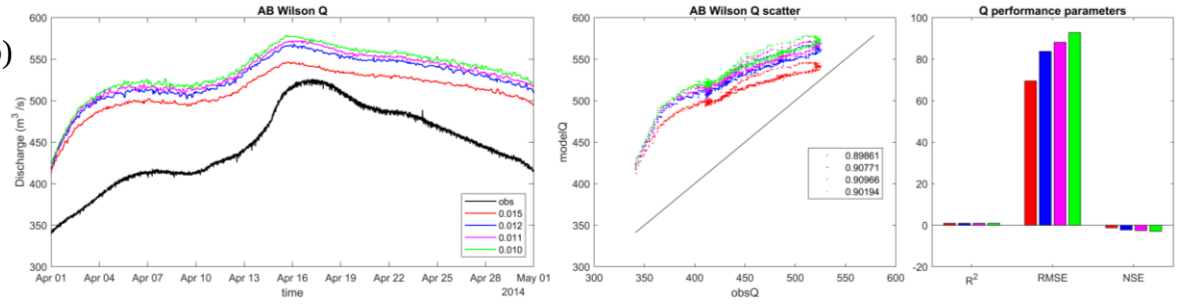

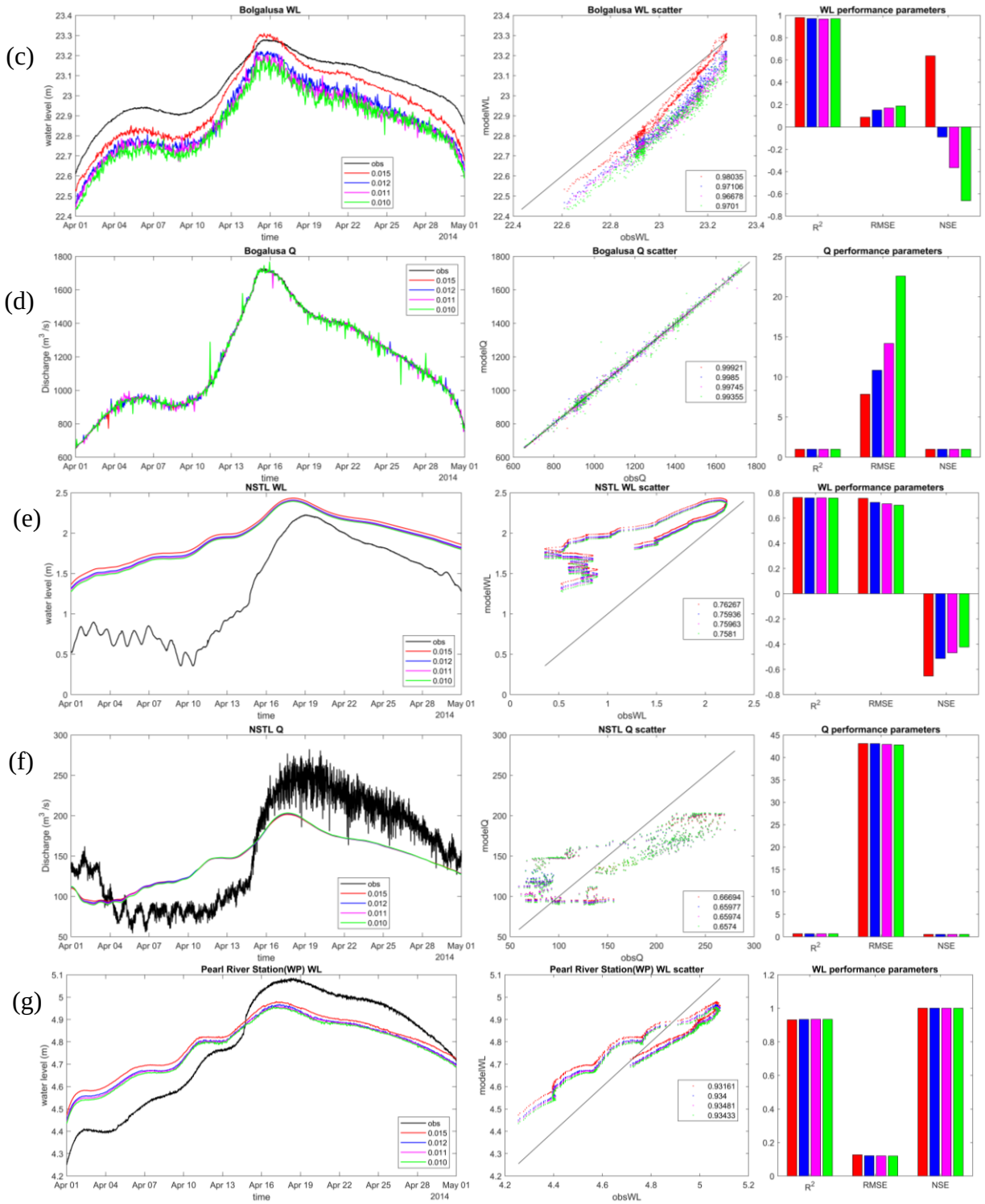

Figure 3.6 *The stage hydrographs (WL) and Discharge hydrographs (Q) at various stations along the channel in April 2014, their corresponding scatter plot and a bar plot showing the performance parameters R^2, RMSE, and NSE.*

Table 3.1 *Performance Parameters at stations at rivers Lower Pearl, West Pearl, and East Pearl for July 2014.*

Time	USGS Station	Manning's n	WL			Q		
			R^2	RSR	NSE	R^2	RMSE	NSE
Jul-14	Bogalusa	0.015	0.998	0.132	0.939	1.000	1.304	0.999
		0.012	0.996	0.079	0.973	1.000	1.093	1.000
		0.011	0.997	0.062	0.983	1.000	1.121	0.999
		0.01	0.995	0.066	0.981	1.000	1.261	0.999
	AB Wilson	0.015	0.99	0.86	-2.80	0.99	20.23	0.82
		0.012	0.99	0.82	-3.48	0.99	18.04	0.81
		0.011	0.99	0.80	-3.27	0.99	18.62	0.79
		0.01	0.99	0.78	-3.05	0.99	18.23	0.80
	Pearl River at Pearl River	0.015	0.97	0.13	1.01			
		0.012	0.97	0.22	1.02			
		0.011	0.97	0.08	1.00			
		0.01	0.97	0.17	1.01			
	NSTL	0.015	0.60	0.15	0.30	0.60	13.21	-0.13
		0.012	0.74	0.12	0.60	0.78	12.03	0.03
		0.011	0.73	0.11	0.64	0.65	12.28	-0.02
		0.01	0.77	0.11	0.66	0.79	11.86	0.05

Table 3.2 *: Performance Parameters at stations at rivers Lower Pearl, West Pearl, and East Pearl for April 2014.*

Times	USGS Stations	Manning's n	WL			Q		
			R^2	RMSE	NSE	R^2	RMSE	NSE
Apr-14	Bogalusa	0.015	0.980	0.088	0.638	0.999	7.844	0.999
		0.012	0.971	0.152	-0.090	0.998	10.826	0.998
		0.011	0.967	0.170	-0.365	0.997	14.161	0.997
		0.01	0.970	0.188	-0.661	0.994	22.549	0.993
	AB Wilson	0.015	0.965	0.211	0.592	0.899	69.475	-1.222
		0.012	0.966	0.254	0.408	0.900	83.841	-2.235
		0.011	0.965	0.269	0.336	0.872	88.274	-2.586
		0.01	0.967	0.290	0.227	0.891	92.851	-2.968
	Pearl River at Pearl River	0.015	0.932	0.127	1.001			
		0.012	0.934	0.121	1.001			
		0.011	0.935	0.120	1.001			
		0.01	0.934	0.119	1.001			

Table 3.2 (Continued)

	NSTL	0.015	0.763	0.756	-0.652	0.667	43.083	0.536
		0.012	0.759	0.724	-0.514	0.660	43.069	0.536
		0.011	0.760	0.713	-0.468	0.660	42.905	0.540
		0.01	0.758	0.702	-0.422	0.657	42.783	0.542

3.4 Run for 2014 and 2015

The model was run for 2014 and 2015 for the calibrated n values at the Lower Pearl, East Pearl, and West Pearl Rivers. The water level hydrographs and flow hydrographs are plotted in Figure 3.7 for 2014, which also shows the scatter plot, the bias of the model, and the regression line of the model vs. observed, with a 95% confidence level shaded on the plots. Figure 3.7 also shows the model performance parameters, R^2, RSR, NSE, PBIAS, MS, and KGE, in bar plots. The water level hydrograph at AB Wilson suggests the cross-section overestimates the low water levels during the dry season of July to December, but the Wilmott Model Skill (MS) higher than 0.8 suggests the water level is well predicted in the model. On the other hand, the model closely captures the base flow for discharge (from July to December 2014) but overestimates the Peak flow by about 50 m^3/s and up to 110 m^3/s in wet months. But an NSE value higher than 0.5 and a KGE value of 0.64 suggests the model's predictive capability is good for discharge at this station. The station at Wilson Slough (Figure 3.7 (c)) is also added to the figure, where the discharge data for only dry months are available. Analysis of model performance is done only in the times when observed data is available at this station. The model again overpredicts the high flows but captures the low flows, and although the peaks are missed, PBIAS values and KGE values suggest the model still performs well. Unfortunately, high flows are not available for full comparison.

For the NSTL (Figure 3.7 (d) and (e)) station on East Pearl River, the peaks in water level are overestimated but the peaks in discharge are underestimated. On the other hand, the station captured tidal fluctuations in both water level and discharge as shown by the high value of R^2 (>0.85 for water level and >0.65 for discharge). The Pearl River Station at Pearl River (Figure 20 (f)), for West Pearl River, shows the model matches the water level well during that time (R^2>0.95, 4% PBIAS, MS, and KGE scores >0.9). The comparison in discharge between NSTL and AB Wilson suggests that the flow division at the bifurcation is nearly 50-50 at high flows but becomes around 80-10 at low flows where West Pearl River receives most flows while the remaining 10% goes to the floodplain. This is further investigated in the next section of the chapter.

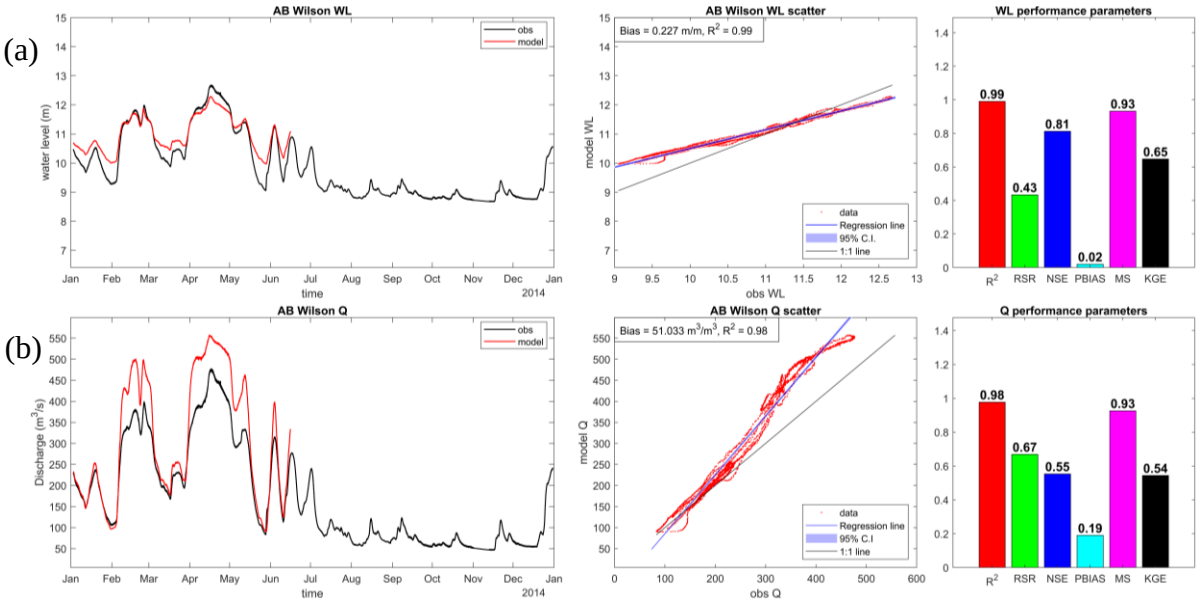

Figure 3.7 *The Discharge and water level hydrographs and each station, the scatter plot, and the performance parameters for the year 2014.*

Figure 3.7 Continued

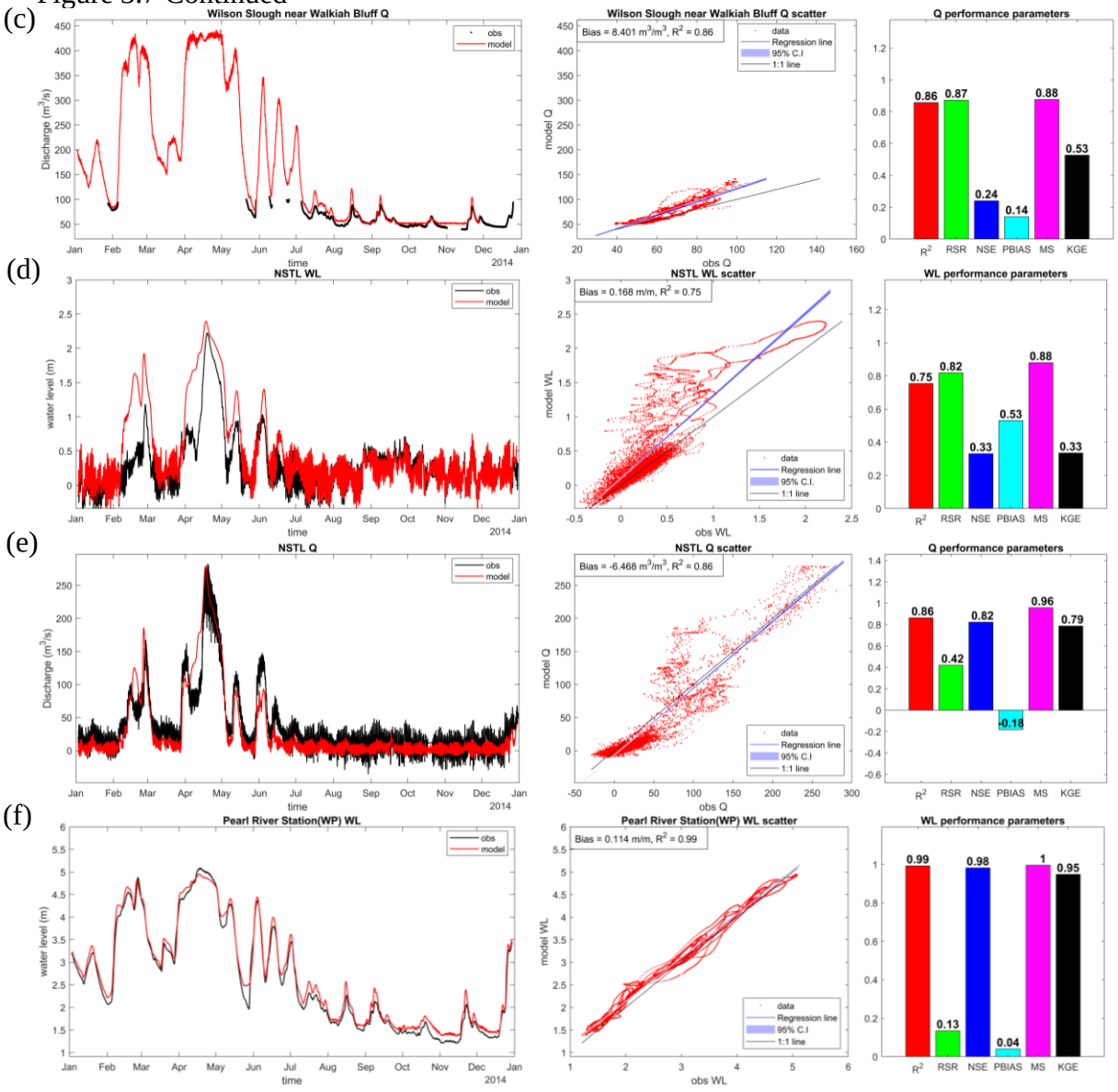

The water level hydrographs and flow hydrographs are plotted for 2015 and are shown in Figure 3.8. Similar to the 2014 results, the model seems to capture the peaks in water level at station AB Wilson, overestimating for the dryer months. But the Wilmot skill (0.85) and R^2 (0.99) greater than 0.8 suggest the model captures the water level well. For this year as well, the peak discharge is overestimated by around 100 m^3/s but a high value of R^2(0.97), NSE (0.81), KGE (>0.6), and a lower value of PBIAS (12%) suggest the model

is performing well. The 2015 results at the station at Wilson Slough are like 2014, the low flows are captured but the peaks are overpredicted, according to the performance parameters, the model is performing well at this station with high values of R^2 (0.96), NSE (0.74), and KGE (0.57) and low values of RSR (0.51) and PBIAS (9%).

However, it seems to be a different scenario for the station NSTL at East Pearl. The tidal influence at this station creates a challenge which is causing the modeled water level and discharge to be underpredicted and to have unsatisfactory performance for most statistical parameters for water levels and some parameters (RSR and PBIAS) for discharge. The high model skill and KGE values for discharge indicate that the model has the capability to capture discharge variations. More on this station will be discussed in the next chapter. The model is performing well at the water level station at West Pearl, with high values of R2 (0.98), NSE (0.95), and Wilmott Skill, MS (0.95) and low values of RSR (.22) and PBIAS (7%). The model captures the peak and water level well while missing the lower water levels during the dry period, a trend seen in its upstream stations AB Wilson and Wilson Slough, for dry months. The model was also run for 2019 and 2020 until July, Table 3.3 shows the statistics for all 4 years: 2014 (Jan – Dec), 2015 (Jan – Dec), 2019 (Jan – Dec), and 2020 (Jan – Dec). Performance parameters indicate the model performed better in 2019 than in 2015 with a high R2 (> 0.9), high NSE (>0.75), MS score (>0.9), and KGE (>0.55) and low PBIAS (< 10%) and RSR (< 0.7) at stations AB Wilson and Pearl River at Pearl River. Only the station at Wilson Slough performed poorly in discharge as seen by NSE (-3.57) and RSR (2.14) values which are because the model could not capture the base flow.

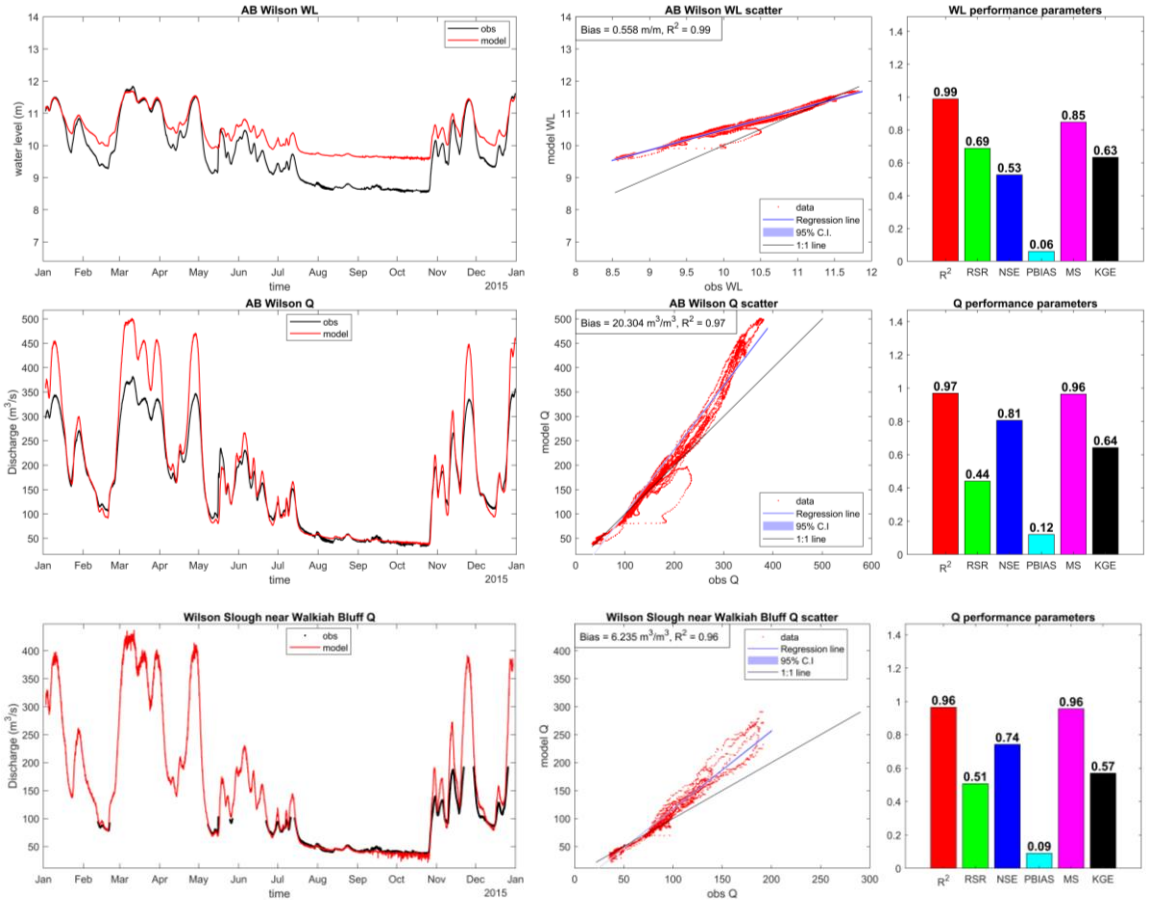

Figure 3.8*: The Discharge and water level hydrographs and each station, the scatter plot, and the performance parameters for the year 2015.*

Figure 3.8 Continued.

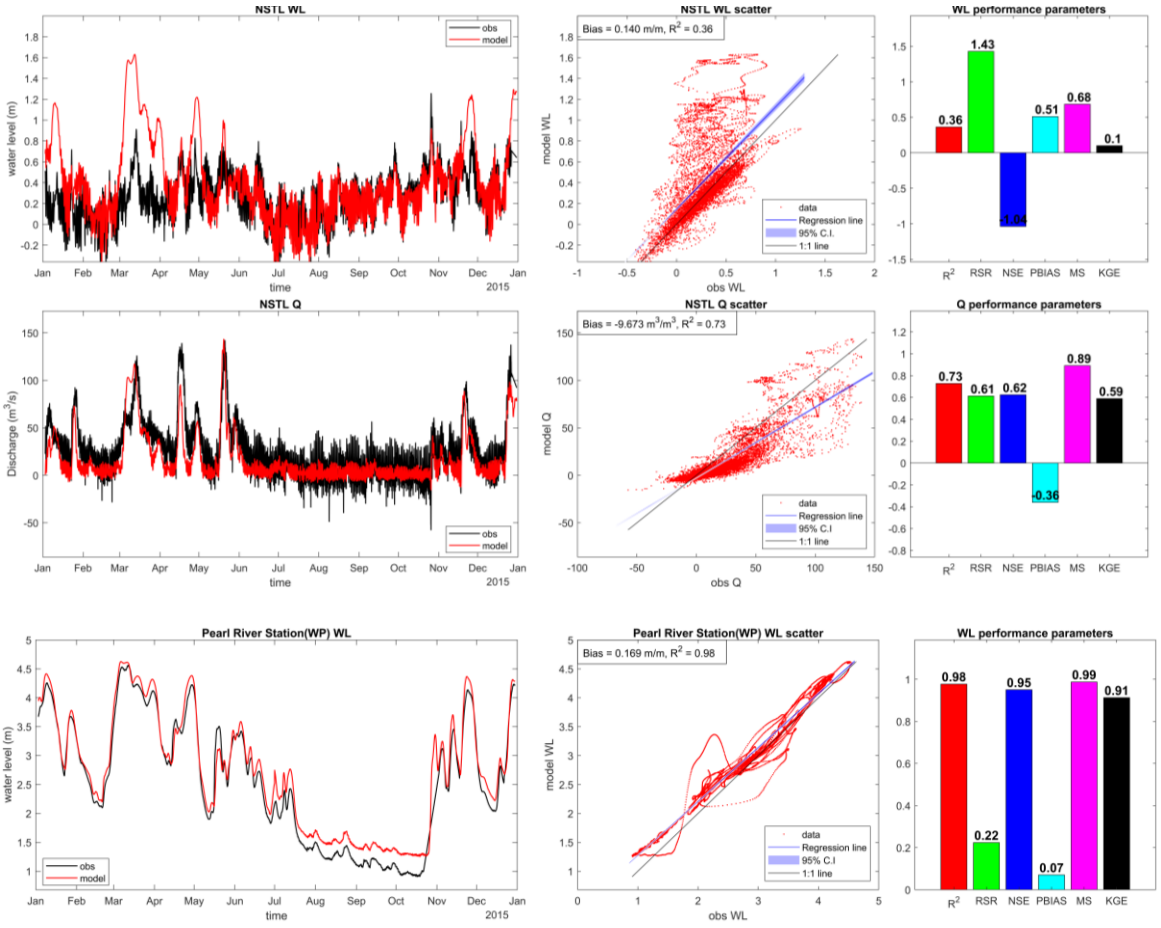

The parameters suggest NSTL performed satisfactorily as well. The performance parameters suggest the model performed better at all stations (With the exception of the station at Wilson Slough) during the verification years of 2019 and 2020. This might be because 2019 and 2020 were wet years with mean Bogalusa discharge of 500 m^3/s and 550 m^3/s, respectively compared to 350 m^3/s in 2015 and 500 m^3/s in 2014.

Table 3.3*: Performance parameters at USGS stations for 2014, 2015, 2019 and 2020*

	Station	WL						Q					
		R^2	RSR	NSE	PBIAS	MS	KGE	R^2	RSR	NSE	PBIAS	MS	KGE
2014	AB Wilson	0.99	0.62	0.61	0.06	0.87	0.64	0.99	0.40	0.84	0.14	0.97	0.65
	Wilson Slough							0.89	0.81	0.35	0.10	0.90	0.45
	NSTL	0.75	0.82	0.33	0.53	0.88	0.33	0.86	0.42	0.82	-0.18	0.96	0.79
	Pearl River at Pearl River	0.99	0.13	0.98	0.04	1.00	0.95						
2015	AB Wilson	0.99	0.69	0.52	0.06	0.85	0.63	0.97	0.44	0.81	0.12	0.96	0.64
	Wilson Slough							0.96	0.51	0.74	0.09	0.96	0.57
	NSTL	0.36	1.42	-1.03	0.51	0.68	0.10	0.72	0.62	0.62	-0.36	0.89	0.59
	Pearl River at Pearl River	0.98	0.22	0.95	0.07	0.99	0.91						
2019	AB Wilson	0.99	0.43	0.81	0.02	0.93	0.60	0.99	0.38	0.86	0.09	0.97	0.68
	Wilson Slough							0.97	0.53	0.72	0.14	0.95	0.70
	NSTL	0.73	0.88	0.23	0.34	0.87	0.43	0.84	0.45	0.79	-0.25	0.94	0.71
	Pearl River at Pearl River	0.99	0.16	0.97	0.03	0.99	0.91						
2020	AB Wilson	0.97	0.48	0.77	0.02	0.91	0.56	0.97	0.27	0.93	0.05	0.98	0.84
	Wilson Slough							0.70	0.64	0.59	0.05	0.90	0.78
	NSTL	0.80	0.63	0.60	0.26	0.92	0.64	0.90	0.38	0.85	-0.23	0.95	0.70
	Pearl River at Pearl River	0.99	0.11	0.99	0.00	1.00	0.94						

CHAPTER IV – DISCUSSION

This chapter will go in-depth into the results for further analysis and explain the capabilities of the model. It will break down each of the results into similar sections where the unsteady flow run, and bathymetry results will be analyzed.

4.1 Unsteady State Run

The modeled water level results indicate an upper cap of 12.5 m at AB Wilson which the model does not seem to exceed even if the observed water levels do (See Figures 3.7 (a) and 3.8 (a)). This might be owed to recent topographic data which does not allow the water level to increase, or it might be owed to too deep a synthetic channel cross section at the station. The theory on deeper bathymetry in the model is fortified by the model results for low water levels where the model again displays a lower cap where the water level does not go below approximately 10 m. The discharge at Bogalusa was lower during 2015, but the overestimation was higher, suggesting flow must have spilled into the floodplain and reduced the flow inside the river before reaching this station (See Figure 1.1 or 2.1 (b) for station location). The lack of flow into the floodplain may be due to the high values of Manning's n assigned to the floodplain (0.10), whereas in reality, it may have been much lower. An experiment was conducted for a short period of time varying Manning's n in the floodplain (Figure A3 in the appendix) and it suggests that a lower value of Manning's n in the floodplain could have decreased the peak flow in the model. It must be mentioned at this point that the peak flow in AB Wilson was not recorded and was generated with a rating curve using measured water level, so the peak values of the observed are also subject to uncertainty.

The discharge in Wilson Slough reflects the discharge of AB Wilson and is also shown in the model (Figure 3.7 (c) and 3.8 (c)). The peak values could not be generated through a rating curve like AB Wilson because the station did not have water level data. There was a barrier installed at the mouth of West Pearl, Walkiah Bluff (See Figure A4 in Appendix), an earthen trapezoidal weir to prevent East Pearl from drying up in the dry periods (Roberts, 2012). But the structure became ineffective as of 2019 according to several news reports (Picayune Times (2023, April 20)) and is reflected in the model as well, so the model might be showing discharge distribution at the bifurcation in the current situation (where the barrier is not as effective). The water level at Pearl River Station in West Pearl performs well, predicting the high and low waters in both dry and wet seasons as suggested by the performance parameters, since it is 26 km upstream of the coastline, the tidal variations are not seen in the water level, in the observations or the model results. The same cannot be said about NSTL, the station at East Pearl (Figure 1.1). NSTL station is also 26 km upstream of the mouth of the East Pearl and this discrepancy between tidal influence between Pearl River at Pearl River station (at West Pearl) vs NSTL (at East Pearl) can be explained by both the smaller slope of the East Pearl compared to West Pearl allowing for tides to propagate farther upstream during the wet season and also by the fact that West Pearl carries a larger riverine discharge not allowing the tidal current to go as far upstream in the West compared to East Pearl.

The tidal discharge is consistently underestimated at NSTL, and the water level overtops at a lower discharge than what is observed. This suggests that the cross-section at this channel might be wider and deeper than reality, to prevent over-topping within the model. The decrease in Manning's n of the floodplain seems to have reduced the discharge

and increased the water level further in the model, suggesting the error in the model might lie in the cross-section itself. There is a lag between the water level and discharge at the station in the observations which is captured in the model as well. For further understanding, the tidal influence is removed from the water level and discharge of both the observation and the model time series at NSTL by passing the data through a low-pass filter function in MATLAB. The function filtered the hourly data using a half -amplitude period of 48 hours and is shown in Figure 4.1. Comparing Figure 4.1 with Figures 3.7 (d & e) and 3.8 (d & e) shows that although the performance parameters remain almost the same, the observed and modeled riverine water level and discharge variations can be seen much clearer, with the model overestimating high water levels and discharge and underestimating the low water levels and discharge.

Figure 4.1 also shows the variation in water level and discharge is similar to the water level in AB Wilson (Figure 3.7 (a & b) & 3.8 (a & b)) suggesting if the tidal influence is removed and only the riverine flow is considered, the model aptly captures the pattern. Wind is one of the dominating factors forcing flow into East Pearl, the south easterly winds from Lake Borgne during summer and fall drive saline water into East Pearl (White & Simmons, 1988) HEC-RAS Shallow Water Equation does not account for wind forces (Munoz et al. 2021; Bush et al., 2022). This might be one of the reasons why the tidal flow was not driven upstream towards NSTL which observations suggest it should. Also, we later see that most of the East Pearl inflow is directed to Little Lake in the model which might not be the case. So, bathymetric measurements are suggested in the entire downstream river sections to ensure the flow in this complex area can be captured and modeled accurately.

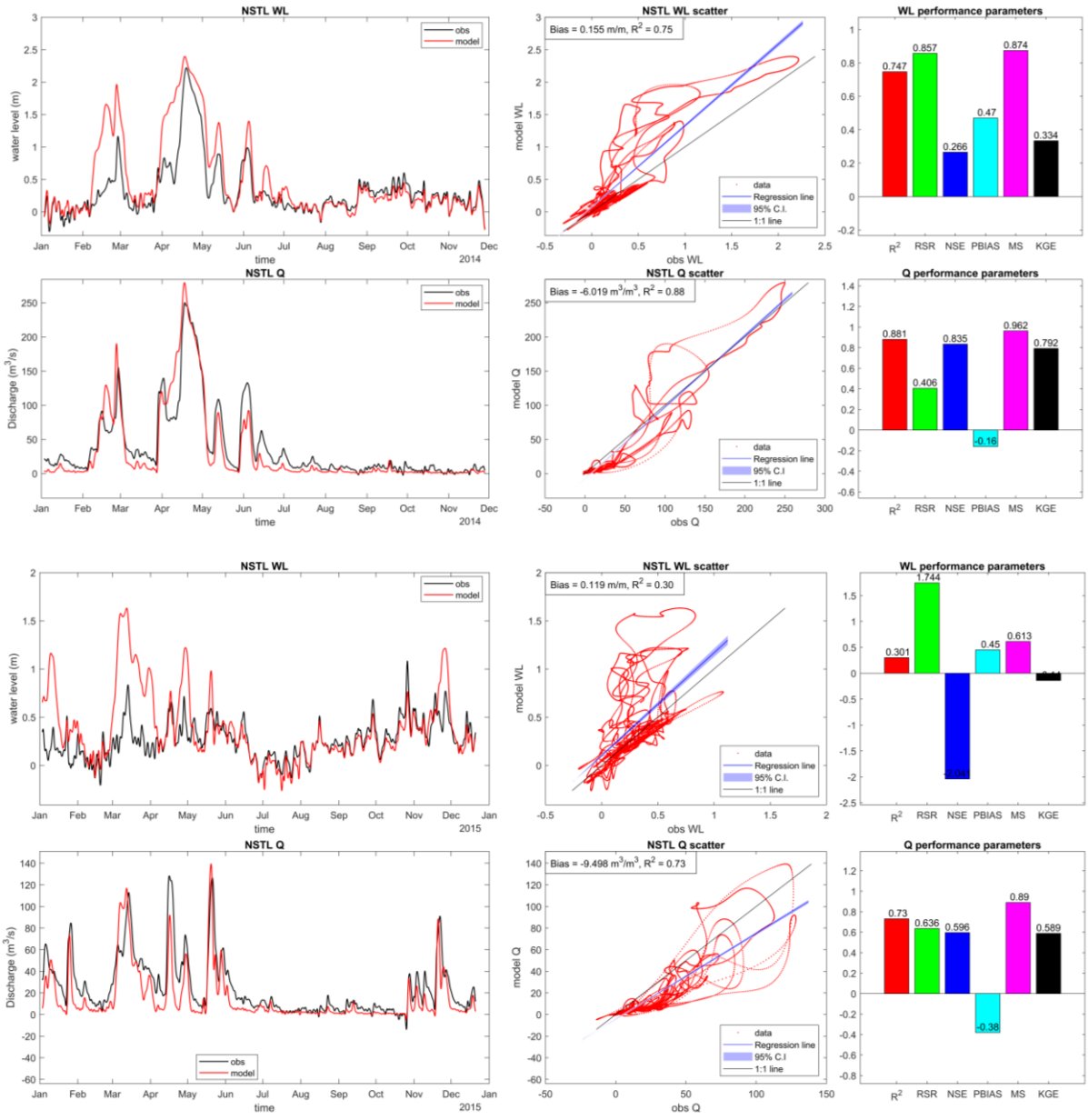

Figure 4.1 *: The discharge and water level at NSTL station (East Pearl) with tidal influence removed from both model results and measurements during the 2014 and 2015 runs.*

4.2 Discharge Distribution:

One of the main objectives of this thesis was to determine if the 60-40 Bogalusa discharge division at the Pearl River outlet for West and East Pearl, respectively, as currently implemented in the ROMS simulations as a river forcing condition, was a valid

decision or not. The results of unsteady flow during 2014 and 2015 were considered to investigate the ratio where the maximum and minimum flow percentage at each branch outlet and inlet of the river system was determined. For simplicity, the river system is grouped into 3 sections shown in Figure 4.2 and the discharge distribution was found for the wet period and dry period because modeling suggested the response to the river was different depending on the river inflow.

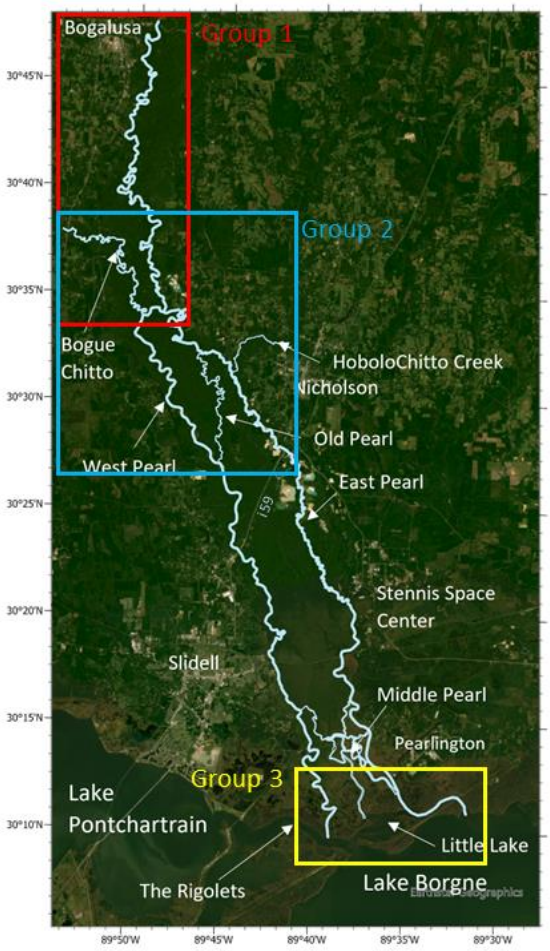

Figure 4.2 *: The study area division into three groups to understand the flow division of the river at each group.*

The first group, Group 1 (Figure 4.2 & 4.3), is focused on the Lower Pearl including the bifurcation that branches Lower Pearl into East and West Pearl, i.e., Bogalusa, AB Wilson (at the split), West East Pearl. This group would investigate the percentage of flow at each channel inlet and how these play into the dynamics downstream. The second group (Group 2, Figure 4.2 & 4.4) is a more complex and dynamic one, focusing on the inlet of channel branches: Bogue Chitto, West Pearl, Old Pearl, East Pearl, and Hobolochitto. Flow from West Pearl meets the flow from Bogue Chitto after the split and merges with the flow from Old Pearl downstream. Old Pearl diverts flow from East Pearl to West Pearl, leaving East Pearl nearly dry in low flow conditions while the flow from Hobolochittos acts as the main source for East Pearl during that time. The last group (Group 3, Figure 4.2, 4.6, 4.7) is for the downstream section of the river at the coastline focusing on the outlets of West Pearl, East Pearl, and Little Lake. This is the main section of concern for this study, where the ratio of outflow is to be determined and will be provided to ROMS. It is critical to state that the analysis is for one year (2014), so the values and percentages will not remain the same for another year or another month. The point is to state which channel receives the bigger percentage of flow and if the channel continues to receive the bigger percentage in wet or dry conditions.

Figure 4.3 shows the flow rates and the percentage distribution of flow in the concerned outlets and inlets calculated with respect to the flow at Bogalusa for Group 1. Figure 4.3 (a) shows flow rates and percentages during wet periods while Figure 4.3 (b) shows the flow rates and percentages for dry periods. In the wet periods, more flow spills into the floodplain where AB Wilson receives only 32% of the maximum flow in Bogalusa while 68% of the flow spills into the floodplain before reaching the bifurcation

downstream. The flow in AB Wilson splits into the West and East Pearl by 25.1% and 7.2% respectively. This refutes the hypothesis that there is 50-50 split between East and West Pearls at high flow condition. In the dry season, only 13% of the flow goes into the floodplain and most flow stays within the river with 87% of the low flow reaching AB Wilson.

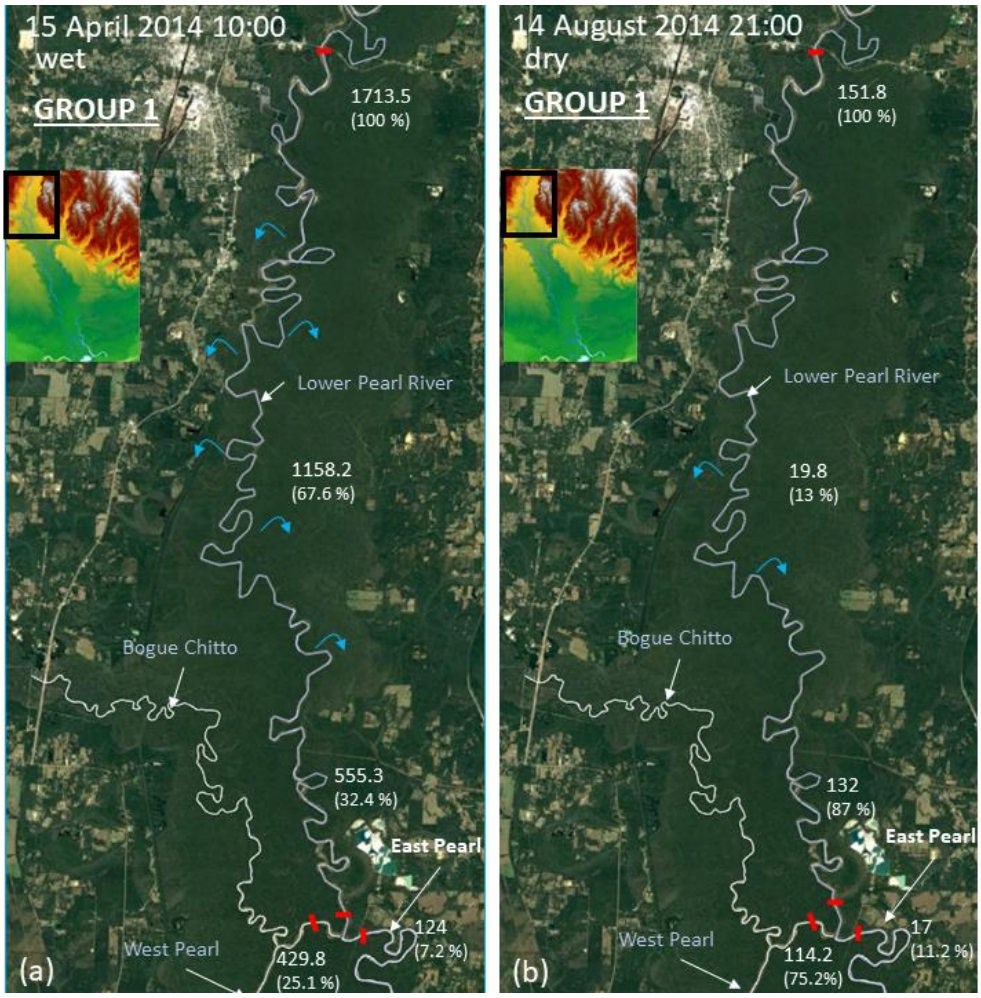

Figure 4.3 *: Group 1 of the river section, showing Bogalusa, AB Wilson, and the bifurcation forming East and West Pearl Rivers for (a) wet period in April 2014 (b) dry period on August 2014. Numbers show the flowrate in m^3/s at identified red cross-sections and values in parenthesis show the percentage of that flow with respect to the flow in Bogalusa.*

Again, West Pearl is the dominating branch, receiving 75.2% of the flow from the dry period flow from Bogalusa while East Pearl only receives around 11.2%, agreeing to the hypothesis that West Pearl is the dominant river branch at the split during low flow conditions. The branches and tributaries make Group 2 (Figure 4.4) more complex than Group 1. For the wet season (Figure 4.4 (a)), more than 50% of the flow from Bogalusa spills into the floodplain, and this flow in the floodplain contributes to the flow in Bogue Chitto as the flow downstream of it is much larger than the flow upstream. Profile plot of the West Pearl between bifurcation point and Bogue Chitto outflow does not show restriction to flow in West Pearl refuting the hypothesis that Bogue Chitto inflow will create a restriction.

The flow from Bogue Chitto combines with West Pearl and flows in the floodplain again merges with West Pearl north of Old Pearl as seen in Figure 4.4 (a). This section suggests that most flows in the floodplain return to the West Pearl River before interstate I59 (location shown in Figure 4.2) as seen that it has 81% of the flow of Bogalusa before the merge with Old Pearl. It is also important to note that the flow from Bogue Chitto is also added to the flow of West Pearl at this point, so the total inflow in the river branch is 135% of the flow at Bogalusa. Over on East Pearl's side, it's seen that an additional 1.3 % flow from the floodplain also returns to East Pearl, increasing its flow so that it receives 8.5% of the maximum flow from Bogalusa. But most flow in East Pearl is diverted into West Pearl through Old Pearl which receives 7% of the flow from Bogalusa leaving East Pearl with very low flows (~27 m^3/s). East Pearl is again replenished by Hobolochitto flow to be 2.5% of Bogalusa's flow. This further shows that north of I59 West Pearl is still the dominating branch at high flow conditions.

The scenario in the dry season (Figure 4.4(b)) is quite similar at downstream sections of Group 2 after Old Pearl merges into West Pearl, with West Pearl carrying more than 100% of Bogalusa flow at low flow conditions, indicating it is carrying both Bogalusa and Bogue Chitto flow. The exception at the dry scenario is the condition at East Pearl. The section of the East Pearl downstream of the Old Pearl split completely dries up with little to no flow. It only gets replenished by flow from Hobolochitto. It gets more complex as we go downstream due to the tidal influence from the Little Lake, East, and West Pearl boundaries at the coastline.

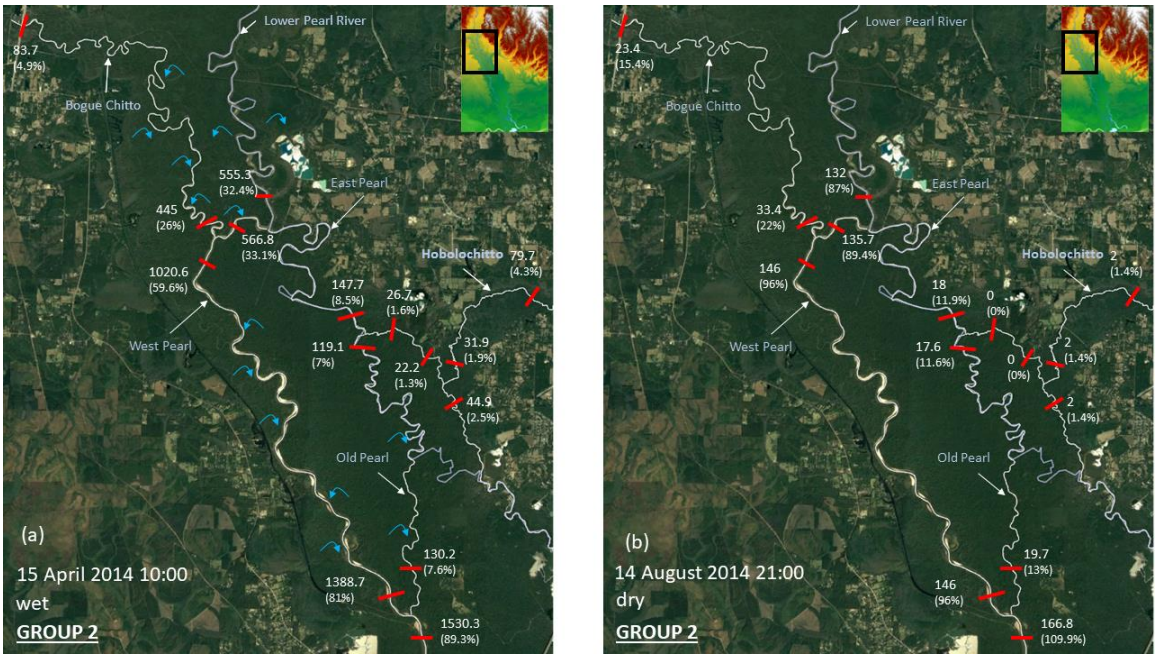

Figure 4.4 *: Group 2 of the river section, showing the tributaries Bogue Chitto for West Pearl, Hobolochitto for East Pearl, and Old Pearl for (a) the wet period on April 2014 and (b) the dry period on August 2014. Numbers show the flow rate in m^3/s at identified red cross-sections and values in parenthesis show the percentage of that flow with respect to the flow in Bogalusa.*

The initial model result at East Pearl showed extremely high discharge varying between 500 m^3/s to 1000 m^3/s where the flow moves into and out of the river outlet, displaying the tidal nature of the flow. Higher flow (around 1000-1500 m^3/s) flowing into

East Pearl and around 500 m^3/s flowing out. This result initially seemed unrealistic, but there was a year of discharge data available at the USGS gage station CSX railroad (See Table 1.1). Figure 4.5 shows the discharge variation for the USGS gage station at CSX railroad, the closest station to the East Pearl outlet. The discharge varies from 500 m^3/s to -500 m^3/s daily, the model also shows a daily variation of discharge at the East Pearl boundary, but unlike the observation, the model suggests the flow in East Pearl is negative throughout the dry season. This difference may be attributed to the differences in 2009 and 2014 conditions. The discharge distribution presented in the downstream section of the river (Group 3) is presented in Figure 4.6 for the wet period and in Figure 30 for the dry period.

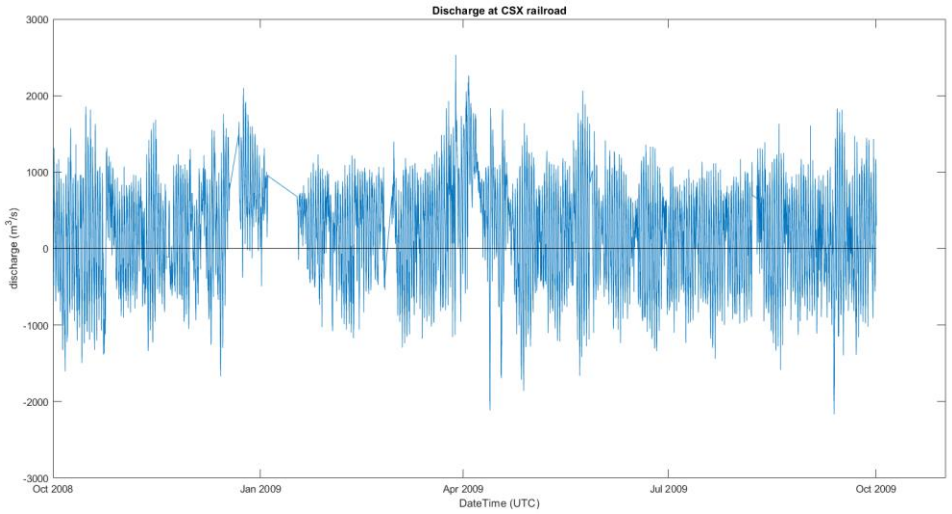

Figure 4.5 *Discharge at USGS gage station 301141089320300, CSX Railroad, for the only duration of time the data was available.*

The flow rate, flow directions, and distribution get complex at the downstream zone due to the tidal water level of all three outlets. But for the wet period, the river dominated the tide as seen in Figure 29, where the discharge distribution at the highest inflow from

Bogalusa was selected. Water flows out through the river currently, with West Pearl and Little Lake having similar discharges, and almost double their discharges flow out of East Pearl. The Middle Pearl channels act to divert most of the flows in the floodplain back into East Pearl and Little Lake, through which flow also moves into West Pearl. Nearly 44% of the flow comes out from East Pearl alone while half of that flows from each of the other two outlets (24% from West Pearl and 19% from Little Lake). It is important to note here that Little Lake outlet does not exist in the ROMS model and considering West Pearl and Little Lake discharges combined (42.5%) amounts to almost equal to that of East Pearl. The discharge distribution plot in Group 3 confirms the hypothesis that East Pearl is the dominant river branch during high river inflows as the flow into East Pearl is almost double the discharge through West Pearl at high flow conditions (during April). Comparing the discharge at the outlets (on April 15, 2014) from Figure 4.6 and the ADCP survey (on March 2) for 2020 (Figure 1.2 (b)) suggests flow coming out from West Pearl is higher than it is predicted by the model. This might be because less flow was allowed to spill into the floodplain and was retained in the river. This is also seen in the flow coming from Middle Pearl channels which is around ~100 m^3/s lower than the surveyed data, suggesting they transfer more flow from the floodplain.

The flow through Little Lake is lower in the survey than what is predicted by the model. This might be because less flow is being transferred in the Little Lake and flowing out of it. According to the survey, around 38% of the flow from East Pearl is diverted into Little Lake whereas the model suggests it is around 12%. Further investigation is needed to analyze the percent distribution of other years to understand if this difference is due to the peak flow value or due to a bathymetry mismatch between the DEM and reality.

Flow distribution is more complex in the dry season when the flow from Lake Borgne enters East Pearl as shown in Figure 4.7, the discharge distribution of the downstream section during August 2014, the month when the river discharge is low. The model suggests water flows into East Pearl from the Sound and exits through Little Lake and West Pearl. It must be mentioned that the boundary downstream is a prescribed boundary and does not allow barotropic waves to radiate out and this might be creating a pressure gradient, causing the flow to move upstream through East Pearl and out through West Pearl and Little Lake. Unfortunately, there is no surveyed flow data during the dry period so the model's results cannot be verified.

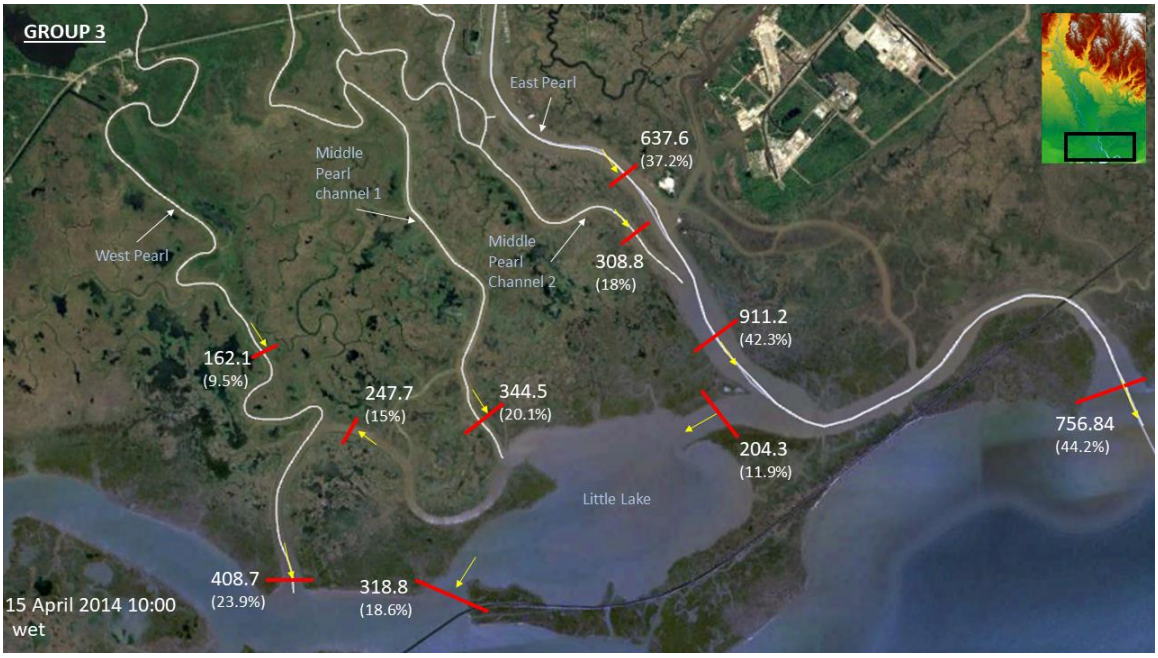

Figure 4.6 *The discharge distribution at Group 3 of the river section, showing the Middle Pearl channels, and the three outlets of Pearl: Little Lake, East, and West Pearls for the wet period on April 2014. Numbers show the flowrate in m^3/s at identified red cross-sections and values in parenthesis show the percentage of that flow with respect to the flow in Bogalusa.*

Further investigation is required with field surveys for a prolonged period in this region, specifically for the dry season. The flow division for the dry season at low flow

conditions disproves the hypothesis that at low flow conditions, both East and West Pearl have the same amount of discharge. Although the magnitude of the flow from both branches is similar, the directions are opposite.

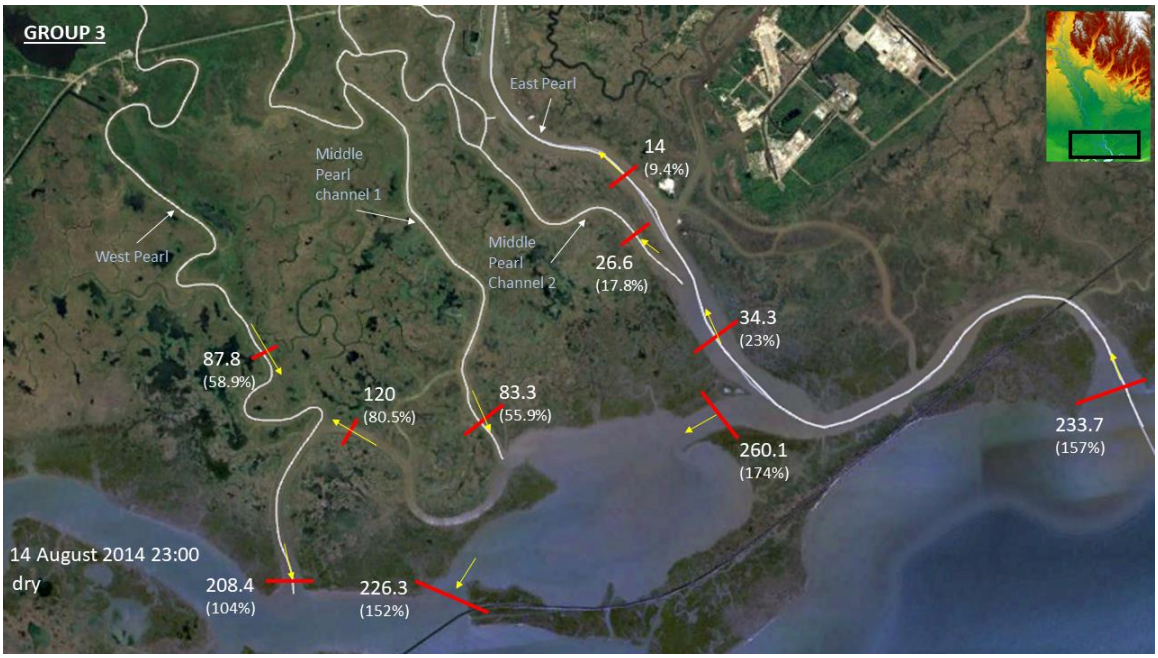

Figure 4.7 *: The discharge distribution at Group 3 of the river section, showing the Middle Pearl channels, and the three outlets of Pearl: Little Lake, East, and West Pearls for the dry period in August 2014. Numbers show the flowrate in m^3/s at identified red cross-sections and values in parenthesis show the percentage of that flow with respect to the flow in Bogalusa.*

The discharge from the three outlets was de-tided to see how the variation in the outflow compared with the total inflow from Bogalusa, Bogue Chitto, and Hobolochitto. Figure 4.8 shows the time-series plot of the discharge variation for the total inflow (black dotted line), combining Bogalusa, Bogue Chitto, and Hobolochitto Creeks, tidal discharge at the outlets (light blue and light orange), the de-tided discharge variation at the outlet of Little Lake and West Pearl combined (solid blue line), and East Pearl (solid orange line) and their combined de-tided discharge (solid purple line) for 2014. The discharge at Little Lake and West Pearl were combined due to their proximity and because both outlets are

treated as one in the ROMS model. Figure 4.8 shows that the flow of (Little Lake + West Pearl), in solid blue, and the flow of East Pearl, in solid orange line, are mirror images, suggesting flow coming into East Pearl flows out through the other two outlets. The flow in all three outlets is added to get the purple line, which has almost the same discharge pattern as the combined inflow (black dashed line). In the wet period, during high river discharge, the flow at all three outlets is positive, with East Pearl having similar discharge as West Pearl and Little Lake combined. During wet periods, the average flow in East Pearl is positive, flow going downstream. But during dry periods, especially when the total inflow is less than or equal to 100, the flow in average flow in East Pearl becomes negative, suggesting East Pearl flows upstream most of the time. The positive value of both purple and black dashed lines in the dry month suggests all the river inflow is exiting through West Pearl and Little Lake combined during the dry season. This suggests that all flow from the two inflows move out of Little Lake and West Pearl in the dry season. This can be seen in Figure 30 where a discharge of about 157% of that of Bogalusa enters East Pearl while the discharge leaving the Little Lake is almost like that amount.

The flow is mostly from West Pearl at low flow conditions where it is the dominating branch as seen from the upstream section while the East Pearl has very low riverine discharge values. This can be further seen in Figure 24, where the performance parameters for discharge suggest the de-tided discharge at NSTL (at East Pearl) compared better with the de-tide observed discharges in 2014. Although the same parameters showed poor model performance when the de-tided discharge was compared at the same station in 2015, this may be because 2015 was a year where the Bogalusa discharge was low and tide-dominated, so the de-tided discharge (showing mainly discharge due to river inflow)

performed poorly. But for 2019 and 2020, the model performed well since both these years had high mean and peak discharge from Bogalusa. However, this analysis cannot be verified due to the lack of observed data, so the discharge analysis presented for the dry months in Figure 30 should be verified with field measurements conducted in the area.

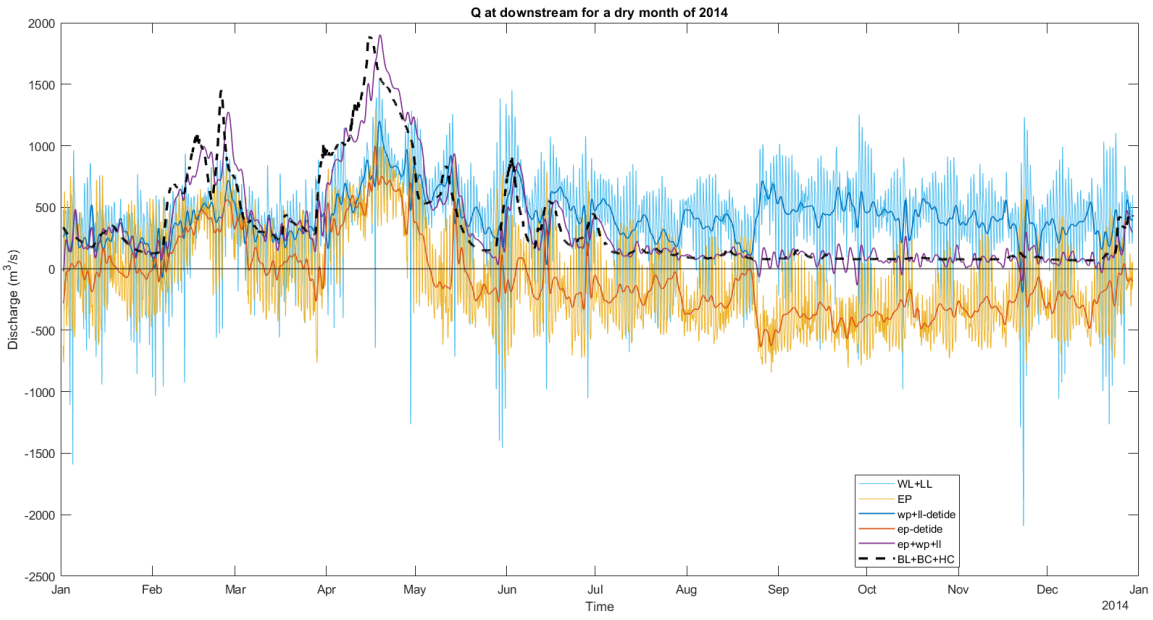

Figure 4.8 *: The model tidal flow at East Pearl (light orange), West Pearl + Little Lake combined (light blue), de-tide discharge at East Pearl (solid orange) and West Pearl + Little Lake combined (solid blue). It also shows (Bogalusa+Bogue Chitto) flow in a dashed black line. The solid purple line shows the discharge of (East Pearl+West Pearl+Little Lake).*

4.3 Volume Accumulation:

Volume accumulation at each of the inflows and outflows was also analyzed from the model. In the wet season, around 7.47 billion m^3 of flow from Bogalusa, 1.18 billion m^3 from Bogue Chitto, and 0.25 billion m^3 from Hobolochitto all contribute to 8.91 billion m^3 of water upstream. 7.42 billion m^3 of water comes out from both West Pearl and Little Lake combined while a net volume of 1.87 billion m^3 exits East Pearl alone, resulting in 8.81 billion m^3 of water coming out of the Lower Pearl River outlet. In this wet period of

about 6 months, about 105 million m^3 of water remains in the floodplain (marshlands and swamps). In the dry season, for a period of 6 months from July to December, 1.27 billion m^3 of water from Bogalusa adds with 0.36 billion m^3 of water from Bogue Chitto, and 0.05 billion m^3 from Hobolochitto upstream resulting in 1.69 billion m^3 of water coming from upstream. Downstream, a total of 6.14 billion m^3 flows through West Pearl and Little Lake while 4.49 billion m^3 of water flows into East Pearl, resulting in a total of 1.65 billion m^3 of water exiting the river downstream. A net volume of 38 million m^3 of water remains within the system in the floodplains or marshlands, which are sustained even in dry conditions. This shows what a significant role the marshlands have in the lower Pearl basin in storing water and how the upstream flow in the East Pearl is maintaining the marshlands. The marshlands maintain the balance and accounting for this would be crucial while the river forcing for the ocean model ROMS is configured.

Volume accumulation is plotted for the whole of 2014 to understand the movement of inflow and outflow and is shown in Figure 4.9. The figure shows the total volume of water (in a billion m^3) entering the study area at upstream boundaries, i.e., from Bogalusa, Bogue Chitto, and Hobolochitto Creeks, in blue bar for each month of 2014. The volume of water leaving each month from West Pearl (WP), Little Lake (LL), and East Pearl (EP) outlets at the coastline are shown in red, yellow, and purple bars respectively. The months with positive total volumes for all three outlets (WP, LL, and EP) in Figure 4.9 show that there is an outflow from all three outlets during high-flow conditions. The outflow volume in East Pearl is higher than the outflow in West Pearl in those months suggesting that East Pearl is the dominant river branch at high flow conditions in Bogalusa. When the upstream inflow goes below a certain threshold value in dry months, water flows into the East Pearl

outlet at the downstream boundary indicated by the negative monthly total flow volumes. The green line shows the net volume of water in the study area system which is an indicator of storage within the wetland system in the Lower Pearl floodplain. The net storage is positive in the wet periods when the river inflows are higher, and negative in the dry season, where the water from marshlands is being flushed out into the Sound. The net volume for wet and dry periods is positive, showing how the marshlands maintain the water balance in the system right after high flow (May) and when the river inflow is low (July). Figure 4.9 also shows that the volume of water into East Pearl is almost double the volume of water leaving West Pearl and Little Lake combined for April when the volume from river inflows is highest in the year.

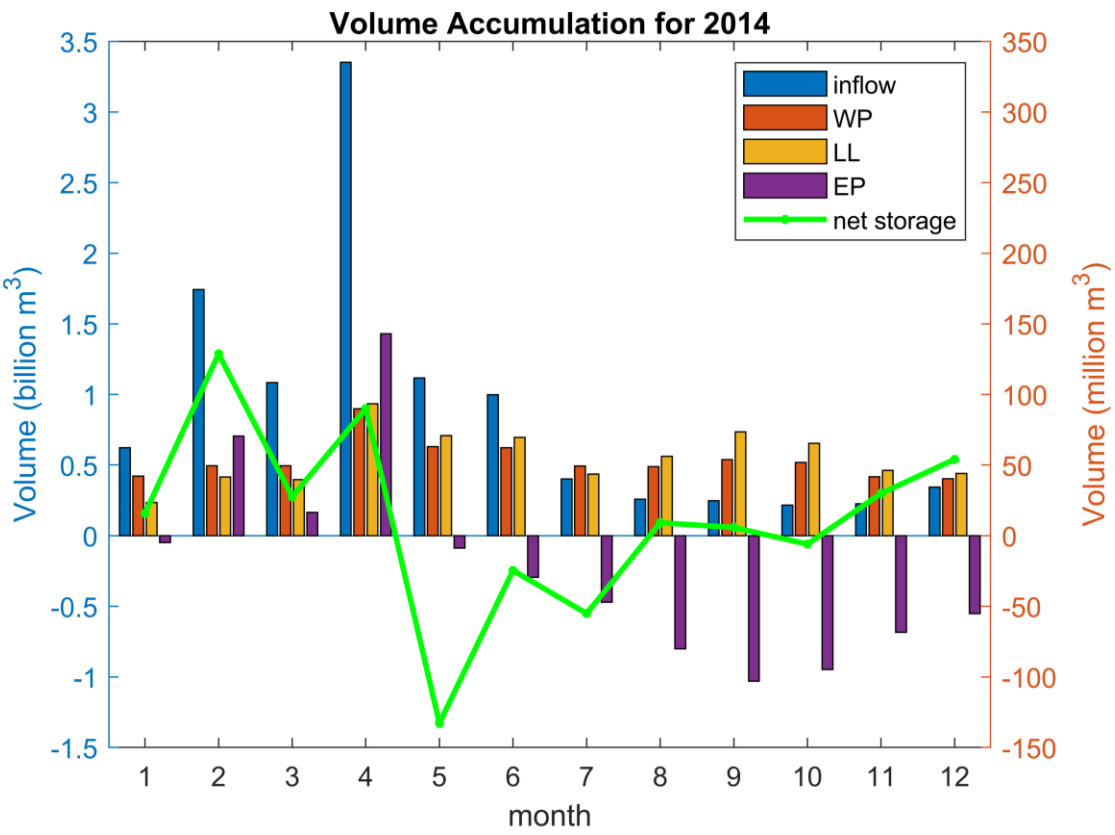

Figure 4.9 *: Total accumulated outflow volume of water for each month of 2014 for each Pearl River outlet at the coastline, West Pearl (WP), Little Lake (LL), East Pearl (EP), along with total inflow volume entering the river at the upstream boundaries, and the net storage shown as the difference between inflow and outflow.*

But it is imperative to state, HEC-RAS is a depth average model, and it does not represent 3D behavior. The flow at group 3, at the outlet, is more complex consisting of flow mixing and wave interaction in 3D so the flow represented by HEC-RAS might not be entirely valid.

CHAPTER V – CONCLUSION

The work presented in this study aimed to understand the flow dynamics upstream of the Lower Pearl River as it bifurcates and downstream of it as it spills into the Mississippi Sound. There is a knowledge gap on how much freshwater comes out from each of the Pearl branches and this study aimed to fill that gap to better understand how the freshwater from Pearl might affect the Sound, salinity, and temperature, and eventually impact the oyster production. The approach to this study was through hydrodynamic modeling which seemed the most cost-effective way to assess the flow for a large study area and for a long duration, instead of fitting and calibrating a limited number of discharge gages at a limited number of stations. This study also aimed to assess if the traditional 60-40 ratio, by which Pearl discharge at Bogalusa was thought to be divided into West Pearl and East Pearl Rivers, was applicable throughout the year. HEC-RAS was used as the model of choice and during initial modeling attempts, bathymetric data gaps proved to be the greatest challenge for modeling activities. So, during the modeling process, a novel technique was introduced to fit a synthetic meandering bathymetry into a DEM to better represent rivers in 2D modeling which are otherwise too small to be captured in satellite imagery, do not have extensive survey bathymetric data, and have tributaries and distributaries.

Although there is room for improvement, particularly in increasing the depth and meandering nature of the river, the study shows synthetic bathymetry can be used to capture the riverine flow (shown in Figures 3.5 and 3.6). However, this bathymetry equation is not applicable to braided river systems yet. Calibration and validation during 2014 and 2015 respectively showed the discharge and water level in stations, AB Wilson, Wilson Slough

near Walkiah Bluff, Pearl River at Pearl River, and NSTL, was captured with good accuracy (R2 >0.9, RSE <0.75, NSE >0.6, MS >0.8, KGE > 0.5). Though the low water values in AB Wilson was overestimated and high-water values were underestimated, the bias was less than 0.6 m. The model does not include sediment transport hence likely missing erosion in wet, high flow periods and deposition in dry, low flow periods. The model performance for discharge predictions was better at all stations than for water level predictions. However, the NSTL station showed particularly low performance during 2015 having a large PBIAS (-36 %) for discharge and showing low performance through all parameters for water level, where the model under-predicted the tidal range in discharge and water level but during high river flows the water level was over-estimated and discharge was underestimated.

The tidal influence in East Pearl is high, as seen by the observation in Figures 3.7, 3.8, and 4.1. The tidal range in the model was very low, suggesting the tidal flow entering East Pearl would be even higher than what the model predicts. This suggests the downstream driver of the tide could not be captured by the model. One reason might be the lack of wind forcing in the HEC-RAS model which did not allow the tides to move further upstream as they should have. The other reason might be the synthetic bathymetry, which should be even deeper than what is used. The bed material might have been scoured at the Lower Pearl before the split, which is suggested by the last 14 years of riverbank shift, which could make up for the difference in water level at AB Wilson station. Since then, boundary used is not a soft boundary allowing waves to propagate and mix, a pressure gradient might have been created between the outlet boundaries within the model causing the upstream from East Pearl to flow out through Little Lake and instead of traveling

upstream further into the river. Waves were also not included in the ADCIRC model providing river boundary for West Pearl and Little Lake which might also prevent the tide from going upstream as much into the East Pearl. The flow in Bogue Chitto is a small percentage of Bogalusa's flow and a backwater effect was not observed, refuting the hypothesis.

The flow analysis suggests the West Pearl receives higher flow than East Pearl upstream in wet conditions, rejecting the hypothesis. In the dry months, West Pearl still receives a higher percentage of the flow from Bogalusa, supporting the hypothesis. So West Pearl is the dominant river branch both in the wet and dry seasons, although higher flow is allocated to East Pearl at the bifurcation during wetter months when compared to dry months. West Pearl is still the dominant river branch downstream of Old River, but this scenario is reversed south of I59, where most flow from West Pearl spills into the floodplain between the two branches. The flow in the floodplain is transferred back into East Pearl and West Pearl at the downstream section. The Middle Pearl channels serve a huge role in this, carrying almost as much flow from the floodplain as West Pearl and diverting the flow from floodplain into Little Lake and East Pearl. So much so that it is hypothesized that East Pearl would have at least the same amount of flow as West Pearl at the river outlets. Thus, at the downstream section, the scenario from upstream is reversed for high flow conditions, when East Pearl is the dominant branch having nearly the same total outflow as West Pearl and Little Lake combined, proving the hypothesis correct. But the tidal influences change this scenario in the dry months where the magnitude of flow in both East and West Pearl is the same, as hypothesized, but the direction of flow is usually the opposite, rejecting the hypothesis. The model suggests all the riverine flow comes out

from Little Lake and West Pearl combined, whereas water flows into East Pearl upstream i.e., zero flow comes out through East Pearl. This finding supports the information received during meetings with The Mississippi Department of Marine Resources (personal communication). Unfortunately, there is no discharge data downstream of East Pearl to agree with or refute this statement. It must be emphasized that the results from HEC-RAS are 2D results in an area where the hydrodynamics are likely to be 3D in nature due to stratification. Using a 3D model with salinity variations would produce a better representation of flow dynamics and is recommended in the future.

The model is not perfect, and the results might be more accurate with more modifications to the bathymetry, boundary conditions as well as calibration parameters but the point of this study is to start a conversation and to assess if the predicted discharge conditions/distributions can be used to predict the salinity distribution in the Mississippi Sound instead of using a constant discharge ratio which might seem unrealistic.

APPENDIX A – Model Results for 2019

Figure A1: The Water level (WL) and flow (Q) hydrographs, the respective scatter plots and performance parameters comparing observation and model at stations AB Wilson, Wilson Slough near Walkiah Bluff, Pearl River at Pearl River and NSTL for 2019.

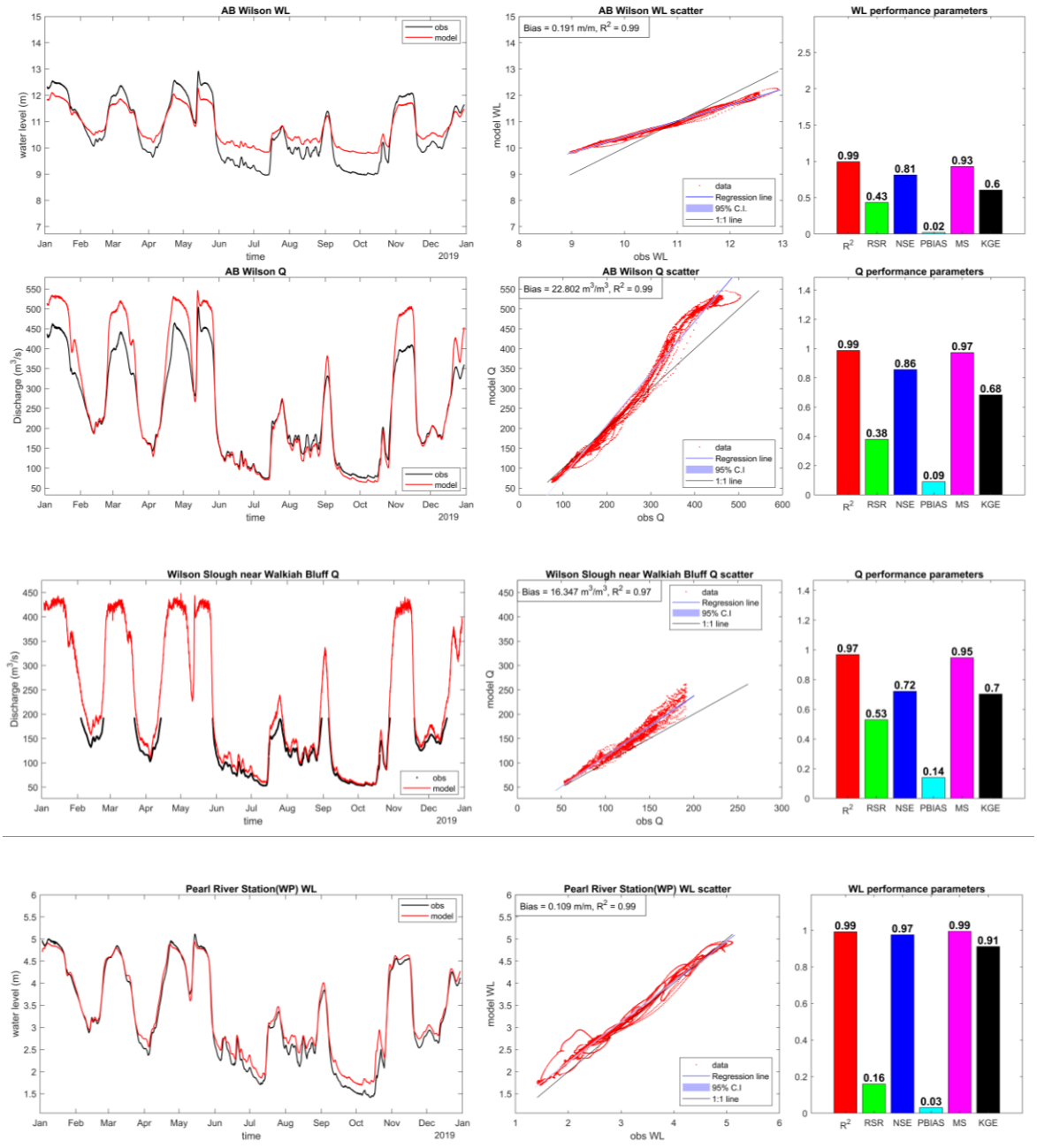

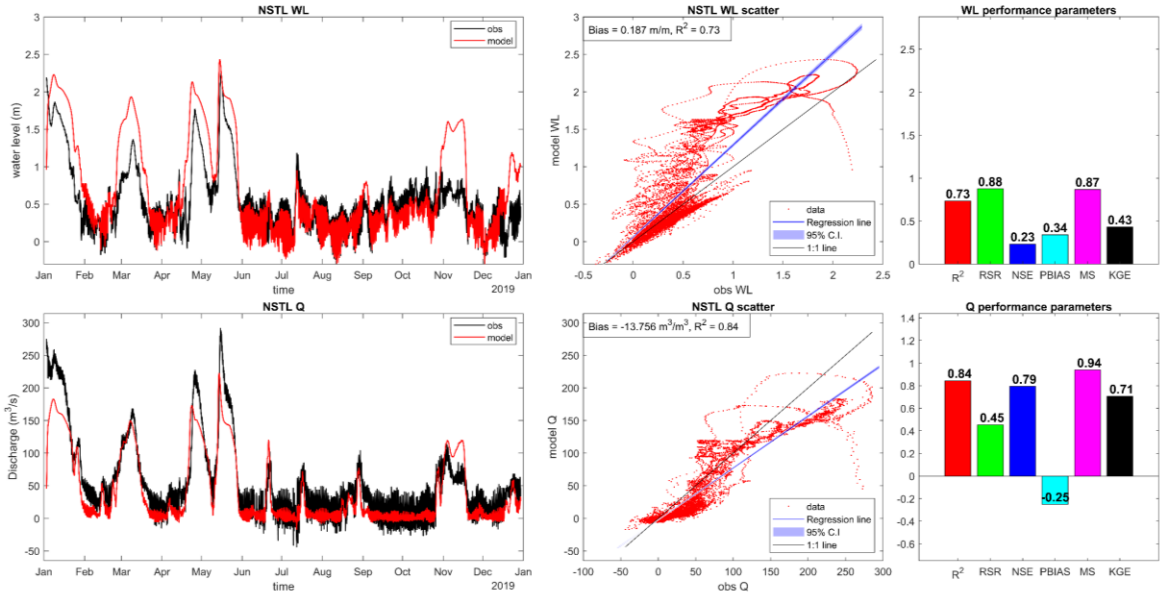
NSTL WL
obs
model
water level (m)
Jan Feb Mar Apr May Jun Jul Aug Sep Oct Nov Dec Jan
time
2019
NSTL WL scatter
Bias = 0.187 m/m, R2 = 0.73
model WL
obs WL
data
Regression line
95% C.I.
1:1 line
WL performance parameters
0.73
0.88
0.23
0.34
0.87
0.43
R2 RSR NSE PBIAS MS KGE
NSTL Q
obs
model
Discharge (m3/s)
Jan Feb Mar Apr May Jun Jul Aug Sep Oct Nov Dec Jan
time
2019
NSTL Q scatter
Bias = -13.756 m3/m3, R2 = 0.84
model Q
obs Q
data
Regression line
95% C.I
1:1 line
Q performance parameters
0.84
0.45
0.79
-0.25
0.94
0.71
R2 RSR NSE PBIAS MS KGE

APPENDIX B – Model Results for 2020

Figure B.1 *: The Water level (WL) and flow (Q) hydrographs, the respective scatter plots and performance parameters comparing observation and model at stations AB Wilson, Wilson Slough near Walkiah Bluff, Pearl River at Pearl River and NSTL for 2020*

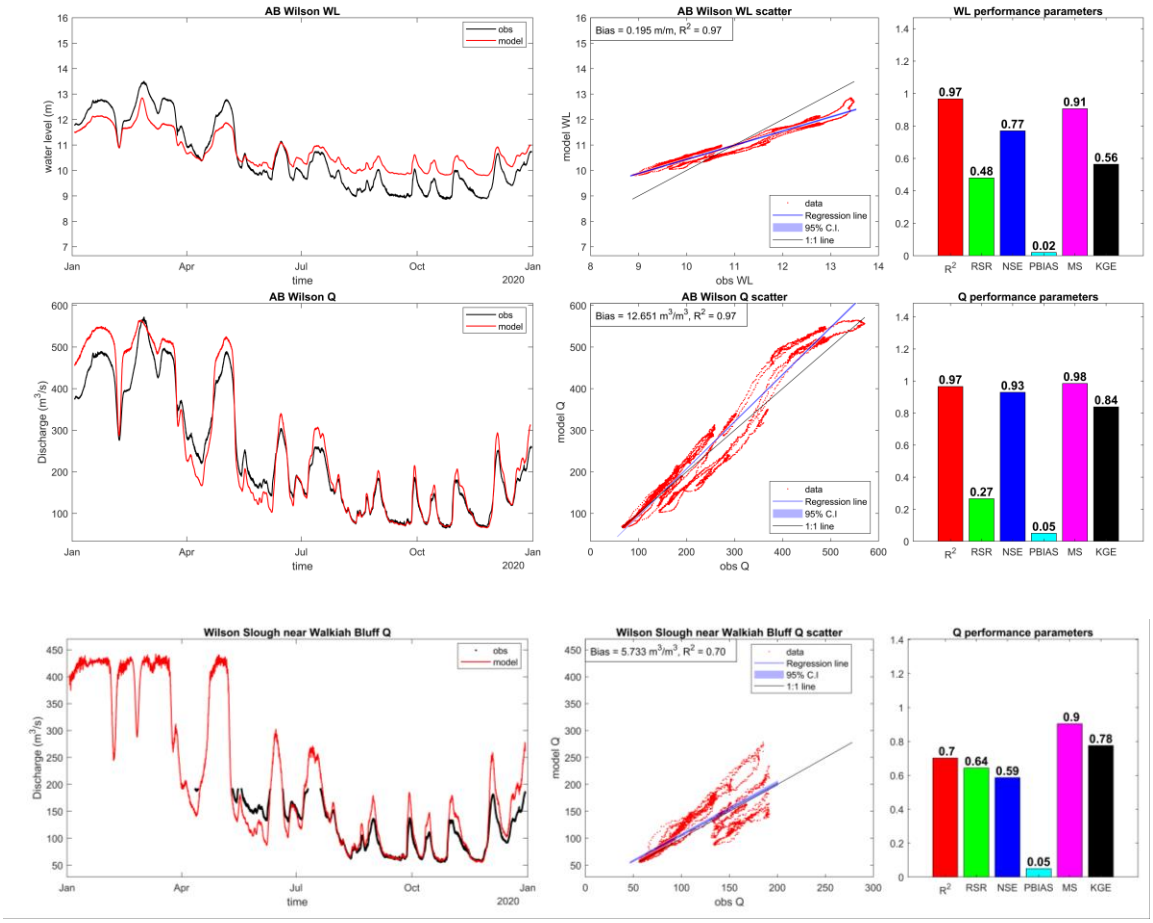

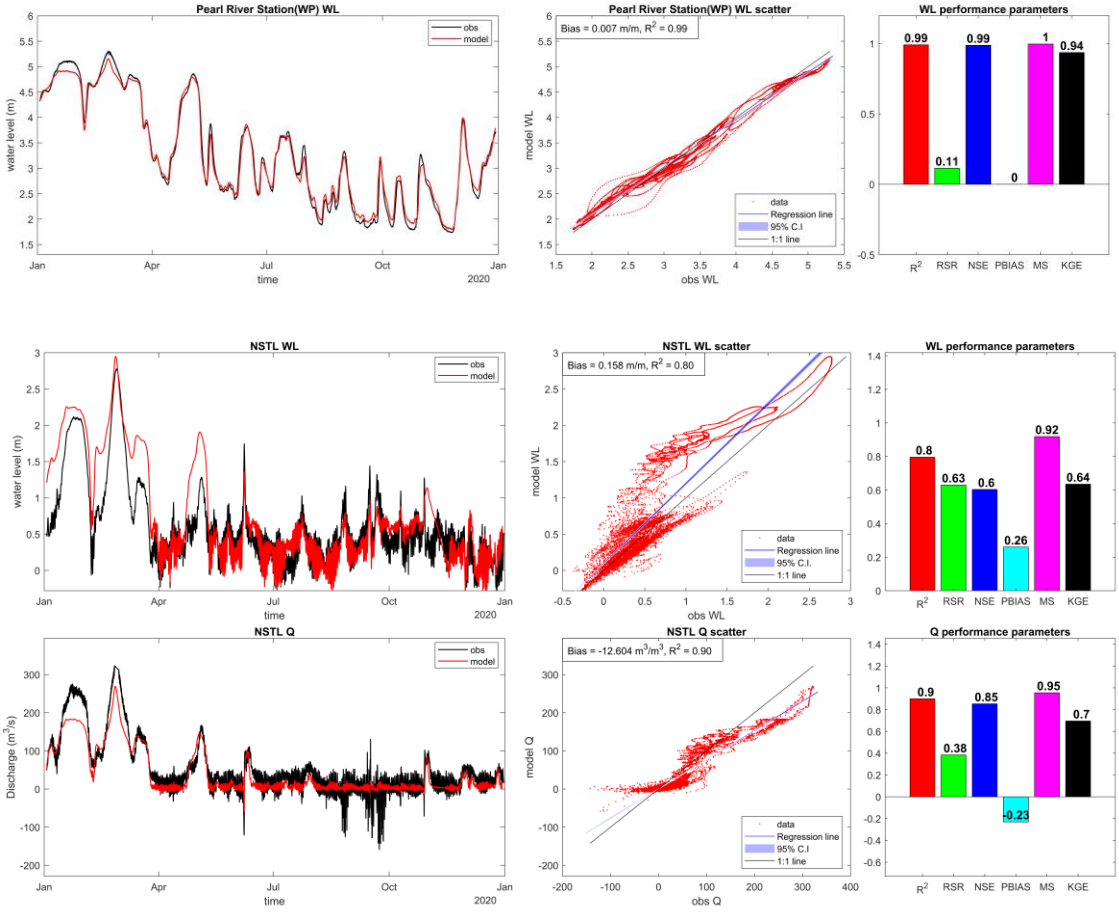
Pearl River Station(WP) WL
obs
model
water level (m)
time
Jan
Apr
Jul
Oct
Jan
2020
Pearl River Station(WP) WL scatter
Bias = 0.007 m/m, R2 = 0.99
model WL
obs WL
data
Regression line
95% C.I
1:1 line
WL performance parameters
0.99
0.11
0.99
0
1
0.94
R2
RSR
NSE
PBIAS
MS
KGE
NSTL WL
NSTL WL scatter
Bias = 0.158 m/m, R2 = 0.80
WL performance parameters
0.8
0.63
0.6
0.26
0.92
0.64
NSTL Q
Discharge (m3/s)
NSTL Q scatter
Bias = -12.604 m3/m3, R2 = 0.90
model Q
obs Q
Q performance parameters
0.9
0.38
0.85
-0.23
0.95
0.7

APPENDIX C – Model Results for Variable Manning's n at floodplain

Figure C1: The modeled water level (WL) and discharge (Q) hydrographs with variable Manning's n value in the floodplain, the scatterplots and the performance parameters at stations Bogalusa, AB Wilson and NSTL for February 2014.

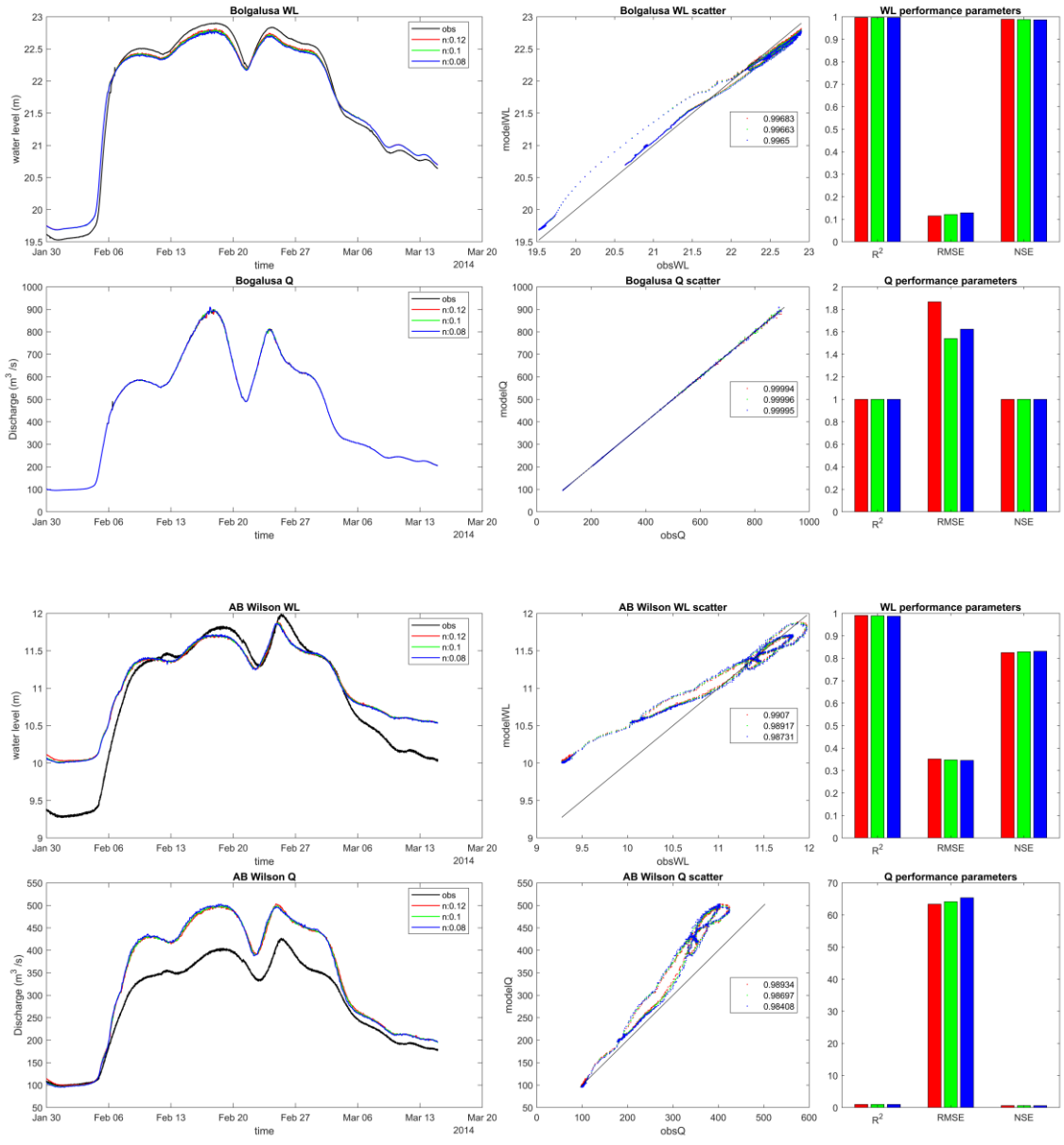

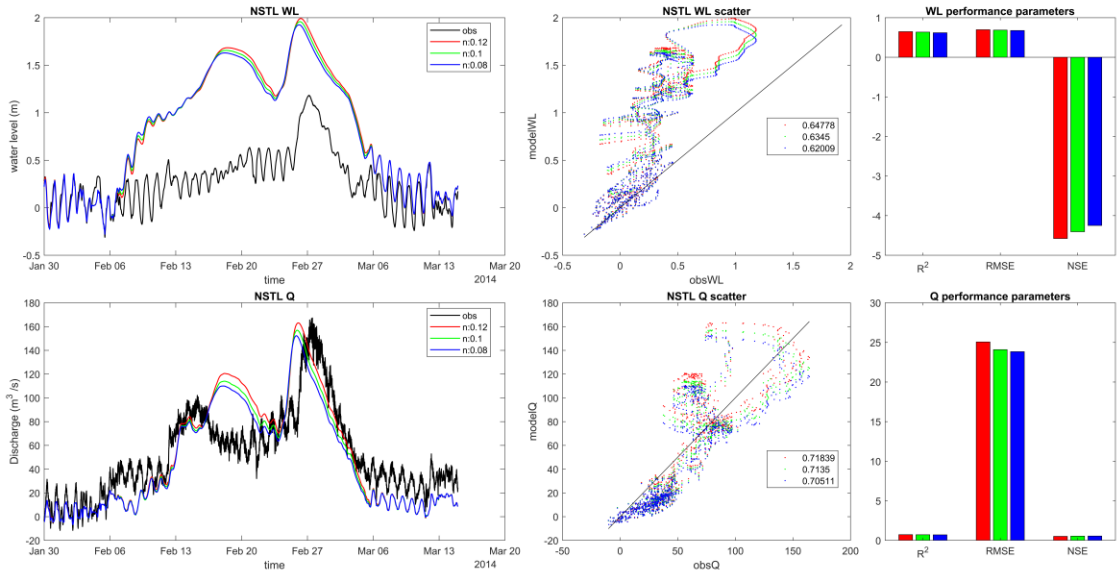
NSTL WL
obs
n:0.12
n:0.1
n:0.08
water level (m)
time
Jan 30
Feb 06
Feb 13
Feb 20
Feb 27
Mar 06
Mar 13
Mar 20
2014
NSTL WL scatter
modelWL
obsWL
0.64778
0.6345
0.62009
WL performance parameters
R2
RMSE
NSE
NSTL Q
Discharge (m3 /s)
NSTL Q scatter
modelQ
obsQ
0.71839
0.7135
0.70511
Q performance parameters

APPENDIX D – Walkiah Bluff

Figure D1: Walkiah Bluff, an earthen barrier at the mouth of West Pearl

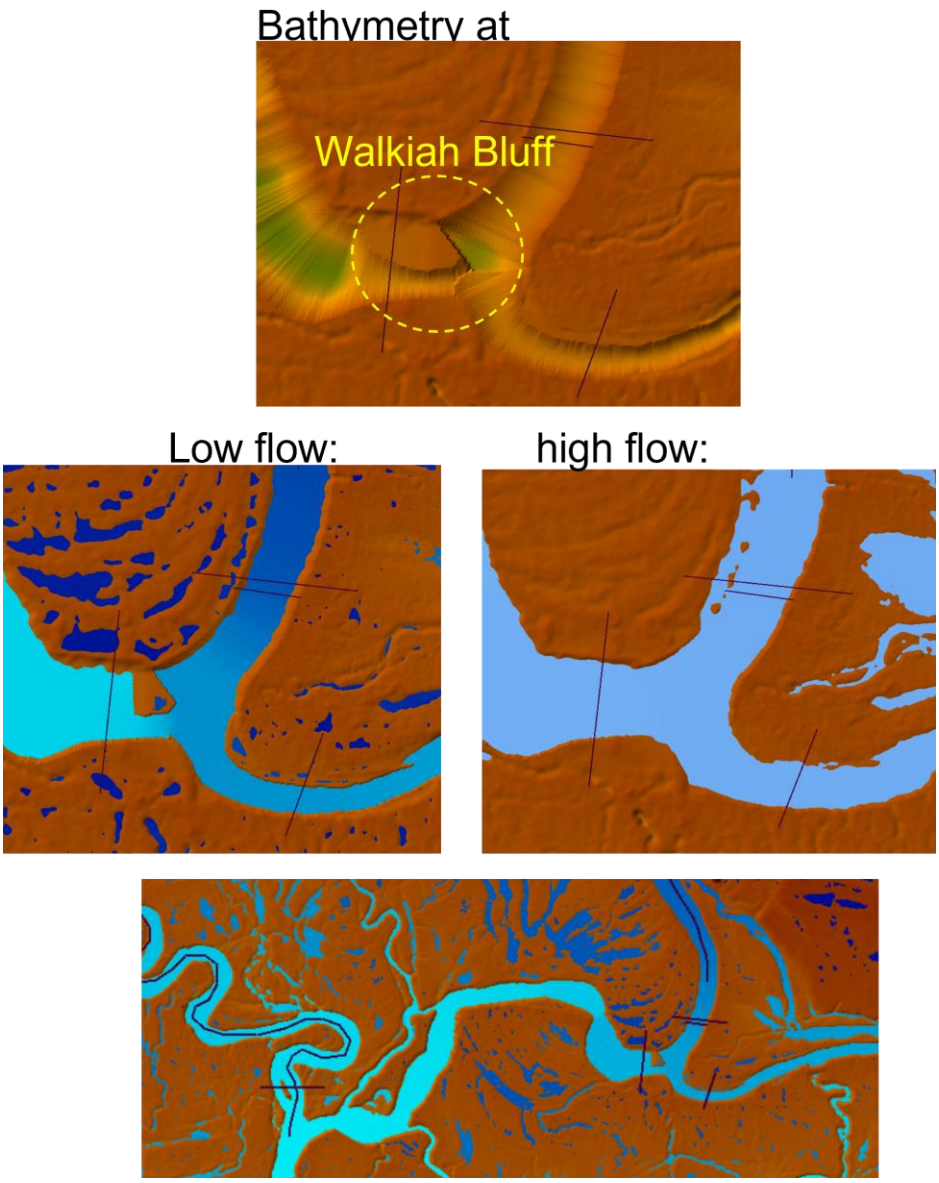

APPENDIX E – Model Results with meandering and non-meandering

Figure E1: Modeled water level (WL) and discharge (Q) hydrographs with meandering and non-meandering bathymetry of DEM at stations AB Wilson, Pearl River at Pearl River and NSTL for July 2014.

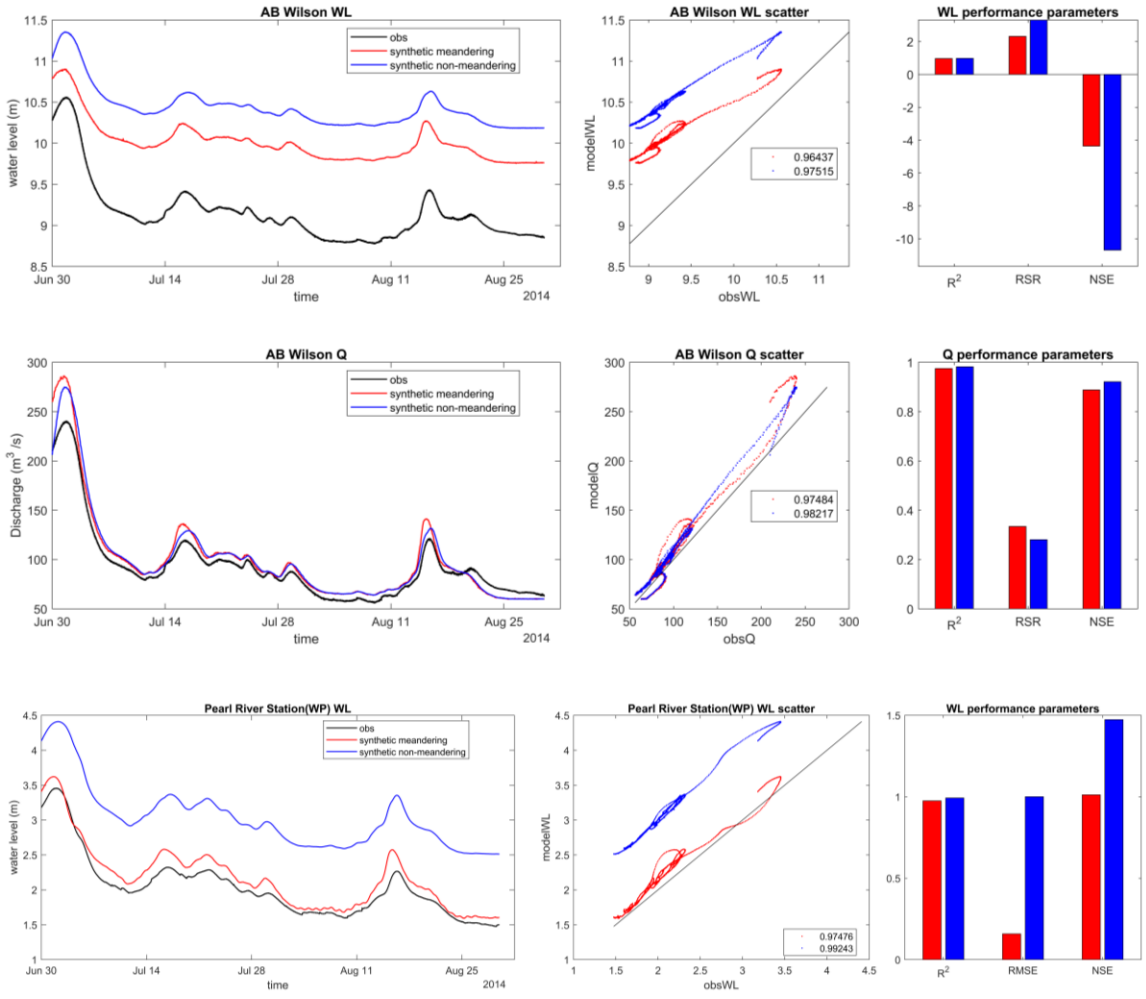

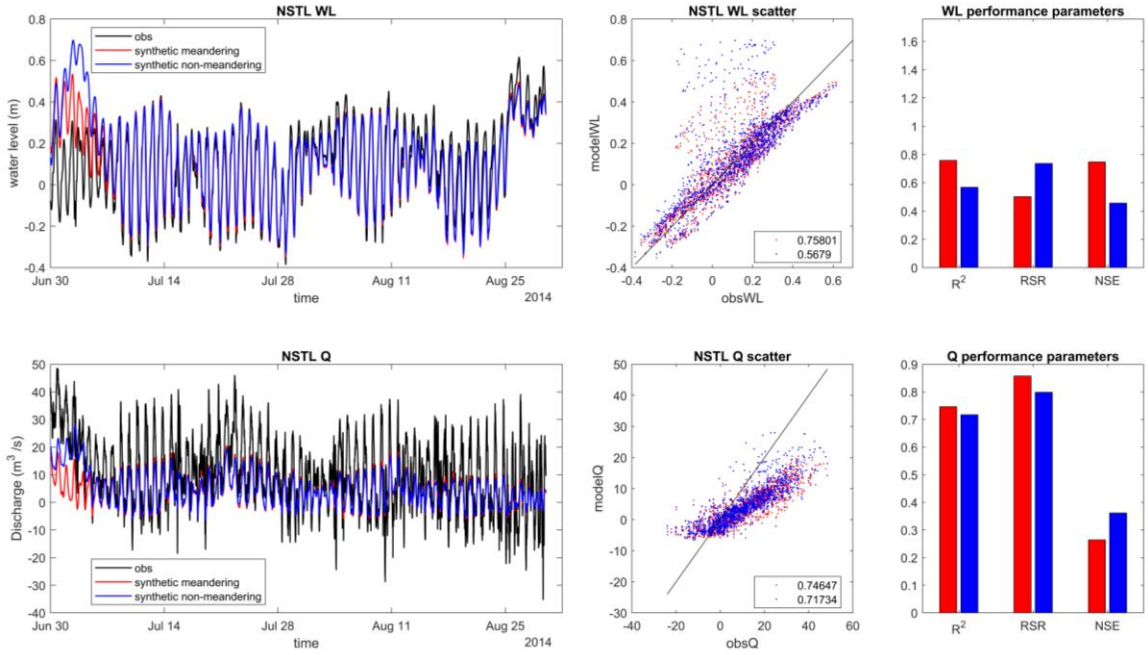
NSTL WL
obs
synthetic meandering
synthetic non-meandering
water level (m)
time
Jun 30
Jul 14
Jul 28
Aug 11
Aug 25
2014
NSTL WL scatter
modelWL
obsWL
0.75801
0.5679
WL performance parameters
R2
RSR
NSE
NSTL Q
Discharge (m3/s)
NSTL Q scatter
modelQ
obsQ
0.74647
0.71734
Q performance parameters

REFERENCES

Adriance, J., Marx, J., Bourque, C., & Britt, C. (2018). An Overview of Louisiana Department of Wildlife and Fisheries Data Collected in the Vicinity of Lake Pontchartrain and Lake Borgne from 2004 to 2017, as related to the MRGO Rock Dam Closure in 2009; La Dept. Wild. Fish. Marine Fisheries Section Tech. Rept.: Baton Rouge, LA, USA, 31.

Ahsan, Q., Blumberg, A. F., Li, H., & Blaha, J. (2002). The calibration/validation of a Mississippi Sound/Bight model. In OCEANS'02 MTS/IEEE (Vol. 2, pp. 823-833). IEEE.

Alarcon, V. J., & McAnally, W. H. (2012, June). Using hydrodynamic modeling for estimating flooding and water depths in grand bay, Alabama. In International Conference on Computational Science and Its Applications (pp. 578-588). Springer, Berlin, Heidelberg.

Altinakar, M., McGrath, M. Z., Ramalingam, V. P., & Omari, H. (2010). 2D modeling of big bay dam failure in mississippi: Comparison with Field Data and 1D Model Results. River Flow 2010, 547-554.

Armandei, M., Linhoss, A. C., & Camacho, R. A. (2021). Hydrodynamic modeling of the Western Mississippi Sound using a linked model system. Regional Studies in Marine Science, 44, 101685.

Armstrong, B. N., Cambazoglu, M. K., & Wiggert, J. D. (2021, September). Modeling the impact of the 2019 Bonnet Carré Spillway opening and local river flooding on the Mississippi Sound. In OCEANS 2021: San Diego–Porto (pp. 1-7). IEEE.

Astite, S. W., Medjerab, A., Belabid, N. E., El Mahmouhi, N., El Wartiti, M., & Kemmou, S. (2015). Cartography of flood hazard by overflowing rivers using hydraulic modeling and geographic information system: Oued El Harrach case (North of Algeria). Revista de Teledetección, (44), 67-79.

Bhuyian, M. N. M. (2019). Development of Morphologically Consistent Digital Elevation Model for Improving Riverine Flood Impact Assessment in Data-Poor Areas (Doctoral dissertation, Tennessee Technological University).

Bhuyian, M. N. M., Alford, A., & Blackwood, D. (2019, December). Estimating Spatio-temporal Error of LiDAR DEM along Two Morphologically Active Rivers in West Tennessee. In AGU Fall Meeting Abstracts (Vol. 2019, pp. EP51E-2132).

Bhuyian, M. N., & Kalyanapu, A. (2020). Predicting Channel Conveyance and Characterizing Planform Using River Bathymetry via Satellite Image Compilation (RiBaSIC) Algorithm for DEM-Based Hydrodynamic Modeling. Remote Sensing, 12(17), 2799.

Bigelow, E. M., Chamberlain, S. D., Council, P. R. C. H. M., & Planning, P. R. C. (2001). Pearl River County, Mississippi Hazard Mitigation And Flood Protection Plan.

Blain, C. A., & Cambazoglu, M. K. (2019). Development of a Forecast Model for the Lower Pearl River Basin. Naval Research Lab Stennis Detachment Stennis Space Center, MS, University of Mississippi.

Brunner, G.W. HEC-RAS, River Analysis System Hydraulic Reference Manual. Available online:

https://www.hec.usace.army.mil/software/hecras/documentation/HECRAS_4.1_Reference_Manual.pdf (accessed on 1 May 2017).

Bunya, S., Dietrich, J. C., Westerink, J. J., Ebersole, B. A., Smith, J. M., Atkinson, J. H., ... & Roberts, H. J. (2010). A high-resolution coupled riverine flow, tide, wind, wind wave, and storm surge model for southern Louisiana and Mississippi. Part I: Model development and validation. Monthly weather review, 138(2), 345-377.

Bush, S. T., Dresback, K. M., Szpilka, C. M., & Kolar, R. L. (2022). Use of 1D Unsteady HEC-RAS in a Coupled System for Compound Flood Modeling: North Carolina Case Study. Journal of Marine Science and Engineering, 10(3), 306.

Cambazoglu, M. K., & Haas, K. A. (2011). Numerical modeling of breaking waves and cross-shore currents on barred beaches. Journal of waterway, port, coastal, and ocean engineering, 137(6), 310-323.

Cardoso de Salis, H. H., Monteiro da Costa, A., Moreira Vianna, J. H., Azeneth Schuler, M., Künne, A., Sanches Fernandes, L. F., & Leal Pacheco, F. A. (2019). Hydrologic modeling for sustainable water resources management in urbanized karst areas. International Journal of Environmental Research and Public Health, 16(14), 2542.

Castaneda-Gonzalez, Mariana, Annie Poulin, Rabindranarth Romero-Lopez, Richard Arsenault, François Brissette, Diane Chaumont, and Dominique Paquin. "Impacts of regional climate model spatial resolution on summer flood simulation." EPiC Series in Engineering 3 (2018): 372-380.

Cho, J., Bosch, D., Vellidis, G., Lowrance, R., & Strickland, T. (2013). Multi-site evaluation of hydrology component of SWAT in the coastal plain of southwest Georgia. Hydrological Processes, 27(12), 1691-1700.

Chow, V. T. (1959). Design of channels for uniform flow. Open—Channel Hydraulics; McGraw Hill: New York, NY, USA.

Chow, V. T. (1959). Determination of hydrologic frequency factor. *Journal of the Hydraulics Division*, *85*(7), 93-98.

Chowdhury, M. E., Islam, A. S., Lemans, M., Hegnauer, M., Sajib, A. R., Pieu, N. M., ... & Bhuyan, A. (2023). An efficient flash flood forecasting system for the un-gaged Meghna basin using open source platform Delft-FEWS. Environmental Modelling & Software, 161, 105614.

DeHaan, H., Stamper, J., Walters, B., 2012. Mississippi river and tributaries system 2011 post-flood report: documenting the 2011 flood, the corps? response, and the performance of the MR & T system. USACE, Mississippi Valley Division, Vicksburg, MS.

Denapolis T, and J Lopez (2020) Habitat suitability analyses for the Eastern oyster, Crassostrea virginica, of the Pontchartrain Basin Estuary, Southeast Louisiana, in 2019. Lake Pontchartrain Basin Foundation, Costal and Community Program, 68 pp

Ding, Y., Altinakar, M. S., Jia, Y., Kuiry, S. N., Zhang, Y. X., & Goodman, A. (2012). Simulation of storm surge in the Mississippi Gulf Coast using an integrated coastal processes model. In Proceeding of ASCE-EWRI congress (pp. 20-24).

Dortch, M. S., Zakikhani, M., Noel, M. R., & Kim, S. C. (2007). Application of a water quality model to Mississippi Sound to evaluate impacts of freshwater diversions. Engineer research and development center Vicksburg MS environmental lab.

Duan, S., Bianchi, T. S., & Sampere, T. P. (2007). Temporal variability in the composition and abundance of terrestrially-derived dissolved organic matter in the lower Mississippi and Pearl Rivers. Marine Chemistry, 103(1-2), 172-184.

Eleuterius, C.K., 1976. Mississippi Sound: Salinity Distribution and Indicated Flow Patterns. Sea Grant Publication MASG-76-023, Ocean Springs, MS.

Fink, P., Bodi, G., & Haider, S. (2006). Abschätzung des Vertrauensbereichs von berechneten Hochwasser-Spiegellagen. Österreichische Wasser-und Abfallwirtschaft, 58, a15-a18.

Gelati, E., Decharme, B., Calvet, J. C., Minvielle, M., Polcher, J., Fairbairn, D., & Weedon, G. P. (2018). Hydrological assessment of atmospheric forcing uncertainty in the Euro-Mediterranean area using a land surface model. Hydrology and Earth System Sciences, 22(4), 2091-2115.

Goolsby, D. A., Battaglin, W. A., Aulenbach, B. T., & Hooper, R. P. (2000). Nitrogen flux and sources in the Mississippi River Basin. Science of the Total Environment, 248(2-3), 75-86.

Gori, A.; Lin, N.; Smith, J. Assessing Compound Flooding From Landfalling Tropical Cyclones on the North Carolina Coast. Water Resourc. Res. 2020, 56, e2019WR026788. [CrossRef]

Gupta, H. V., Kling, H., Yilmaz, K. K., & Martinez, G. F. (2009). Decomposition of the mean squared error and NSE performance criteria: Implications for improving hydrological modelling. Journal of hydrology, 377(1-2), 80-91.

Gupta, H. V., Sorooshian, S., and Yapo, P. O.: Toward improved calibration of hydrologic models: Multiple and non-commensurable measures of information,Water Resour. Res., 34, 751–763, https://doi.org/10.1029/97WR03495, 1998.

Horritt, M.S.; Bates, P.D. Evaluation of 1D and 2D numerical models for predicting river flood inundation. J. Hydrol. 2002, 268, 87–99. [CrossRef]

Jahandideh-Tehrani, M., Helfer, F., Zhang, H., Jenkins, G., & Yu, Y. (2020). Hydrodynamic modelling of a flood-prone tidal river using the 1D model MIKE HYDRO River: calibration and sensitivity analysis. Environmental Monitoring and Assessment, 192, 1-18.

Jain, S. K., & Sudheer, K. P. (2008). Fitting of hydrologic models: a close look at the Nash–Sutcliffe index. Journal of hydrologic engineering, 13(10), 981-986.

Jones, K. E., Dahl, T. A., & Corum, Z. P. (2018). Modeled Sedimentation in the Lower White River Countyline Levee Setback, Washington State: Comparison of 1D (HEC RAS) and 2D (AdH) Results. ERDC-CHL Vicksburg United States.

Knoben, W. J., Freer, J. E., & Woods, R. A. (2019). Inherent benchmark or not? Comparing Nash–Sutcliffe and Kling–Gupta efficiency scores. Hydrology and Earth System Sciences, 23(10), 4323-4331.

Kulp, M., Yocum, T., Courtis, A. (2020). Flow distribution at the mouth of the Pearl River using synoptic ADCP. Lake Pontchartrain Basin Foundation.

Lahmers, T. M., Hazenberg, P., Gupta, H., Castro, C., Gochis, D., Dugger, A., ... & Wang, Y. H. (2021). Evaluation of NOAA national water model parameter calibration in semiarid environments prone to channel infiltration. Journal of Hydrometeorology, 22(11), 2939-2969.

LeFavour, G., & Alsdorf, D. (2005). Water slope and discharge in the Amazon River estimated using the shuttle radar topography mission digital elevation model. Geophysical Research Letters, 32(17).

Lian, J. J., Xu, K., & Ma, C. (2013). Joint impact of rainfall and tidal level on flood risk in a coastal city with a complex river network: a case study of Fuzhou City, China. Hydrology and Earth System Sciences, 17(2), 679-689.

McAlpin, J., Ross, C., & McKnight, J. (2019). Houston Ship Channel and Vicinity Three-Dimensional Adaptive Hydraulics (AdH) Numerical Model Calibration/Validation Report. ERDC Vicksburg United States.

McKay, P., & Blain, C. A. (2009, October). Toward developing a hydrodynamic flow and inundation model of the Lower Pearl River. In OCEANS 2009 (pp. 1-8). IEEE.

Mejia, A. I., & Reed, S. M. (2011). Evaluating the effects of parameterized cross section shapes and simplified routing with a coupled distributed hydrologic and hydraulic model. Journal of Hydrology, 409(1-2), 512-524.

Moriasi, D. N., Arnold, J. G., Van Liew, M. W., Bingner, R. L., Harmel, R. D., & Veith, T. L. (2007). Model evaluation guidelines for systematic quantification of accuracy in watershed simulations. Transactions of the ASABE, 50(3), 885-900.

Muñoz, D. F., Yin, D., Bakhtyar, R., Moftakhari, H., Xue, Z., Mandli, K., & Ferreira, C. (2022). Inter-model comparison of Delft3D-FM and 2D HEC-RAS for total water level prediction in coastal to inland transition zones. JAWRA Journal of the American Water Resources Association, 58(1), 34-49.

Nilsson, C., & Berggren, K. (2000). Alterations of riparian ecosystems caused by river regulation: Dam operations have caused global-scale ecological changes in riparian ecosystems. How to protect river environments and human needs of rivers remains one of the most important questions of our time. BioScience, 50(9), 783-792.

Pan, T., Wu, S., Dai, E., & Liu, Y. (2013). Estimating the daily global solar radiation spatial distribution from diurnal temperature ranges over the Tibetan Plateau in China. Applied Energy, 107, 384-393.

Pappenberger, F.; Beven, K.; Horritt, M.; Blazkova, S. Uncertainty in the calibration of effective roughness parameters in HEC-RAS using inundation and downstream level observations. J. Hydrol. 2005, 302, 46–69. [CrossRef]

Parra, S. M., Sanial, V., Boyette, A. D., Cambazoglu, M. K., Soto, I. M., Greer, A. T., ... & Dinniman, M. S. (2020). Bonnet Carré Spillway freshwater transport and corresponding biochemical properties in the Mississippi Bight. *Continental Shelf Research*, *199*, 104114.

Pathak, S. R. (2013). Application of 2D Hydrodynamic and Sediment Transport Model AdH in Weeks Bay, Alabama (Doctoral dissertation, Mississippi State University).

Patrick, R. 1995. Rivers of the United States: Volume II Chemical and physical characteristics. John Wiley and Sons, Inc.

Pearl River Basin Team (2000) Pearl River Basin 2000 Status Report. [http://www.deq.state.ms.us].

Picayune Times (2022, April 20). St Tammany Parish comments on the Pearl River Basin, Mississippi Section 211. https://www.picayuneitem.com/2023/04/st-tammany-parish-comments-on-the-pearl-river-basin-mississippi-section-211-feasibility-study-integrated-draft-feasibility-and-environmental-impact-statement/

Ray, T., Stepinski, E., Sebastian, A., & Bedient, P. B. (2011). Dynamic modeling of storm surge and inland flooding in a Texas coastal floodplain. Journal of Hydraulic Engineering, 137(10), 1103-1110.

Roberts, A.L. (2012). Flooding Concerns on the Lower Pearl River Near Walkiah Bluff. Mississippi Water Resources Conference (pp. 115-126)

Rogelis, M. C., Werner, M., Obregón, N., & Wright, N. (2016). Hydrological model assessment for flood early warning in a tropical high mountain basin. Hydrology and Earth System Sciences Discussions, 1-36.

Sandeep, K. K., Armstrong, B. N., Cambazoglu, M. K., & Wiggert, J. D. (2021, December). An assessment of the mixed layer salinity balance in the river-dominated coastal region of northern Gulf of Mexico using a high-resolution numerical model. In AGU Fall Meeting 2021. AGU.

Sandeep, K. K., Armstrong, B., Cambazoglu, M. K., & Wiggert, J. D. (2020, December). Impact of river discharge on the seasonal variability of salinity in the Mississippi

delta region: A modeling approach. In AGU Fall Meeting Abstracts (Vol. 2020, pp. OS013-06).

Sankar, M.S., Dash, P., Lu, Y. et al. Seasonal changes of trace elements, nutrients, dissolved organic matter, and coastal acidification over the largest oyster reef in the Western Mississippi Sound, USA. Environ Monit Assess 195, 175 (2023). https://doi.org/10.1007/s10661-022-10719-z.

Santos, L., Thirel, G., & Perrin, C. (2018). Pitfalls in using log-transformed flows within the KGE criterion. Hydrology and Earth System Sciences, 22(8), 4583-4591.

Schmalz, J.R.A. (1983). The Development of a Numerical Solution to the Transport Equation (Reports 1, 2, 1st 3). U. S. Army Engineer Waterways Experiment Station, Vicksburg, MS.

Schönfelder, L. H., Bakken, T. H., Alfredsen, K., & Adera, A. G. (2017). Application of HYPE in Norway, Assessment of the hydrological model HYPE as a tool to support the implementation of EU Water Framework Directive in Norway (No. 2017, p. 00737). SINTEF Energy Research, report.

Shiller, A. M., Shim, M. J., Guo, L., Bianchi, T. S., Smith, R. W., & Duan, S. (2012). Hurricane Katrina impact on water quality in the East Pearl River, Mississippi. Journal of Hydrology, 414, 388-392.

Sklar, F. H., & Browder, J. A. (1998). Coastal environmental impacts brought about by alterations to freshwater flow in the Gulf of Mexico. Environmental management, 22(4), 547-562.

Soto, I.M., Crooke, B., Seegers, B., Cetinic, I., Cambazoglu, M.K., Armstrong, B. (2023) "Spatial and temporal characterization of cyanobacteria blooms in the Mississippi

Sound and their relationship to the Bonnet Carré Spillway openings", Harmful Algae. (accepted).

Tetra Tech. Inc. (2018). Hydrodynamic and Water Quality Modeling Report for the Lower Pearl River, Mississippi. Draft Report for Mississippi Department of Environmental Quality.

Thorne, C., Harmar, O., Watson, C., Clifford, N., & Biedenham, D. (2008). Current and historical sediment loads in the Lower Mississippi River. Nottingham Univ (United Kingdom) Dept of Geography.

Timbadiya, P. V., P. L. Patel, and P. D. Porey. "A 1D–2D coupled hydrodynamic model for river flood prediction in a coastal urban floodplain." Journal of Hydrologic Engineering 20.2 (2015): 05014017.

Turner, R. E. (2006). Will lowering estuarine salinity increase Gulf of Mexico oyster landings?. Estuaries and Coasts, 29(3), 345-352.

Vinogradova, N., Vinogradov, S., Nechaev, D. A., Kamenkovich, V. M., Blumberg, A. F., Ahsan, Q., & Li, H. (2005). Evaluation of the northern Gulf of Mexico littoral initiative model based on the observed temperature and salinity in the Mississippi Bight. Marine Technology Society Journal, 39(2), 25.

Wang, X., Cai, Y., & Guo, L. (2013). Variations in abundance and size distribution of carbohydrates in the lower Mississippi River, Pearl River and Bay of St Louis. Estuarine, Coastal and Shelf Science, 126, 61-69.

Ward, G. M., Harris, P. M., & Ward, A. K. (2005). Gulf Coast rivers of the southeastern United States. Rivers of North America, 125-178.

Warren, B. (2013, August 27). Hurricane Isaac memories strong one year later in Slidell, St. Tammany Parish. The Times-Picayune. (NOLA.com). Available at: https://www.nola.com/news/weather/article_08d6959b-0a80-5965-8c7d-1fde79e69211.html#:~:text=But%20Isaac%20pushed%20a%20massive,in%20a%20handful%20of%20areas.

White, D.A. & Simmons, M. J. (1988). Productivity of the Marshes at the Mouth of the Pearl River, Louisiana. Castanea, Vol. 53, No. 3, (pp. 215-224). Southern Appalachian Botanical Society.

Wijayarathne, D. B., & Coulibaly, P. (2020). Identification of hydrological models for operational flood forecasting in St. John's, Newfoundland, Canada. Journal of Hydrology: Regional Studies, 27, 100646. https://doi.org/10.1016/j.ejrh.2019.100646.

Williams, C. N., Cornford, S. L., Jordan, T. M., Dowdeswell, J. A., Siegert, M. J., Clark, C. D., Swift, D. A., Sole. A., Fenty. I., & Bamber, J. L. (2017). Generating synthetic fjord bathymetry for coastal Greenland. The Cryosphere, 11(1), 363-380.

Williams, J. J., & Esteves, L. S. (2017). Guidance on setup, calibration, and validation of hydrodynamic, wave, and sediment models for shelf seas and estuaries. Advances in civil engineering, 2017.

Willmott, C. J. (1981). On the validation of models. Physical geography, 2(2), 184-194.

Yochum, S. E., Goertz, L. A., & Jones, P. H. (2008). Case study of the Big Bay Dam failure: Accuracy and comparison of breach predictions. Journal of Hydraulic Engineering, 134(9), 1285-1293.